The Thesis Committee for Thanawut Worawutthichanyakul
Certifies that this is the approved version of the following thesis:

Unstable Immiscible Displacement Study in Oil-Wet Rocks

APPROVED BY
SUPERVISING COMMITTEE:

Supervisor:

Kishore K. Mohanty

Mojdeh Delshad

Unstable Immiscible Displacement Study in Oil-Wet Rocks

by

Thanawut Worawutthichanyakul, B.E.

Thesis

Presented to the Faculty of the Graduate School of

The University of Texas at Austin

in Partial Fulfillment

of the Requirements

for the Degree of

Master of Science in Engineering

The University of Texas at Austin

May 2016

Dedication

To my family.

Acknowledgements

First and foremost, I would like to thank my thesis supervisor, Dr. Kishore K. Mohanty for his guidance and support throughout this research. Whenever I ran into a trouble or had questions about my research or writing, I was able to reach him. It was a true pleasure and honor to work with him. In addition, I would like to thank Dr. Mojdeh Delshad for being a reader of my thesis and providing valuable advice and feedback.

I am grateful to be surrounded by people who have been very supportive and helpful: Shashvat for teaching me the experiments procedures when I started working on my research, Dr. Erik Dao and Robin for helping me with experimental setup, Haishan for teaching the effective fingering model concept and guiding me during the simulation process, Gary Miscoe for providing me the experimental materials, Dr. Dicarlo and Tianbo for supporting me during the CT scan experiment. My completion of this project could not have been accomplished without these people.

I would also like to thank my research group members: Pinaki, Himanshu, Taylor, Ruth, Krishna, Chammi, Almas, Songyang, and Prateek for their friendship and all their helps. I had a great time working with all of you. I would like to extend a thank you to Barbara Messmore for a work schedule reminder and a secret recipe.

In addition, I also owe a thank you to PTTEP for providing me the opportunity and funding to study here. This is one of the best experiences in my life.

Finally, I must express my gratitude to my family and to all my friends here in Austin, especially the IGSM group, for giving me the support and continuous encouragement throughout my graduate school life.

Abstract

Unstable Immisible Displacement Study in Oil-Wet Rocks

Thanawut Worawutthichanyakul, M.S.E

The University of Texas at Austin, 2016

Supervisor: Kishore K. Mohanty

Displacement of a viscous fluid by a lower viscosity immiscible fluid (such as waterflood of the viscous oil) in a porous medium is unstable. The displacement front generates viscous fingers which lead to less oil recovery efficiency. Another important problem related to instability in immiscible flow is the lack of reservoir modeling to capture viscous fingerings in simulation grid blocks.

Few approaches to represent this phenomenon in reservoir modeling have been proposed previously. A dimensionless scaling group (viscous finger number) has been suggested which have a power-law relationship with the breakthrough recovery and cumulative recovery in unstable core floods. The relative permeability used in large grid-block simulations has been modified to so-call "pseudo-relative permeability" on the basis of the dimensionless group, thus incorporating the effect of fingers in waterflood predictions.

However, the previous proposed models were constructed from experiments only in water-wet systems. This research extends the recent viscous fingering models to oil-wet systems. Sandstone cores are treated to alter the wettability to oil-wet. Series of

experimental studies are performed in both water-wet and oil-wet cores. Viscosity ratio, velocity and diameter are varied. It is shown that the previously developed viscous finger number works for the new water-wet experiments. However, for oil-wet experiments, the correlating dimensionless number is different. A pseudo-relative permeability model has been developed for oil-wet cores. The core flood experiments have been matched by the new pseudo-relative permeability model. This pseudo-relative permeability model can be used for reservoir simulation of viscous oil waterfloods and polymer floods.

Table of Contents

List of Tables

List of Figures

CHAPTER 1: INTRODUCTION

1.1 MOTIVATION

As conventional resources are being depleted, global energy is shifting toward an unconventional trend. According to Meyer et al. (2007), one of the most important unconventional reserves is the heavy oil consisting of approximately 3.4 trillion barrels of original oil in place (OOIP). Heavy oil is different from light oil due to the property of high viscosity at the reservoir temperature. Viscous oil has been producing through various enhanced oil recovery (EOR) methods, for example, water injection, polymer flooding, in-situ combustion, steam flood and steam-assisted gravity drainage. Steam flood is the most efficient method due to the considerable decrease of oil viscosity, leading to the better displacement in a reservoir.

Although thermal techniques can decrease the viscosity of the oil, it is energy intensive. Water floods or polymer floods are unstable or the viscous fingers occur in immiscible displacement processes such as a waterflood. This is mainly because the displacing fluid usually has a higher mobility than the displaced fluid, thus reducing sweep efficiency and causing early breakthrough of the injected fluid even in homogeneous reservoirs. During reservoir simulation, a classical flow model typically generates optimistic prediction based on relative permeability and capillary pressure concepts due to the lack of viscous fingering effects. This invalidates history matching and production forecast results. For that reason, a fingering model needs to be incorporated in simulations for capturing this phenomenon.

In general, minerals in nature such as silica and limestone are hydrophilic due to their chemical structures and high chemical reactivity with water. However, a large amount of evidence of crude oil's effect on rock wettability indicates that most reservoirs

are at different wettability conditions other than very strong water-wet. However, most studies of unstable immiscible flow have been conducted in a relatively water-wet system. Thus there is a need to conduct both experiments and modeling unstable flow in oil-wet or mixed-wet media. The goal of this study is to understand unstable flow in oil-wet media.

1.2 RESEARCH OBJECTIVES

The objectives of this study are:

1. To identify variables affecting viscous fingerings and their mechanism in an oil-wet system. In this research, the variation of viscosity ratio, displacement velocity, core diameter, and core permeability has been performed in a series of experiments.
2. To obtain a data set of effective-finger model parameters including the maximum fractional area of the finger (a_e), and the exponent affecting shape of the fingers and the bypassed-oil region (β_1 and β_2), and the correlations with scaling groups in an oil-wet system in order to account for fingering in flow simulations.
3. To study the effect of the parameters in scaling groups on the relative permeability in oil-wet sandstones.

1.3 DESCRIPTION OF CHAPTERS

The thesis is organized as follows. The next chapter discusses previous studies of the unstable flow for an immiscible displacement and its issues for reservoir simulation. In chapter 3, the explanation of materials, equipments, and experimental procedures are

presented. Chapter 4 discusses the results and analysis of coreflood experiments. Then, Chapter 5 describes the simulation modeling results including the history matching for all experiments and the analysis of effective-finger model parameters. Finally, the conclusions of thesis and recommendations are summarized in Chapter 6.

CHAPTER 2: LITERATURE REVIEW

2.1 UNSTABLE FLOW IN POROUS MEDIA

2.1.1 Heavy Oil

According to Leimkuhler et al. (2012), unconventional resources can be divided into 3 groups: 1) unconventional reservoirs including source rocks and tight reservoirs; 2) unconventional fluids which consist of heavy oil, natural bitumen, and acid gas; and 3) hydrocarbons that are locked in rocks, for example, oil shale and methane hydrates. Due to the development of production technologies and the increase in exploration cost for new conventional oil basins, heavy oil is becoming one of the main resources to provide supplies around the world. It is defined as the hydrocarbon liquid which has the density equal to or less than 20 ^{o}API gravity and the viscosity greater than 200 cp at reservoir temperature.

Heavy-oil productions typically depend largely on thermal recovery techniques such as steam flooding, cyclic steam stimulation (huff and puff), and steam- assisted gravity drainage (SAGD), etc. These methods significantly decrease the viscosity of hydrocarbon, thus reducing the pressure drop and resulting in the higher oil flow rate. However, there may also be a decrease in the oil relative permeability (k_{ro}) due to an increase in water and gas saturations. Consequently, the rate increase is not in proportion to the oil viscosity that has been reduced. It is also noted that the reduced viscosity is not sufficient to create a favorable flow condition (a unit mobility ratio). As a result, all recovery methods experience instabilities, for instance viscous fingerings and permeability channeling. In this research, we focus on the water (and polymer) injection in heavy oil reservoirs (Figure 2.1).

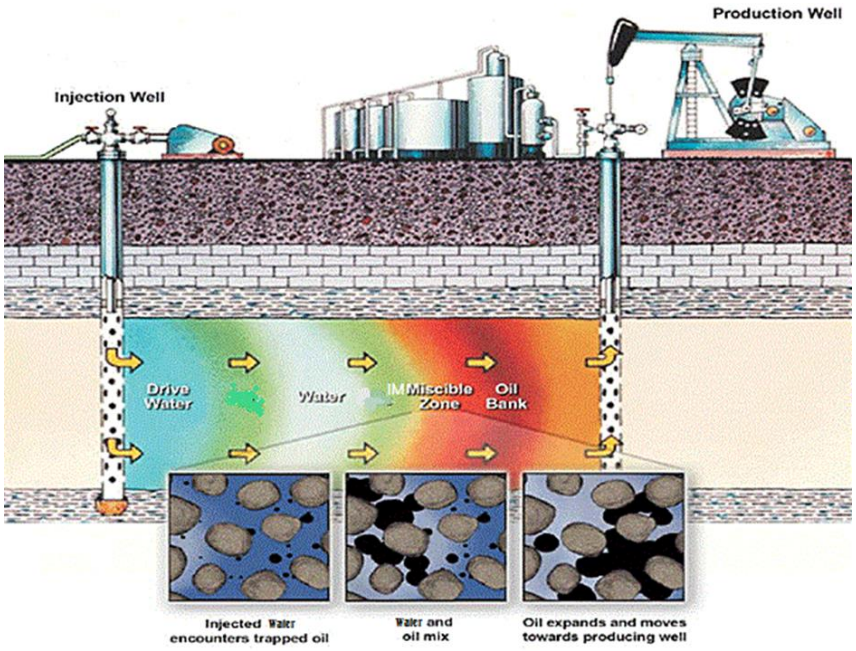

Figure 2.1: Schematic of water injection in an oil reservoir (Patel et al., 2014)

2.1.2 Immiscible Displacement

There are several parameters controlling waterflood recovery. They are divided into two categories. The first group is called 'primary variables', which is directly related to mathematical calculation of oil recovery, for example, initial water saturation, primary recovery efficiency, sweep efficiency, residual oil saturation, and oil shrinkage. Another set of factors called 'secondary variables' are indirectly correlated to the primary variable. For instance, the oil viscosity and the permeability are involved in recovery efficiency and the residual oil saturation or the type of flood will have an effect on sweep efficiency. Callaway (1959) suggests that the waterflood should be initiated at early life of the field before oil shrinkage in the reservoirs since the recovery from the waterflood will be reduced if the reservoirs are already depleted by the solution gas drive.

The method for calculation of oil recovery from a waterflood has been originally established by Buckley and Leverett (1942). A theoretical analysis of the mechanism associated with the displacement of immiscible flood called 'fractional flow equation' is consistent with several experimental results performed by several researchers. The displacing fluid moves from the high saturation zone into the lower saturation zone, thus removing the oil and altering the invaded region into the higher saturation of the displacing fluid. The fractional flow equations for one-dimensional in a two-phase system have been derived from Darcy's equation and material balance analysis. The definition or expression for the fraction of water flowing is as follow.

$$f_w = \frac{1 + \frac{kk_{ro}}{u\mu_o}\left[\frac{\partial P_c}{\partial x} - \Delta\rho g sin \propto\right]}{1 + \frac{k_{ro}\mu_w}{k_{rw}\mu_o}} \tag{2.1}$$

For simplicity, it is often assumed that a reservoir is horizontal (α = 0), incompressible fluids flow in a homogeneous and anisotropic reservoir, and the capillary pressure does not vary much with location ($^{\partial P_c}/_{\partial x} = 0$). Then, the expression reduces to:

$$f_w = \frac{1}{1 + \frac{k_{ro}\mu_w}{k_{rw}\mu_o}} \tag{2.2}$$

The efficiency of the waterflood is controlled by the mobility ratio of the displacing fluid ($^{k_{rw}}/_{\mu_w}$) to the displaced fluid ($^{k_{ro}}/_{\mu_o}$). The lower the ratio of oil viscosity to water viscosity, the better is the displacement efficiency since the oil relatively flows easier. Theoretically, when the oil viscosity is less than or equal to the water viscosity, ideal case for the waterflood process called 'piston-like displacement' can occur. It is the most favorable scenario where the total amount of oil can be reduced to the residual oil saturation in the entire reservoir. However, oil is typically more viscous

than water, causing water to travel faster than oil and leaving oil in by-passed region. As a result, the recovery from an immiscible flood is never complete. This phenomenon is called 'viscous fingerings' and will be discussed in the next section.

Regarding the definition of water fractional flow, the gravity also has an effect on oil recovery in the immiscible process. Due to the difference between fluid densities, gravity forces will contribute to the efficiency in a non-horizontal system. In order to remove such effects, all experiments in this study are conducted in gravity-stabilized conditions where water is injected vertically upward from the bottom and oil is produced from the top of core holder because water is denser than oil.

2.1.3 Viscous Fingering

As stated by Homsy (1987): "Viscous fingering generally refers to the onset of an evolution of instabilities that occur in the displacement of fluids in porous materials". In case of an immiscible displacement, this phenomenon is the formation of patterns typically associated with the variation of fluid properties such as viscosity, density, and interfacial tension at the interface between two fluids. An example of viscous fingerings in the immiscible process (gas-oil system) is shown in Figure 2.2. Regarding the waterflood recovery, oil is displaced by water, which has less viscosity, causing water flow through oil and leaving by-passed oil zone behind. Furthermore, according to the fluid density difference, water is always denser than oil, thus water, when flowing, will segregate by gravity to the bottom of the reservoir, and oil will simultaneously flow upward to the top of the reservoir.

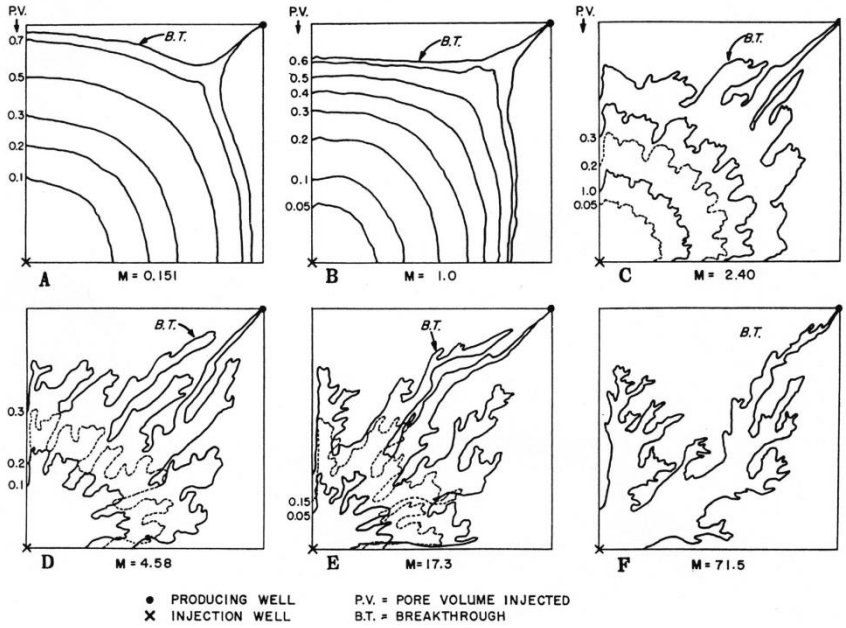

Figure 2.2: Example of unstable immiscible gas-oil displacement for different mobility ratio and the pore volume injected (PV) at the breakthrough in a quarter of five-spot flooding pattern (Green, D. W., & Willhite, G. P., 1998)

The concept can be numerically explained, from Darcy's law in 1-D steady flow in the homogeneous and anisotropic porous medium. Saffman and Taylor (1958) proposed that the instability can occur when 2 fluids flow through the porous medium under gravity and pressure gradient. Considering a stationary coordinate system of oil lies above water with the assumptions that the velocity (V) is uniform and flowing vertically upward, and the interface between oil and water is plane, then the interface is stable if

$$\left(\frac{\mu_2}{k_2}-\frac{\mu_1}{k_1}\right)V+(\rho_2-\rho_1)g>0 \tag{2.3}$$

and unstable if

$$\left(\frac{\mu_2}{k_2}-\frac{\mu_1}{k_1}\right)V+(\rho_2-\rho_1)g<0 \tag{2.4}$$

where μ is the fluid viscosity, k is the permeability, ρ is the density, and the suffix 1 and 2 refer to the upper fluid and the lower fluid, respectively. Since the permeability depends only on porosity and pore size, regarding the tubular porous model, therefore $k_1 = k_2$. Moreover, we know that $\rho_1 < \rho_2$ and $\mu_1 > \mu_2$ because of the fluid properties. In case of oil driving water downward ($V < 0$), the flow is always stable. However, considering the upward flow ($V > 0$), the unstable flow will occur when flow velocity is greater than critical velocity (V_c) as expressed by

$$V > V_c = \frac{(\rho_2 - \rho_1)g}{\left(\frac{\mu_1}{k_1} - \frac{\mu_2}{k_2}\right)} \tag{2.5}$$

On the other hand, if water is placed over oil, then ρ_1 will be higher than ρ_2, and μ_1 will be less than μ_2 resulting in term $\rho_2 - \rho_1 < 0$ and term $\frac{\mu_1}{k_1} - \frac{\mu_2}{k_2} > 0$. This condition makes stable flow impossible.

There also have been many experimental and numerical studies of viscous fingering and its mechanism. Engelberts and Klinkenberg (1951) conducted a series of laboratory experiments in the hydrophilic system and then proposed the term 'viscous fingering'. They concluded that the ultimate recovery of the waterflood was not controlled by displacement parameters but the breakthrough recovery depended on the flow rate and the viscosity ratio. Furthermore, they developed the semi-log relationship between breakthrough recovery and the viscosity ratio at high displacement rates.

Chuoke et al. (1959) presented the relationship of the onset of the macroscopic immiscible instabilities in the uniform porous medium between laboratory results and the predictions. They found that the size of finger depends on the oil viscosity and the interfacial tension. Their experiments also showed that finger widths are larger in the

existence of connate water saturation. This effect may be contributed from the capillary pressure.

According to Hagoort (1974), the numbers of earlier case studies were too few for a general conclusion especially the effect of the capillary force on instability. He demonstrated that the capillary number is proportional to the wavelength of the fingers and if this wavelength is much greater than the system width, the displacement is stable.

Peters and Flock (1981) extended the previous studies by focusing on the relationship between the onset of viscous fingering and the scaling dimensionless number. This was the first attempt to visualize the unstable flow in 3D system. They combined all variables affecting instability into one dimensionless number including viscosity ratio, flow velocity, system dimension and permeability. They also incorporated the wettability number in the scaling group in order to create a unified theory for both water-wet and oil-wet systems.

Peters (1983) studied the relationship between breakthrough recovery and the scaling group (for both linear and radial flows) in cylindrical core. The results showed that recovery data from the model and prototype conform to the radial scaling group which includes displacement rate, water viscosity, core diameter, interfacial tension between the two fluids, porosity, and permeability.

Pavone (1992) developed a molding technique conducted in the porous limestone to examine the two-phase front. This finding shows that the shape of the viscous fingering can be varied depending on flow rate and viscosity ratio. The patterns of flow in the porous medium are also divided into the stable region and the unstable region. The finger width is proportional to the square root of the difference of capillary number. In addition, they also found the linear relationship between relative permeability and fingering factors.

Apart from fluid properties, the heterogeneity also has an effect on the viscous fingering. Even when the fluids have the same viscosity, a non-uniform flow occurs due to the preferential flow in the high permeability layer, leading to an early breakthrough as well. Araktingi and Orr (1993) proposed a computational technique which describes the relation of finger growth and non-uniform permeability system. The shapes of fingers are dependent on a permeability distribution when the distribution has a large variance. In contrast, the finger patterns are similar to those observed in a uniform system if the variation of the permeability distribution is small. Nonetheless, in this research, the scope does not include the unstable fingering in the heterogeneous porous medium.

2.2 WETTABILITY

2.2.1 Definition and Determination

Wettability is described as the tendency of one fluid to spread on a solid surface in the presence of one or more immiscible fluids. The degree of wetting is defined by the equilibrium between repulsive and cohesive forces. The fluid which is preferred to spread than the others is called the wetting fluid. According to Al-Shafei and Okasha (2009), wettability can be either uniform or non-uniform in any system depending on the heterogeneity. In general, water is the first fluid to occupy pore throats in reservoirs and most minerals typically have high energy surfaces, resulting in water-wet reservoirs. However, the crude oil that migrates into the reservoirs later can contain components which affect wetting surfaces, thus altering the wettability. In most cases, water or oil is the wetting phase while gas is always a non-wetting phase. The wetting fluid generally occupies the smaller pore throats while the nonwetting fluid occupies the bigger one. This

phenomenon definitely has an impact on the fluid flow in porous medium and the efficiency in oil recovery process.

Although the wettability is one of the key variables in oil recovery, it is very challenging to quantify. Several methods to measure the wettability have been proposed. According to Buckley (1996), the contact angle measurement and spontaneous liquid imbibitions are the most common methods. At equilibrium, the interfacial tensions are related by Young's Equation:

$$\gamma_{bs} - \gamma_{as} = \gamma_{ab} cos\theta \tag{2.6}$$

where γ_{bs} is the interfacial tension between fluid b and solid, γ_{as} is the interfacial tension between fluid 'a' and solid, γ_{ab} is the interfacial tension between 2 fluids, and θ is the contact angle and measured through the more dense fluid (fluid a in this case). In an oil-water system, fluid 'a' is water and fluid 'b' is oil. If θ is less than 90^o, the solid is said to be water-wet. On the other hand, the solid is preferentially oil-wet if θ is greater than 90^o. However, the solid can be in a neutral situation or the intermediate wettability if the contact angle is approximately 90^o. The illustration of contact angle and interfacial tensions are shown in Figure 2.3. This method provides reliable results; however, there are some disadvantages. For instance, this method requires a flat and homogeneous surface while there is no smooth surface in reservoirs, and this technique also needs a long time to complete.

In spontaneous imbibition measurements, a core initially saturated with oil at the connate water saturation is immersed in water, the amount of spontaneous water imbibition is measured. Capillary pressure is the main driving force in this method (Morrow et al., 1994). The wetting fluid tends to imbibe into the smaller pore space. The rate of increase in wetting fluid saturation depends on the interfacial tension, viscosity of fluid, core geometry, and core surface condition.

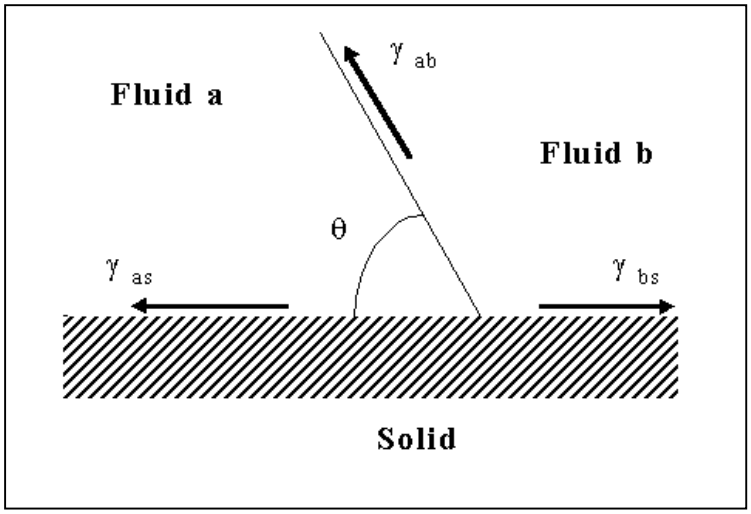

Figure 2.3: Interfacial tensions between fluid a, fluid b, and solid system. (Martys and Ferraris, 1997)

Other methods used to characterize wettability include Amott test and United States Bureau of Mines (USBM) test. Amott wettability test takes the concept of imbibition displacement and the forced displacement into account. The volume of fluid displaced is used to calculate the wettability index of water (I_w) and oil (I_o). The difference between these indices is called Amott wettability index as expressed by:

$$Amott\ Index = I_w - I_o \tag{2.7}$$

Amott index ranges from -1 to 1. When the value is close to 1, rock is indicated as a strongly water-wet rock whereas an index of -1 indicates a strongly oil-wet rock. According to Buckley (1996), these indices can be influenced from various factors consisting of the time interval of spontaneous imbibitions, the initial saturation during primary drainage, and the techniques that are used for forced displacements, thus resulting in biased results.

In 1969, Donaldson proposed the USBM wettability index. This method is based on the relationship between the areas under capillary pressure curves obtained by displacements using a centrifuge. The curves are dependent on the wettability and the pore size distribution. As shown in Figure 2.4, the secondary drainage (area A_1) and forced imbibitions data (area A_2) are measured. The USBM index is calculated as:

$$USBM\ Index = log_{10}\left(\frac{A_1}{A_2}\right) \tag{2.7}$$

Similar to Amott index, the positive values point toward a water-wet system while the negative values indicate oil-wet system.

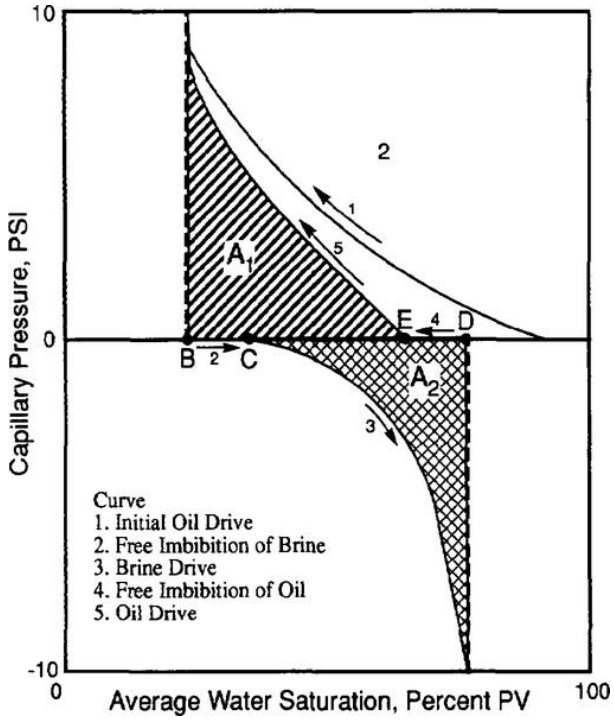

Figure 2.4: Determination of USBM wettability index. "AAPG Wiki". Web. Retrieved 11 Nov 2014.

2.2.2 Effect of Wettability

The wettability significantly affects multiphase flow and rock-fluid interactions including relative permeability, fluid distribution in pore throats, capillary pressure and residual oil saturation, thus controlling the efficiency of the immiscible displacement.

One of the profound effects of wettability is a relative permeability. Owens and Archer (1971) determined that the wetting preference reduces the relative permeability of the wetting phase at a given saturation. For example, the relative permeability to water is low and the relative permeability to oil is high for a water-wet rock compared to an oil-wet rock at any given saturation (Figure 2.5). This is because during the immiscible flood, the wetting fluid tends to attach to the rock surface more than the nonwetting fluid.

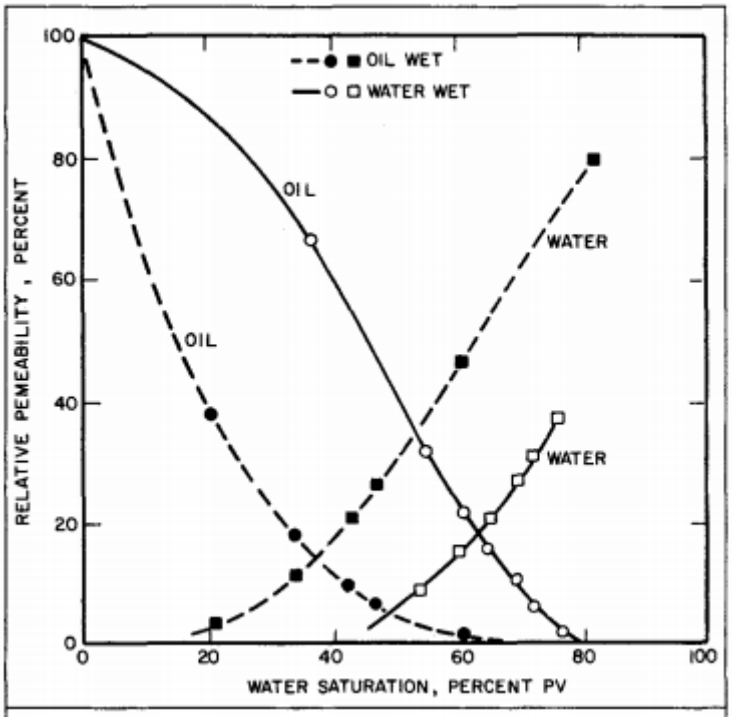

Figure 2.5: Oil-water relative permeability measured with heptane and brine in a water-wet and oil-wet core. (Anderson, 1987)

Anderson (1987) concluded that the wettability controls the waterflood performance by its impact on the flow and spatial distribution of fluids in the porous medium. During the waterflood in water-wet rocks, the injected water tends to imbibe into small to medium pore sizes and oil has a tendency to move to the larger pores. As a result, oil is relatively easily displaced in a water-wet system compared to an oil-wet system, leading to a higher recovery in a water-wet system at similar conditions. Figure 2.6 shows the results of waterflood efficiency for different contact angles.

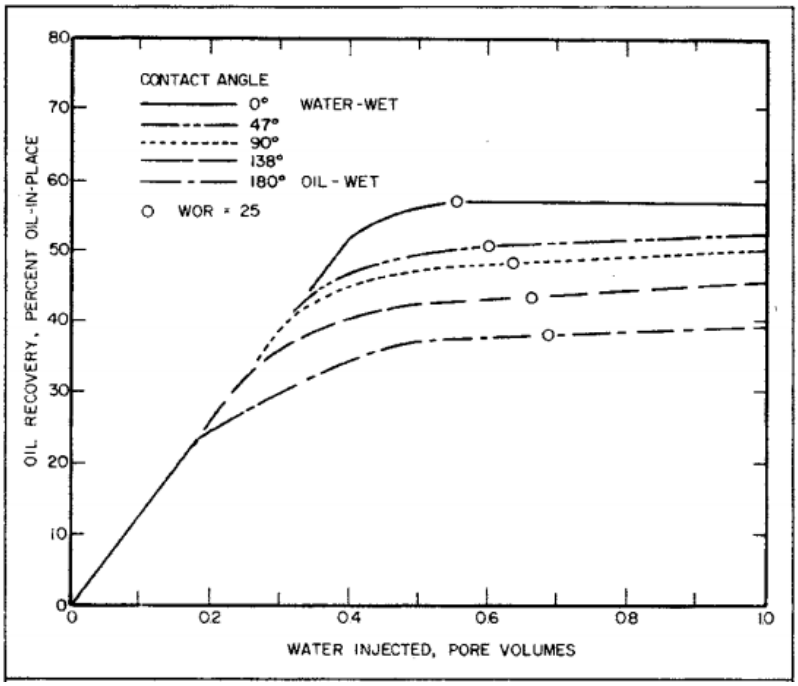

Figure 2.6: Effect of the wettability on waterflood performance calculations, 20-acre five-spot pattern at viscosity ratio of 5 (Owen and Archer, 1971)

The residual oil saturation (ROS) also has been investigated by many researchers. The relation between the ROS and the wettability can be explained by the capillary force which dominates the trapped residual oil. Lorenz et al. (1974) varied the wettability and

measured the average ROS of the sandstone with brine and crude oil (Figure 2.7). The curve reaches the minimum close to a slightly oil-wet condition. This result is consistent with Morrow (1990) that highest displacement recovery can be achieved in a mixed-wet system where surfaces of the larger pores become strongly oil-wet whereas surfaces if the smaller pores remain water-wet. The oil flow occurs in film drainage over the strongly oil-wet surfaces and there is less oil saturation in smaller pores, resulting in the lowest ROS value. This finding inspires the concept of wettability alteration to reduce ROS as low as possible.

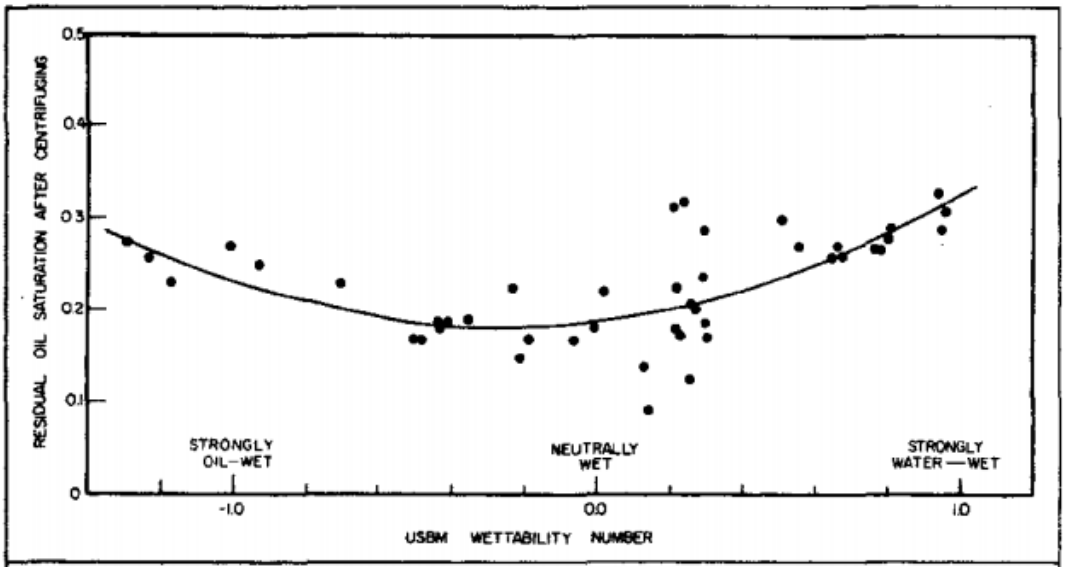

Figure 2.7: Average ROS after centrifuging and USBM wettability index curve in Torpedo sandstone core (Lorenz et al, 1974)

2.3 FINGERING MODEL

The viscous fingering is a major issue in the modeling of heavy oil reservoirs. As the width of the fingers is usually small, very fine grid blocks are required to capture such

phenomenon. However, fine grid blocks cause other problems, for instance, the simulations become computationally expensive and high resolution data is not available (Doorwar and Mohanty, 2015). As a consequence, this method is not practical in field scale reservoir simulations.

Several approaches have been developed in order to take into account the instability. For miscible displacements, Koval (1963) proposed an empirical model predicting the efficiency of an unstable flow through the use of heterogeneity factor and viscosity ratio which is called 'K-factor method'. This technique assumes that the solvent fractional flow behavior is similar to immiscible displacements. Todd and Longstaff (1972) discussed a similar model; however, they applied a mixing rule to calculate an effective viscosity.

According to Fayers (1988), an upscaling model for the miscible flooding called 'fingering function' has been proposed (Figure 2.8). This model suggests that displacing fluid forms fingers which spread linearly through the mixing zone between oil and solvent.

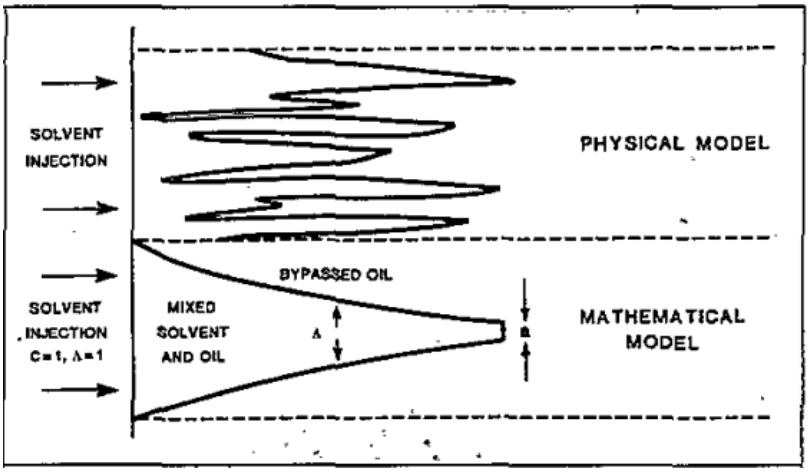

Figure 2.8: Schematic of conceptual model for fingering function (Fayers, 1988)

Fayers and Newley (1988) proposed a model for the effective width of fingers as:

$$\lambda = a + bC_f^{\alpha} \tag{2.8}$$

where λ is the average finger width, a is the initial fractional width of finger, a+b is the final fraction width of finger cross-section when C_f approaches 1, C_f is the normalized concentration of the solvent, and α is the exponent rate for finger growth. This model also captures the heterogeneity of the simulation grid-block through parameter b by assumption of $a + b < 1$ if reservoir is heterogeneous, and $a + b = 1$ if reservoir is completely swept in the homogeneous permeability conditions.

Doorwar and Mohanty (2015) applied the previous theory and developed a "lumped finger model" for immiscible displacements as shown in Figure 2.9. In this case, all fingers are merged into one equivalent finger and there is a region where oil is always trapped called "isolated zone". Parameter C_f become C which is the normalized water saturation instead. Two-phase flow occurs only within the finger whereas single-phase flow of oil can occur in some areas of the unswept zone.

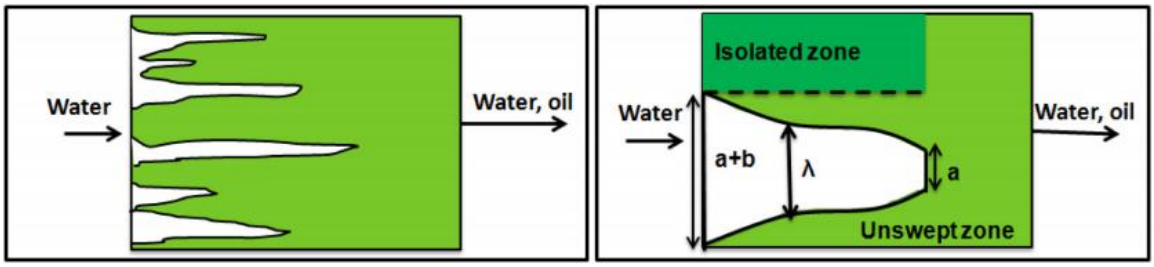

Figure 2.9: (left) Schematic of viscous fingering for the water-oil system; (right) an equivalent averaged finger width of multiple sub-grid fingers (Doorwar and Mohanty, 2015)

They also implemented a pseudo-relative permeability function into the reservoir simulator. Based on a series of experimental and history matching results in a water-wet

rock, they found that this function depends on a dimensionless number which is a product of the capillary number and viscosity ratio to a power of 2 ($N_c\mu_r^2$). Moreover, the model parameters a, b, and the shape exponent (β) also have a correlation with $N_c\mu_r^2$.

Luo et al (2016) proposed an improved effective-finger model since there are some limitations to the lumped model consisting of the discontinuity of finger width at zero water saturation and very large value of exponent β, which makes an unrealistic mathematical logic. As shown in Figure 2.10, all fingers are also combined into one corresponding finger. Nonetheless, the finger fraction is zero at the front of the finger. In terms of regional compartmentalization, there are similar three zones during displacement and no oil single-phase flow at the final state.

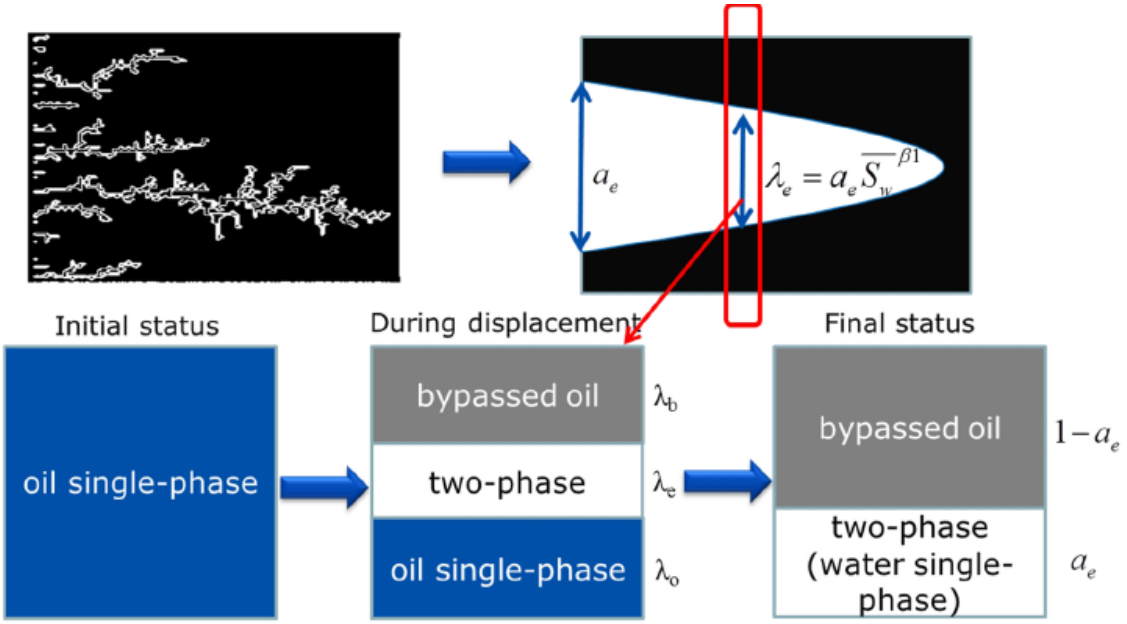

Figure 2.10: Schematic of effective-finger model (Luo et al., 2016)

The fractional finger width (λ_e) and the fractional cross-section of bypassed oil region (λ_b) are expressed by:

$$\lambda_e = a_e \bar{S}_w^{\beta 1} \tag{2.9}$$

$$\lambda_b = (1 - a_e)\bar{S}_w^{\beta 2} \tag{2.10}$$

where a_e is the maximum cross-section of finger, β_1 is the finger growth exponent of two phase region, λ_b is the fractional cross-section of bypassed oil region, and β_2 is the growth rate exponent of λ_b. However, in this case, the domain of normalized water saturation ($\bar{S}_w$) ranges from the initial water saturation to the water saturation corresponding to the effective remaining oil saturation (1-S_{orem}). This is different from the waterflood residual oil saturation (S_{or}) which is the intrinsic property of the rock because S_{orem} also depends on parameter a_e. These parameters alter the relative permeability curves for both water and oil, which represent viscous fingerings flow.

The model parameters in this technique such as a_e and β_1 also show the power-law correlation with the dimensionless scaling group. This method benefits the reservoir simulation by capturing the effect of viscous fingering and providing more accurate predictions without the use of very fine grid simulations.

CHAPTER 3: EXPERIMENTAL PROCEDURES

3.1 PLANNING

A series of experiments is designed to study the effect of parameters including viscosity ratio, injection rate, core diameter, and core permeability on viscous fingering in both water-wet and oil-wet rocks. This is because we want to evaluate the effect of several variables in the viscous finger scaling group (N_c, μ_r, D, k). The fingers will influence oil recovery and pressure drop in each case. The details of coreflood experiments are listed in Table 3.1 and 3.2 for oil-wet and water-wet systems, respectively. The injection velocity shown in these tables is the interstitial velocity $\left(V = \frac{Q}{A\emptyset}\right)$, not the Darcy's velocity.

Experiment No.	Core diameter (inches)	Oil viscosity (cp)	Water viscosity (cp)	Viscosity ratio	Interstitial velocity (ft/day)
1	2	60	60	1	1
2	2	60	1	60	1
3	2	1800	60	30	1
4	2	1800	30	60	1
5	2	1800	14	128.6	1
6	2	1800	5.5	327.3	1
7	2	1800	1	1800	1
8	2	1800	1	1800	0.2
9	2	1800	1	1800	0.05
10	4	60	60	1	1
11	4	60	1	60	1
12	4	1800	1	1800	1

Table 3.1: List of coreflood experiments in oil-wet system

Experiment No.	Core diameter (inches)	Oil viscosity (cp)	Water viscosity (cp)	Viscosity ratio	Interstitial velocity (ft/day)
13	4	60	60	1	1
14	4	60	1	60	1
15	4	1800	1	1800	1

Table 3.2: List of coreflood experiments in water-wet system

3.2 MATERIALS

3.2.1 Formation and Injection Brine

In all the cases, both the formation and injection brines have the same salinity of 0.5 wt% Sodium Chloride (NaCl). In some cases, the viscosity of the water phase is increased by adding glycerol. This is because glycerol and water are completely miscible and the solution is a Newtonian fluid which means a constant viscosity during flow. High purity glycerol (>99.5%) was combined with pure water using the viscosity guideline shown in Table 3.3. However, there are various sources of viscosity table due to different types of the viscometers. Therefore, the volume adjustment of water and glycerol was required after measuring viscosity by AR-G2 rheometer at the room temperature. Finally, we obtained brine solution for injected fluid for each case (5.5, 14, 30, and 60 cp).

VISCOSITY OF AQUEOUS GLYCEROL SOLUTIONS IN CENTIPOISES										
GLYCEROL % wt	TEMPERATURE (°C)									
	0	10	20	30	40	50	60	70	80	90
0	1.7	1.308	1.005	0.8007	0.6560	0.5494	0.4688	0.4061	0.3565	0.316
10	2.4	1.74	1.31	1.03	0.826	0.680	0.575	0.500	-	-
20	3.4	2.41	1.76	1.35	1.07	0.879	0.731	0.635	-	-
30	5.1	3.49	2.50	1.87	1.46	1.16	0.956	0.816	0.690	-
40	8.2	5.37	3.72	2.72	2.07	1.62	1.30	1.09	0.918	0.763
50	14.6	9.01	6.00	4.21	3.10	2.37	1.86	1.53	1.25	1.05
60	29.9	17.4	10.8	7.19	5.08	3.76	2.85	2.29	1.84	1.52
65	45.7	25.3	15.2	9.85	6.80	4.89	3.66	2.91	2.28	1.86
67	55.5	29.9	17.7	11.3	7.73	5.50	4.09	3.23	2.50	2.03
70	76	38.8	22.5	14.1	9.40	6.61	4.86	3.78	2.90	2.34
75	132	65.2	35.5	21.2	13.6	9.25	6.61	5.01	3.80	3.00
80	255	116	60.1	33.9	20.8	13.6	9.42	6.94	5.13	4.03
85	540	223	109	58	33.5	21.2	14.2	10.0	7.28	5.52
90	1310	498	219	109	60.0	35.5	22.5	15.5	11.0	7.93
91	1590	592	259	127	68.1	39.8	25.1	17.1	11.9	8.62
92	1950	729	310	147	78.3	44.8	28.0	19.0	13.1	9.46
93	2400	860	367	172	89	51.5	31.6	21.2	14.4	10.3
94	2930	1040	437	202	105	58.4	35.4	23.6	15.8	11.2
95	3690	1270	523	237	121	67.0	39.9	26.4	17.5	12.4
96	4600	1580	624	281	142	77.8	45.4	29.7	19.6	13.6
97	5770	1950	765	340	166	88.9	51.9	33.6	21.9	15.1
98	7370	2460	939	409	196	104	59.8	38.5	24.8	17.0
99	9420	3090	1150	500	235	122	69.1	43.6	27.8	19.0
100	12070	3900	1410	612	284	142	81.3	50.6	31.9	21.3

Table 3.3: Aqueous glycerol viscosity solutions. IPS Engineering. Retrieved 24 February 2016 from URL http://www.ips-engineering.it/pulp-paper/105-data-book/189-viscosity-of-glycerol-water-solutions

3.2.2 Oil

Two types of mineral oils are used in these experiments. The measured viscosities at room temperature are approximately 60 cp and 1800 cp. Initially, we had planned to use mineral oils diluted by Cyclohexane for different viscosity ratios. Although it can decrease viscosity of the mineral oils, we observed that evaporation of Cyclohexane in the produced volume was significant. Thus, the viscosity ratio was mainly altered by the viscosity of the injection brine.

3.2.3 Core Samples

All coreflood experiments were conducted using Boise sandstones which are outcrop cores. Cores initially were in relatively water-wet system due to their mineral compositions. Two sizes of cores were selected (2-inch and 4-inch in diameter) and both were 1-foot long. Absolute brine permeability was measured in all the cores. Permeabilities are greater than 1 Darcy, which is typical for Boise sandstones. A summary of core properties is listed in Table 3.4.

Core diameter (inches)	Pore Volume (cm^3)	Porosity (%)	Permeability (Darcy)	Length (ft)
2	178.78	30.22	4.02	1
4	695.75	28.15	2.17	1

Table 3.4: Summary of core properties

3.2.4 Other Chemicals

In oil-wet protocol, sandstone cores are treated with two types of silane chemicals: Dichlorodiphenylsilane and Chlorotrimethylsilane. These Chlorosilanes are very toxic and corrosive. They also react with water, generating white substances that can block pore space if the reaction occurs inside the cores. Therefore, the cores were completed dried before treatment with silanes.

Silanes were combined with Hexane and then injected into core. Hexane was also used to check the wettability at core surface. Other solvents related to this study included Toluene and Acetone. They were mainly used to clean the cores after oil-wet process and all coreflood experiments.

3.3 EQUIPMENT

3.3.1 Core Holder

Core holders used in all coreflood experiments were the Hassler Type core holders. With the sleeve provided in core holders, radial pressure was applied to the core samples after injecting water into confining pressure port. This overburden pressure was maintained at 1000 psi for all experiments in order to provide seal and prevent flow along the outer surface of core samples. Stainless steel core holder and Aluminum core holder were selected for experiments of 2-inch diameter core and 4-inch diameter core, respectively (Figure 3.1). Core holders were mounted vertically and kept at the room temperature.

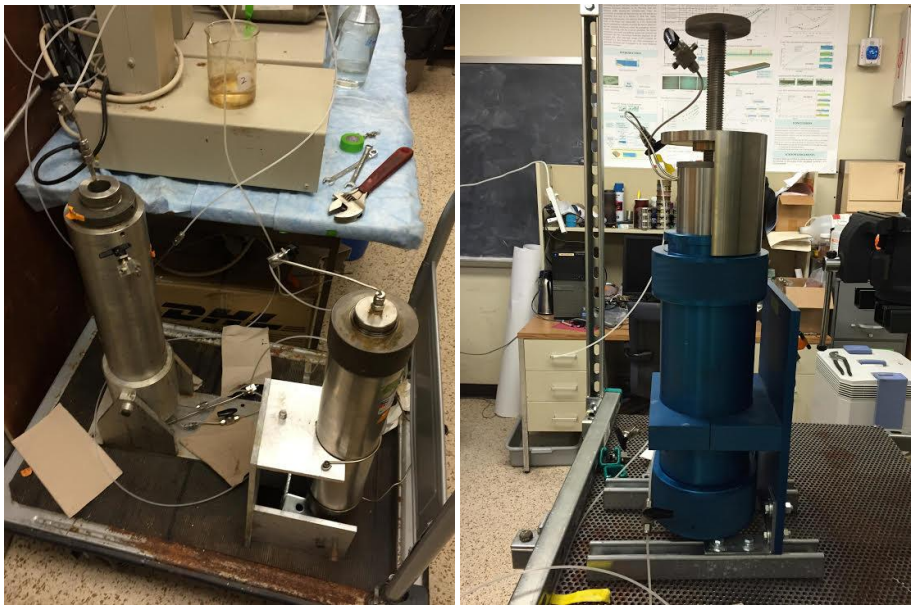

Figure 3.1: (left) Stainless steel core holder for 2-inch core experiments (on the left); (right) Aluminum core holder for 4-inch core experiments

3.3.2 Pump

500D syringe pumps from Teledyne Isco were used to inject fluid during the experiment. The pump volume capacity is approximately 500 ml with the maximum pressure limit of 3750 psi. Brine was filled into the pump and directly injected into the core during the waterflood experiments. However, in other processes such as oil saturation or oil-wet core procedure, brine was pumped into a stainless steel accumulator, which contained oil or solvent inside to prevent corrosion in the pump. In this study, only constant flow rate injection was operated.

3.3.3 Accumulators

There were two types of accumulators involved in these experiments which consisted of a stainless steel accumulator and a glass accumulator. The stainless steel accumulator was a cylinder with a piston inside, containing mineral oil, hexane, and other solvents. The piston separated two fluids in the accumulator which was also mounted vertically. The injected fluid was in the top section of the piston while brine was injected to the bottom part, displacing the top fluid into the core holder. The volume capacity is approximately 1000 ml.

The glass accumulator was used during the cleaning process. There was no piston within this type of accumulator and the operating pressure limit is very low. Injected fluid was filled into the accumulator using vacuum pump which connected to the top part. Then, instead of brine, low pressure air was injected into the top part, pushing liquid to flow through the bottom part of the accumulator into the core holder. The maximum volume for this glass accumulator was about 500 ml.

3.3.4 Pressure Transducer

A pressure transducer was used to record pressure drop between inlet and outlet of the core holder during the waterflood experiments. It converted the pressure drop reading into the voltage signal. This data was sent to a computer and stored in a digital format. Before recording data, a pressure-voltage calibration curve is required to set the scale factor and the offset for the voltage data. This curve was also used to convert the voltage data back into pressure drop.

3.3.5 Fraction Collector

The effluent samples from coreflood experiments were collected using Retriever 500 fraction collector from Teledyne ISCO. Plastic tubes were filled in the racks to collect fluid from the outlet of the core holder. Time interval for each tube was calculated from the injection rate and required the volume for each experiment.

3.3.6 Rheometer

Rheometer was not involved during the coreflood process but it was important for the fluid preparation. All viscosity measurements were taken using AR-G2 rheometer from TA instruments. This rheometer is a combined motor and transducer tool where the lower part (a Peltier plate) is immobile while the upper part (a cone) is connected to the shaft and can rotate. A small volume of fluid sample was dropped onto the Peltier plate, and then the rotational cone was moved toward fluid in order to set the reference position. In all cases, the viscosity was measured over the shear range of 0.1 to 10 sec^{-1} at the temperature of 25^{o}C. Both oil and brine results show Newtonian characteristic (viscosity independent of shear rate).

3.4 METHODOLOGY

3.4.1 Equipment Setup

The schematic of an equipment setup for coreflood experiments is presented in Figure 3.2. An outlet line from pump was connected to the first 3-way union which brine can flow to a stainless steel accumulator and a core holder. However, there was a 2-way valve located between the first and the second 3-way union. This valve was closed during oil saturation or other processes that required an accumulator. In order to record pressure during the waterflood process, a brine line was connected to a pressure transducer through the second 3-way union. A 3-way valve controlled the fluid line before flowing into the core holder. Finally, the outlet of the core holder was connected to the fraction collector for sample collection.

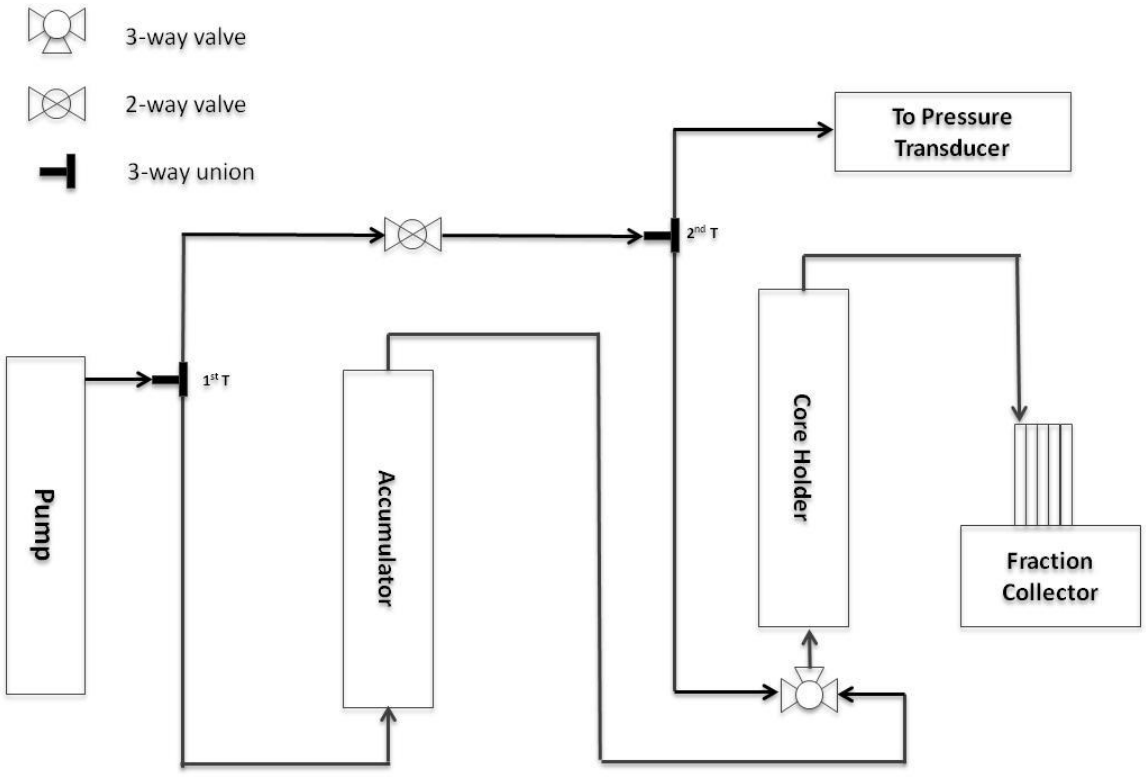

Figure 3.2: A schematic of equipment setup for coreflood experiments.

3.4.2 Oil-Wet Treatment Procedure

The organosilane compounds such as Dichlorodiphenylsilane and Chlorotrimethylsilane consist of silicon molecules with chlorines and hydrophobic organic groups were the main chemicals for the oil-wet core treatment. The general formula of this type of silane is R_nSiCl_{4-n} where R is typically methyl or phenyl and n is equal to 0, 1, 2, or 3. After the reaction with the hydroxyl group (OH) on silicon dioxide surfaces of sandstones, the organic groups were exposed on the surface, thus generating non-hydrophilic wettability.

The following method was followed to generate a completely oil-wet surface at Boise sandstone cores for both 2-inch and 4-inch core diameters in this research. Firstly, the cores were dried in the oven at temperature 120^{o}C for 24 hours. After the cores were cooled down at the room temperature, cores were put into the core holder and connected to a vacuum pump in order to remove any fluid inside dry cores. The cores were then displaced by approximately 2 PV of a 7% solution of Dichlorodiphenylsilane in hexane. Then, nearly 2 PV of hexane was injected into the core holder. The next process was displacing a 7% solution of Chlorotrimethylsilane in hexane for about 2 PV. Then, 5 PV of hexane was pumped into the cores in order to remove free silanes as much as possible. Finally, the cores were cleaned by Toluene and Acetone. The fluid waste after cleaning with Toluene and Acetone had green color. These solvents were continuously injected until the waste color become clear same as the solvents. All wastes were collected in the fume hood and the injected solvents were stored in the stainless steel accumulator. During this process, the pressure drop was frequently checked because if there was any water and silane chemical reaction, it can plug the cores and increase the pressure drop. After oil-wet core treatment process, the cores were placed in the oven for 24 hours. It

was assumed that the pore structure of the core such as pore-size distribution and connectivity was not changed after the process.

To determine the wettability of the surface, hexane and water droplets were placed on the surface of the dry core. Originally, both hexane and water were instantly imbibed into the dry core (water-wet core) because dry pore spaces contained gas which was the most non-wetting fluid. After oil-wet treatment, as shown in Figure 3.3, hexane drop instantly imbibed into the core after it contacted the core surface. On the other hand, water drop could not imbibe into the dry core. These results suggest that the wettability of the core is strongly oil-wet.

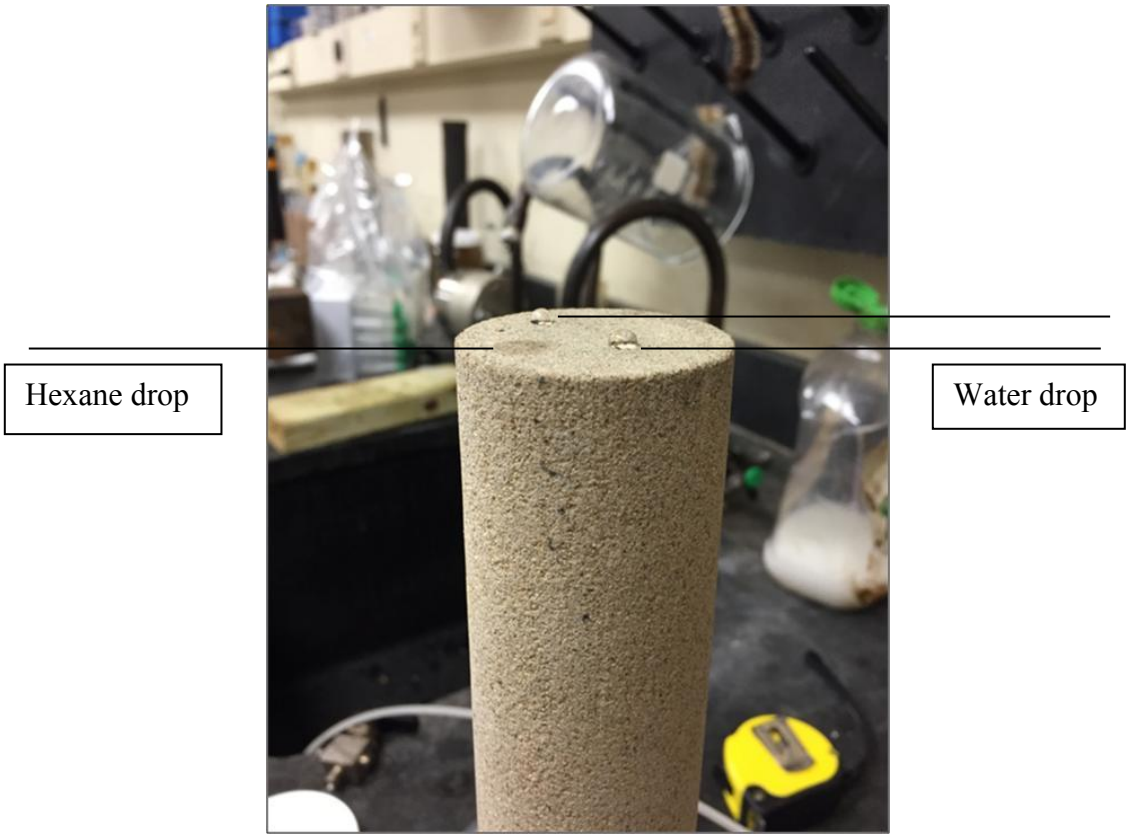

Figure 3.3: Wettability test results on oil-wet 2-inch diameter core.

3.4.3 Coreflood Procedure

Core Property Measurement

Although both 2-inch and 4-inch diameter experiments were conducted in different core holders, most processes were the same. At first, the cores were dried in the oven for 24 hours. After cooling to the room temperature, the dry weight and core geometry were measured. The cores were then wrapped with a plastic layer and applied with the heat to fit with the core size, and loaded into core holder inside the rubber sleeve. After placing the core inside the core holder, the brine was injected into the confining pressure port in order to provide an overburden pressure of 1000 psi. After a few hours, a pressure drop was checked to test the leak of the core holder. Before injection of any fluid into dry cores, the cores were vacuumed using a vacuum pump to remove air.

A porosity of cores in this study was calculated from a pore volume data. The pore volume was obtained from the injected volume of fluid into the dry vacuumed cores. The injected volume can be read from the pump. The porosity of the core then were calculated from the following equation.

$$\emptyset = \frac{PV}{BV} \tag{3.1}$$

where PV is pore volume and BV is bulk volume calculated from a core geometry.

Absolute brine permeability was a permeability measured at 100% water saturation. After cores were saturated with brine, pressure drop across core samples was recorded at different constant brine flow rates. Permeability values were then calculated using Darcy's law by plotting pressure drop versus injection rate. The equation is expressed as:

$$Q = -\frac{kA\Delta P}{\mu L} \tag{3.2}$$

where Q is volume flow rate (cm^3/sec), k is the brine permeability (Darcy) , A is the core surface area (cm^2), ΔP is the pressure drop across the core (atm), μ is the brine viscosity (cp), and L is the length of the core (cm).

Single phase tracer tests were also performed in order to check the homogeneity of core samples. The resident brine was displaced by different salt concentration brines. The effluent salinity was analyzed using a refractometer. The normalized salinity values were plotted against the injected pore volume. In both cores, the results show smooth S-shave curves with the normalized concentration of 0.5 at approximately 1 injected pore volume (Figure 3.4 and Figure 3.5). This implied that the cores were quite uniform.

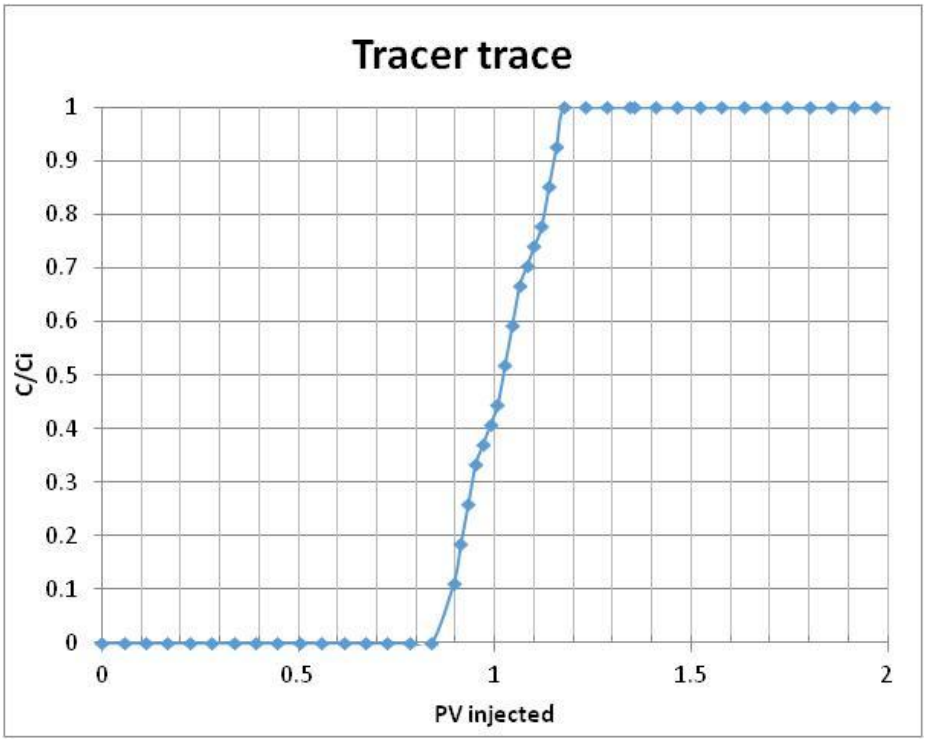

Figure 3.4: Tracer trace results for 2-inch diameter core

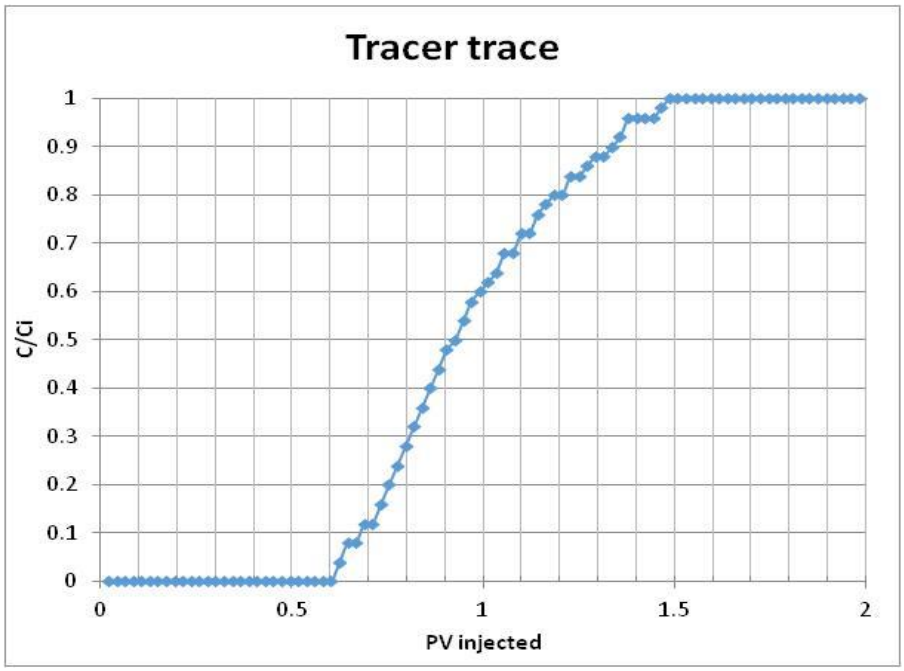

Figure 3.5: Tracer trace results for 4-inch diameter core

Oil Saturation

Oil was injected into the cores using a stainless steel accumulator. In case of oil-wet core experiments, the cores were initially saturated with 100% oil. For the first experiment, oil was injected into the dry vacuumed cores from the bottom of core holders at the constant injection pressure of 200 psi. After the cleaning core process, the cores were saturated with toluene which is completely miscible with the mineral oil. The cores were then saturated with oil at the constant pressure until the viscosity of oil from the outlet reach the value of pure mineral oil.

For water-wet core experiments, the cores were initially saturated with brine. Then, mineral oil was injected into core samples from the top which was a gravity stable displacement. The injection pressure was kept constant at 200 psi. Oil injection continued until there was no water produced from the cores. Initial oil saturation and water saturation were calculated from the collected brine volume after oil saturation process.

Waterflood

Before brine injection of each experiment, the cores were displaced with oil at the designed constant flow rate from the bottom of the core holder until the pressure drop reached a stable point. This data was used to estimate the oil relative permeability at zero water saturation for the oil-wet or the connate water saturation for the water-wet experiments, respectively.

After getting a steady pressure drop, brine was injected directly from the pump into the bottom part of the core holder at the desired constant rate. This process continued for approximately 2 PV of injected brine in most cases. The effluents were collected at the outlet of the cores (top part of the core holder). The fractional flow data was measured from the fluid fraction in each tube and the pressure drop data was recorded by a pressure transducer. This information was used in the data analysis section.

Core Cleaning

The reason to clean core was to remove all liquids from the core in order to measure porosity, fluid saturation, and permeability and to prepare the core for the following coreflood experiments. One issue of core cleaning is that it is difficult to remove all of the adsorbed liquids. This can affect the wettability and coreflood analysis. In an effort to effectively clean cores, a combination of toluene and acetone was used. Toluene is effective in removing hydrophobic compounds while acetone removes the hydrophilic compounds.

CHAPTER 4: COREFLOOD RESULTS AND ANALYSIS

4.1 OIL-WET RESULTS

4.1.1 2-Inch Core

Oil-wet unstable displacement experiments were conducted first in a 2-inch Boise sandstones core. Two main variables were studied: the viscosity ratio (VR $= \mu_o/\mu_w$) and the injection rate. Table 3.1 lists the operating conditions for these experiments. The viscosity ratio is varied in Experiments 1-7. The cumulative recovery results are shown in Figure 4.1. As expected, as the viscosity ratio increases, the breakthrough decreases. A higher viscosity ratio also led to a lower cumulative recovery.

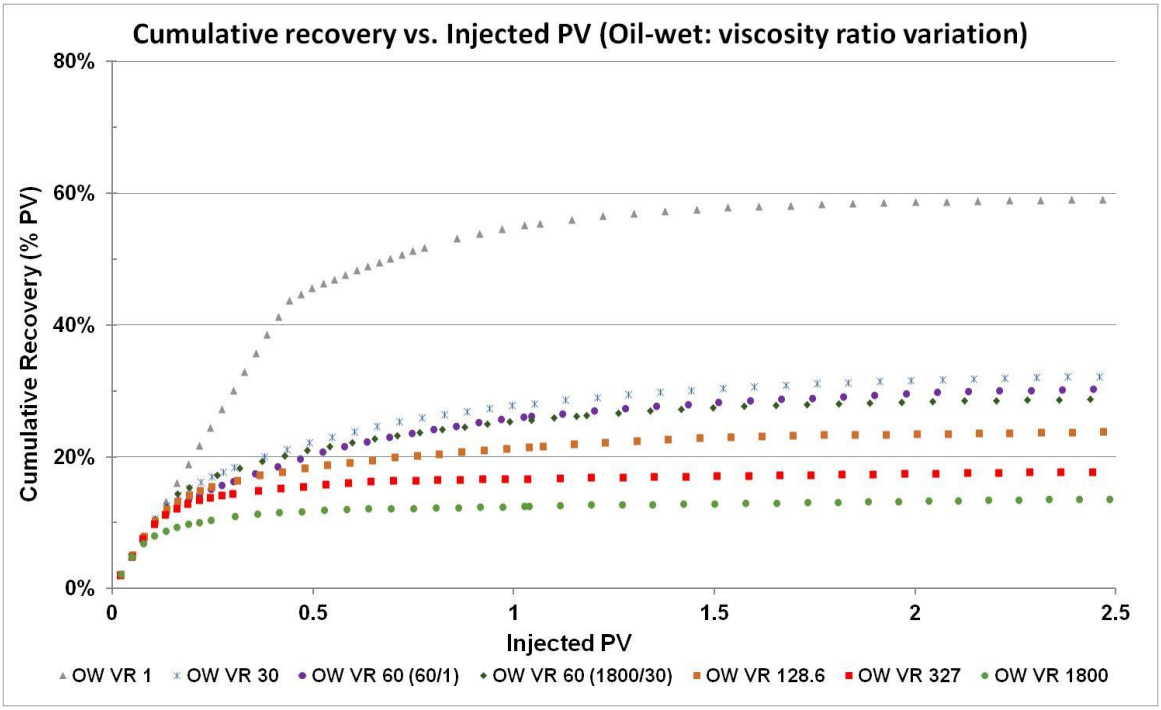

Figure 4.1: Effect of the viscosity ratio on the cumulative recovery (%PV) in the 2-inch core (oil-wet experiments)

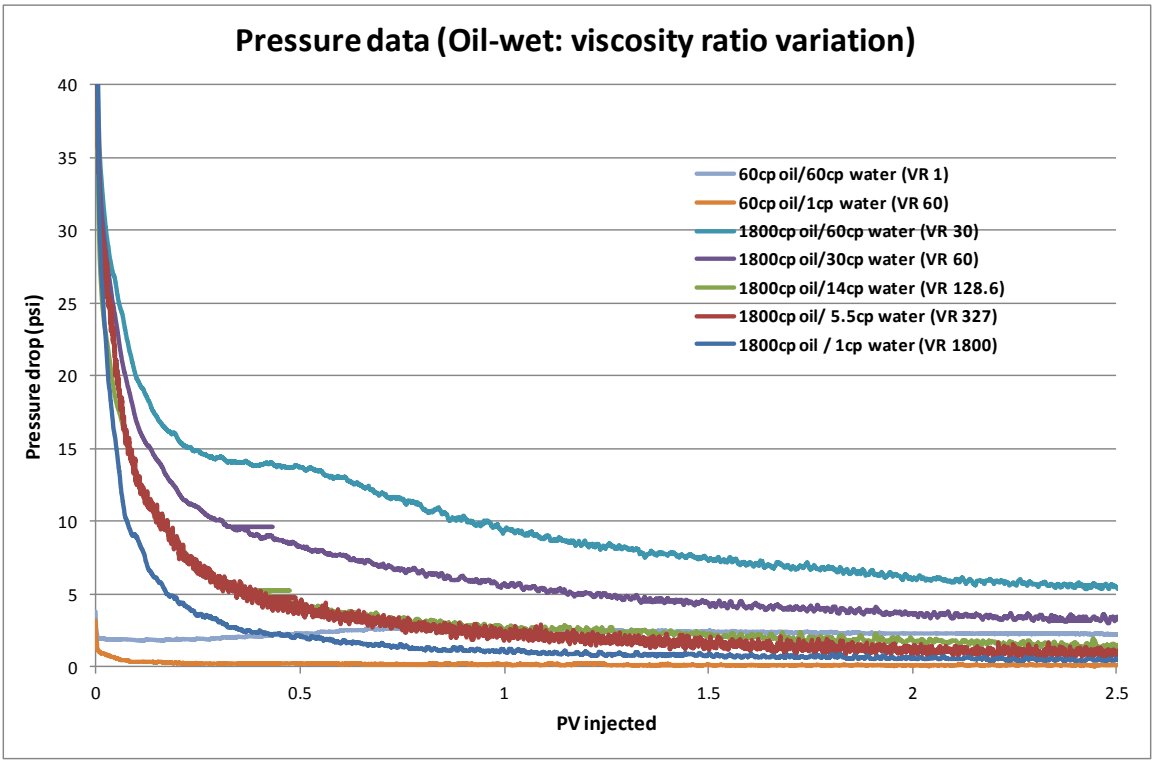

Figure 4.2: Effect of the viscosity ratio on the pressure drop (%PV) in the 2-inch core (oil-wet experiments)

In Experiments 7-9 of Table 3.1, the injection rate was varied, the viscosity ratio was kept constant at 1800. The cumulative recovery results are illustrated in Figure 4.3. As the injection rate increases, the oil recovery increases in the oil-wet rock. This trend is the opposite of that seen in the water-wet system in previous studies (Doorwar, 2015). According to Figure 4.4, the lower injection rate causes higher recovery in water-wet system because water can imbibe into smaller pore spaces and displace more oil as the flow time increases for a given pore volume. In contrast, the lower flow rate resulted in the lower oil recovery and the earlier breakthrough recovery in the oil-wet system. This is because water naturally does not imbibe into smaller pore spaces in strongly oil-wet rock surfaces. The lower flow rate contributes to less pressure drop, as can be seen in Figure

4.5, due to Darcy's flow equation ($v \propto \Delta P$), which leads to less capillary pressure resulting in less oil recovery.

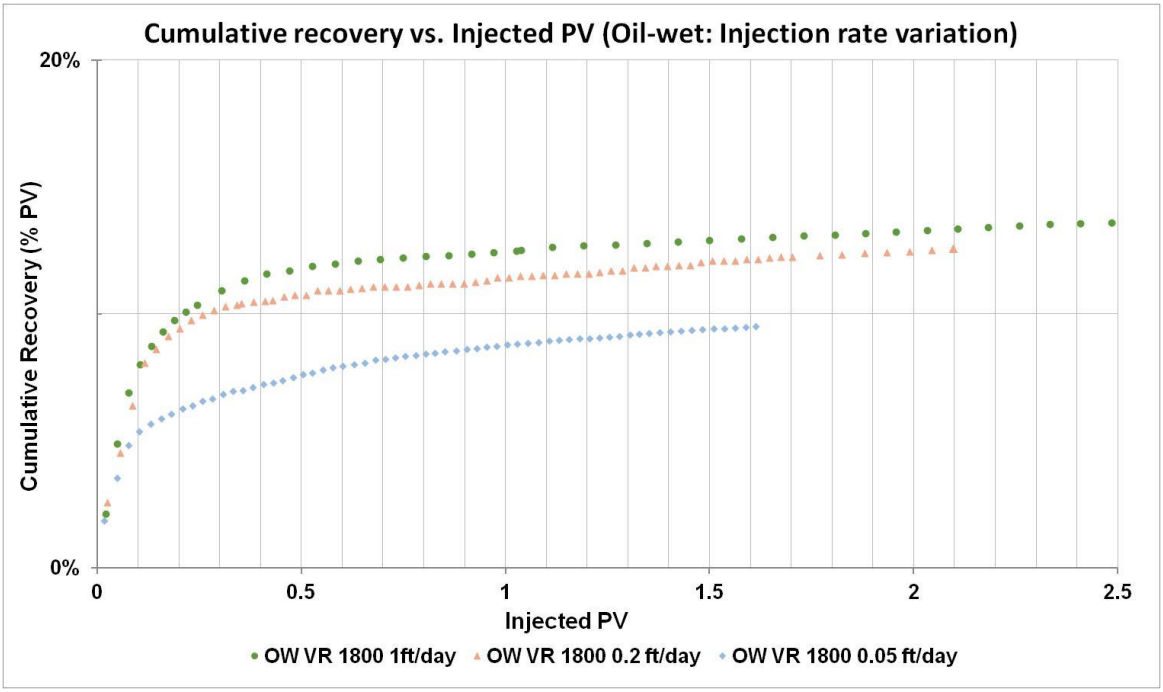

Figure 4.3: Effect of the injection rate on the cumulative recovery (%PV) in the 2-inch core (oil-wet experiments)

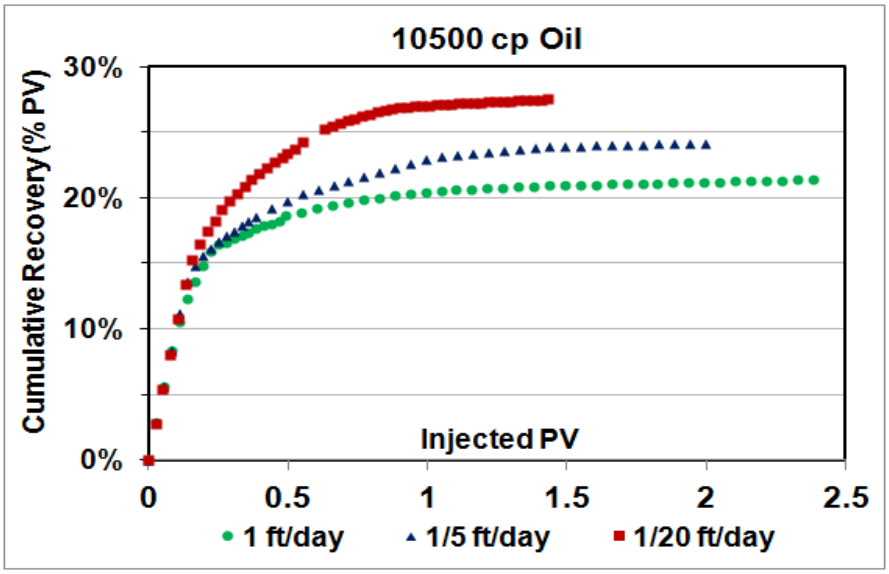

Figure 4.4: Effect of the injection rate on the cumulative recovery (%PV) in water-wet experiments retrieved from the previous study (Doorwar, 2015)

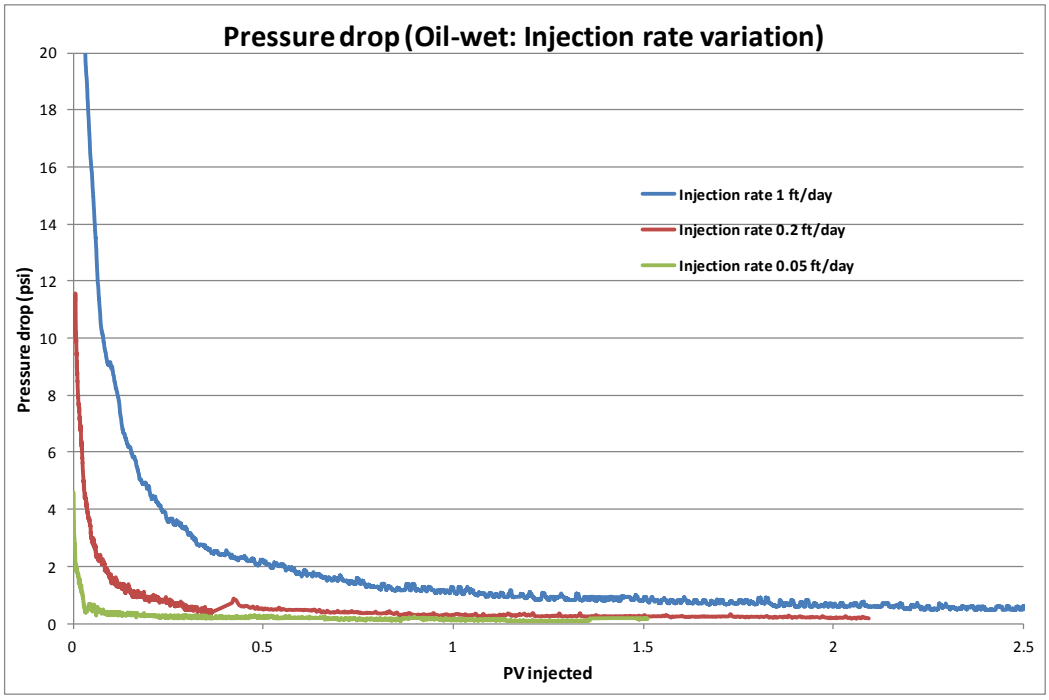

Figure 4.5: Effect of the injection rate on the pressure drop (%PV) in the 2-inch core (oil-wet experiments)

4.1.2 4-Inch Core

Experiments were performed in an oil-wet 4-inch to study the effect of core diameter variation on viscous fingerings. Table 3.1 lists the operating conditions in Experiments 10-12. Only viscosity ratio variation was tested in this case and the results are shown in Figure 4.6. Similar to 2-inch core results, the earlier breakthrough and the lower cumulative oil recovery occurred in higher viscosity ratio experiments. However, when comparing the recovery, the 4-inch core had earlier breakthrough recovery and lower cumulative recovery than the 2-inch core at the same viscosity ratio, suggesting that core diameter also affects unstable flow. Therefore, it is reasonable to include core diameter into viscous fingerings dimensionless groups.

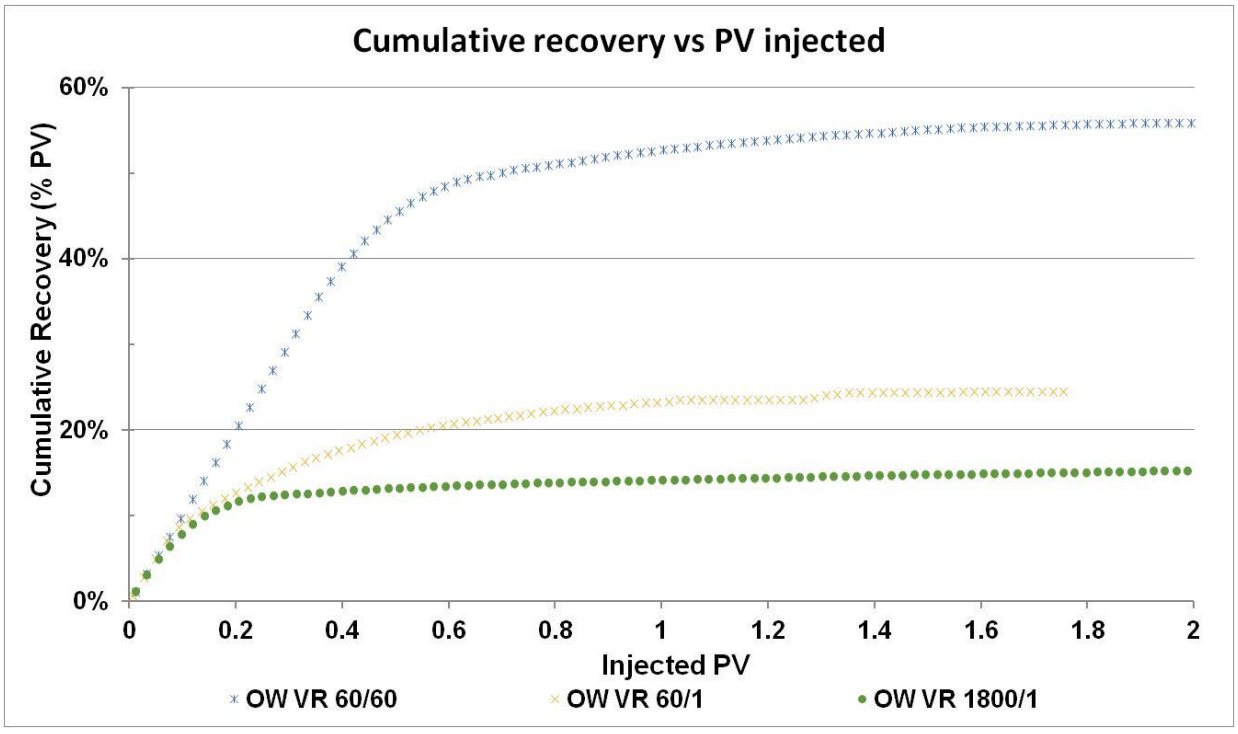

Figure 4.6: Effect of the viscosity ratio on the cumulative recovery (%PV) in the 4-inch core (oil-wet experiments)

4.2 WATER-WET RESULTS

4.2.1 4-Inch Core

In order to compare the results with the oil-wet system, water-wet experiments were conducted in a 4-inch water-wet core at the same conditions. The results are shown in Figure 4.7. As the viscosity ratio increased, the breakthrough occurred earlier and the cumulative oil recovery was slower. Compared to the 2-inch core experiments in the water-wet rock (Doorwar, 2015), 4-inch rock had earlier breakthrough and lower cumulative recovery for the same viscosity ratios.

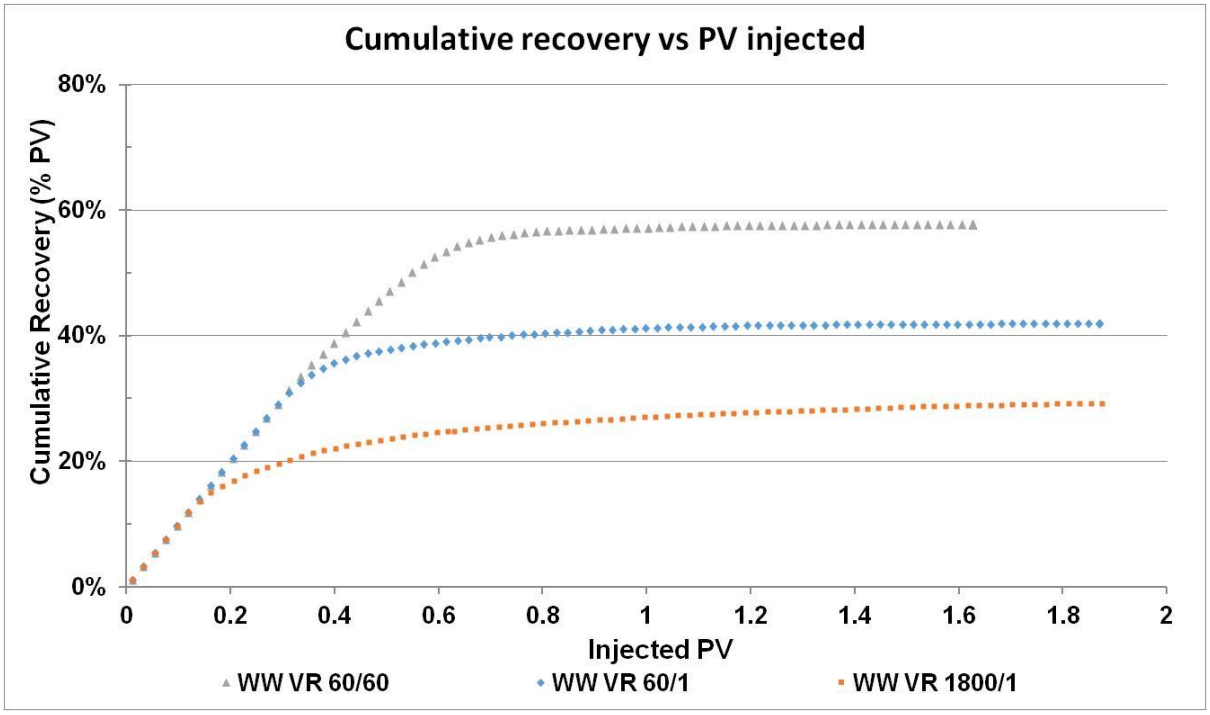

Figure 4.7: Effect of the viscosity ratio on the cumulative recovery (%PV) in the 4-inch core (water-wet experiments)

Figure 4.8 shows the results of both oil-wet and water-wet system 4-inch cores at different viscosity ratios. The cumulative recovery axis was changed to %OOIP for comparison purpose. It is obvious that the oil-wet system yields less oil recovery and earlier breakthrough recovery at the same condition than the water-wet system.

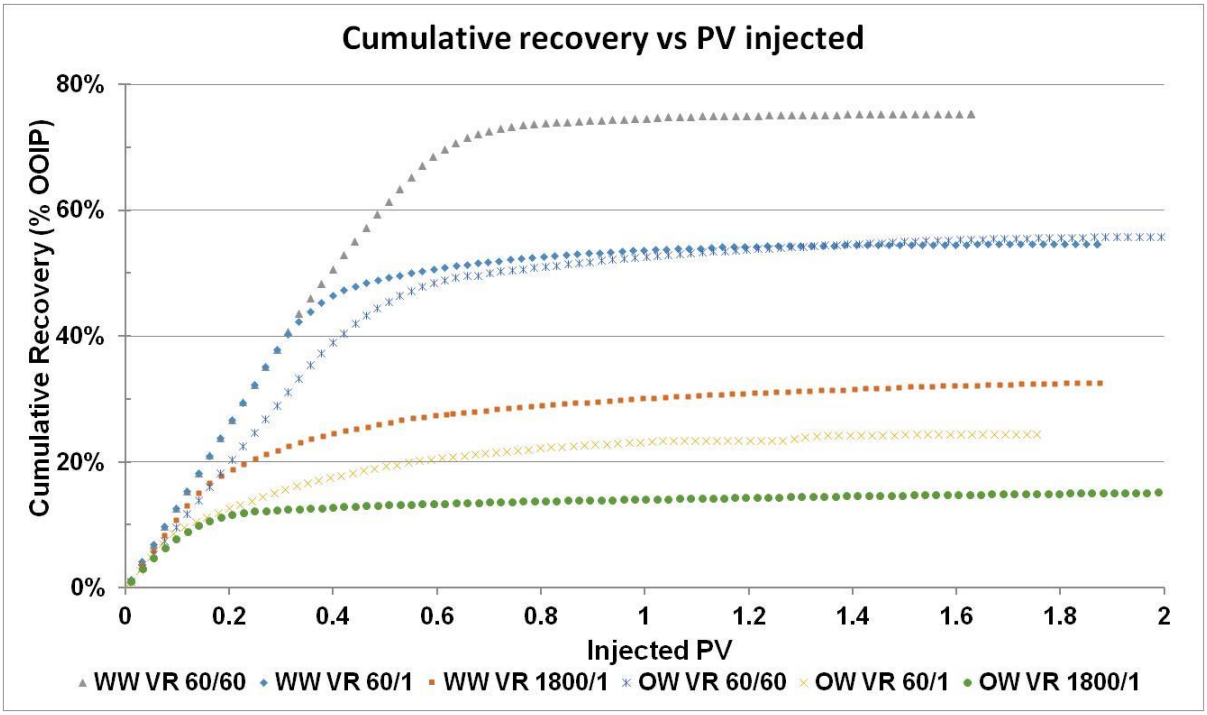

Figure 4.8: Effect of the viscosity ratio on the cumulative recovery (%OOIP) in the 4-inch core (all experiments)

4.3 Data Analysis

4.3.1 Scaling Groups Estimation

Several scaling groups have been plotted against breakthrough recovery and cumulative recovery at 1 to identify the reasonable group that correlates with the experiments. The recovery results are listed in Table 4.1. Additional data from a previous study (Doorwar and Mohanty, 2015) of the 2-inch water-wet core listed in Table 4.2.

Experiment No.	Breakthrough recovery (%PV)	Cumulative recovery at 1 PV (%PV)
1	43.77	55.13
2	9.96	26.08
3	10.58	27.76
4	10.52	25.63
5	10.3	21.3
6	7.56	16.65
7	4.87	12.48
8	4.53	11.42
9	3.53	8.79
10	35.5	52.66
11	8.7	23.18
12	3.03	12.53
13	35.26	57.16
14	30.89	41.17
15	11.77	27

Table 4.1: List of breakthrough recovery and cumulative recovery at 1 PV results conducted in this study

Experiment No.	Core diameter (inches)	Oil viscosity (cp)	Water viscosity (cp)	Viscosity ratio	Injection rate (ft/day)	Breakthrough recovery (%PV)	Cumulative recovery at 1 PV (%PV)
16	2	60	60	1	1	64	63.61
17	2	60	1	60	1	40	47.72
18	2	560	1	560	1	20	33.44
19	2	1440	1	1440	1	14	27.97
20	2	5200	1	5200	1	12	22.01
21	2	10500	1	10500	1	9	20.4
22	2	10500	1	10500	0.2	13	22.83
23	2	10500	1	10500	0.05	15	27

Table 4.2: List of breakthrough recovery and cumulative recovery at 1 PV results retrieved from the previous study (Doorwar and Mohanty, 2015)

$N_c\mu_r^2D^2/k$: Previously Proposed Group

First, the scaling group $N_c\mu_r^2D^2/k$ which has been proposed in a previous study was plotted with the recovery as listed in Table 4.1 and Table 4.2. The definition of capillary number (N_c) in this study is defined as:

$$N_c = \frac{v_w \mu_w}{\sigma_{ow}} \tag{4.1}$$

where v_w is the interstitial velocity ($v_w = Q_w/A\emptyset$), μ_w is the water viscosity, and σ_{ow} is the interfacial tension between oil and water. This expression was originally derived from

$$N_c = \frac{k\Delta P}{\sigma L} \tag{4.2}$$

The μ_r is the viscosity ratio and k is the absolute permeability of the core. The D^2 term refers to the characteristic area of cross-section which is the diameter square for cylindrical cores. The combination of these variables $N_c\mu_r^2D^2/k$ yields a dimensionless scaling group for fingerings. The results for both water-wet and oil-wet experiments were plotted against this group in a logarithmic, scale as shown in Figure 4.9. From this figure, it is obvious that all data do not follow the same trend.

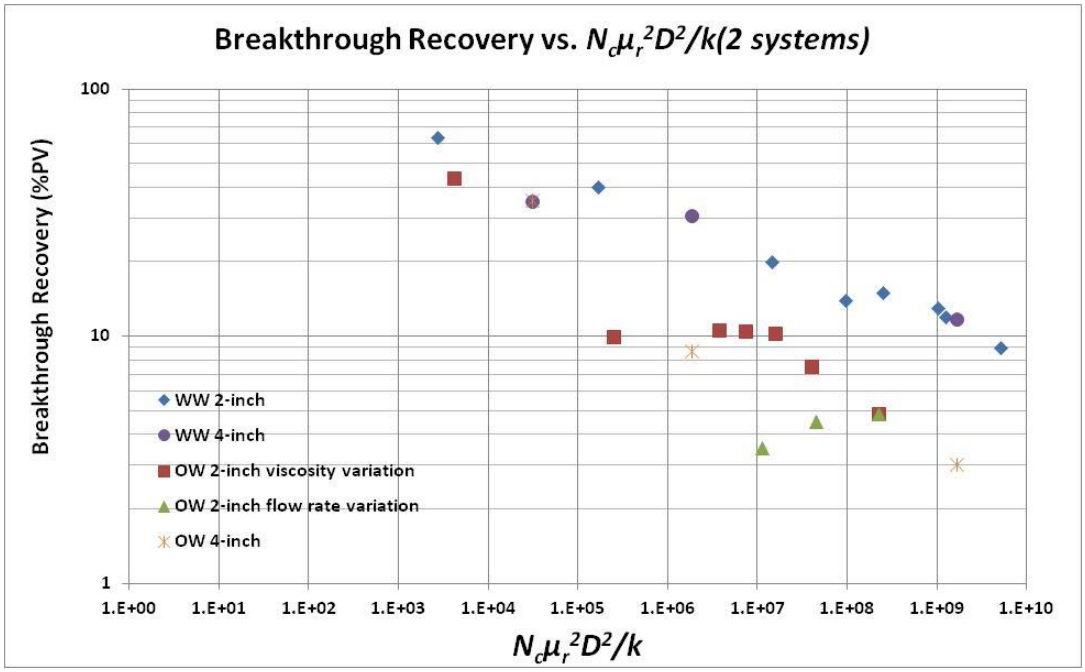

Figure 4.9: Breakthrough recovery (%PV) versus $N_c\mu_r^2D^2/k$ for both water-wet and oil-wet experiments

Figure 4.10 shows the power-law correlation trends drawn separately through water-wet and oil-wet experiments. Breakthrough recovery in the water-wet system provides better correlation than the oil-wet system, as can be seen from R^2 value. The cumulative recovery at 1 PV injected is similar to the breakthrough recovery (Figure 4.11). All the data for water-wet experiments followed the water-wet correlation closely. On the other hand, in oil-wet experiments, the data was divided into 2 trends based on the parameter varied. This is because the slope of flow rate variation results demonstrates an opposite direction to the viscosity ratio variation trend. The results show poor relationship when all the data is combined to one trend line. It suggests that this scaling group is not applicable to oil-wet experiments. Specifically, the exponent of N_c term in scaling group should not be equal to 1.

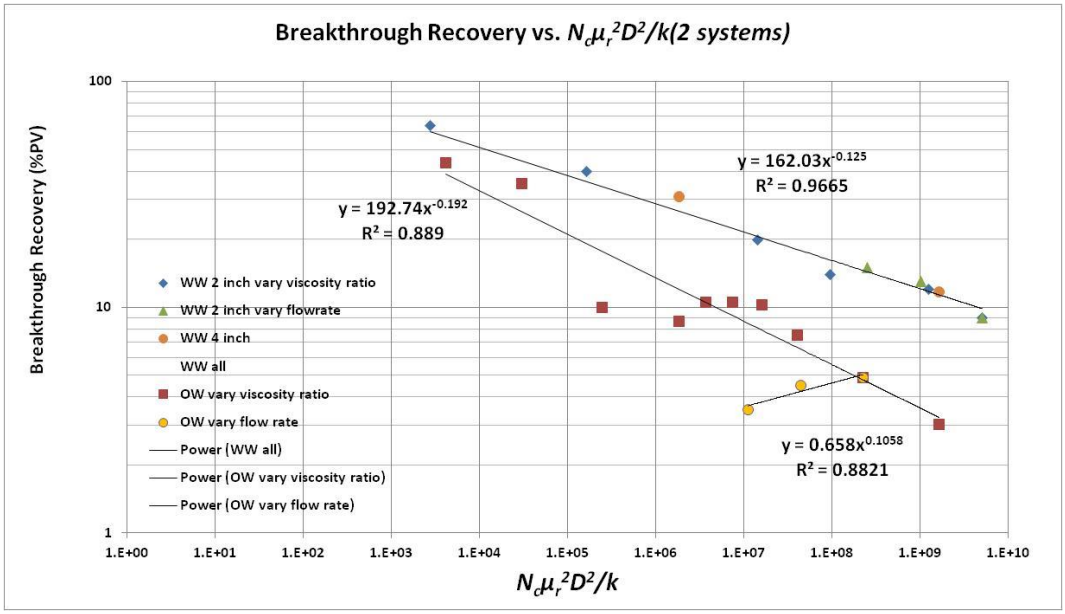

Figure 4.10: Power-law correlation between breakthrough recovery (%PV) and $N_c\mu_r^2D^2/k$ in water-wet and oil-wet experiments

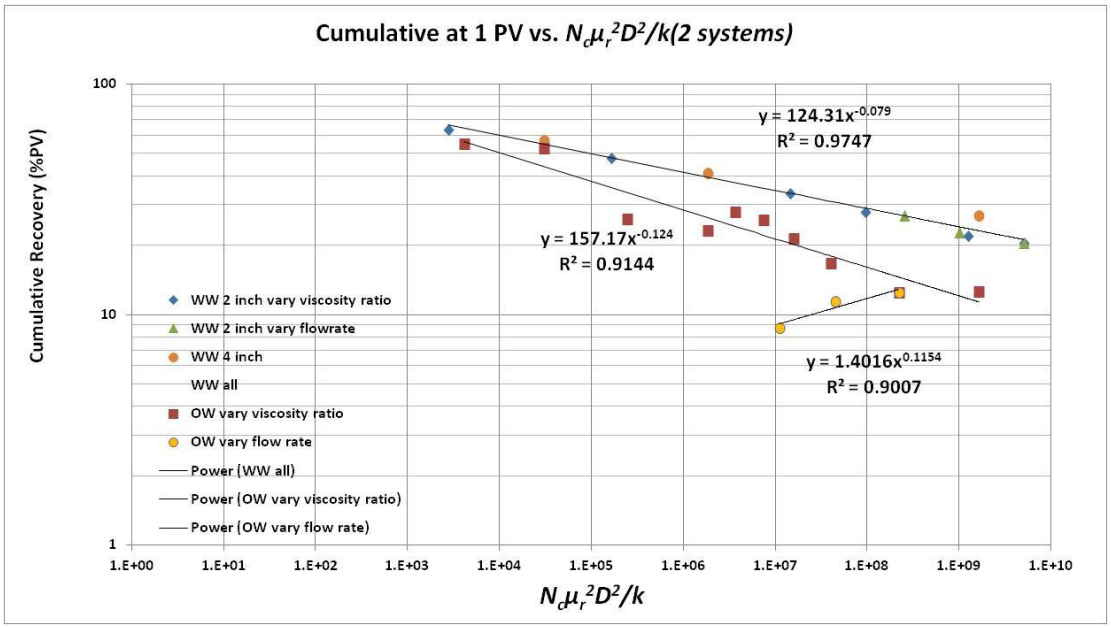

Figure 4.11: Power-law correlation between cumulative recovery at 1 injected PV (%PV) and $N_c\mu_r^2D^2/k$ in water-wet and oil-wet experiments

In general, as waterflood continues, the widths of viscous fingers grow. The cumulative recovery at higher injected pore volumes reflects the maximum effective cross-section of finger (a_e). Therefore, the correlation between cumulative recovery at 1 PV and scaling groups also assists in finding relationship between model parameters and scaling groups.

From Figure 4.10 and 4.11, $N_c\mu_r^2D^2/k$ is a reasonable scaling group for fingering in water-wet rocks, but it is not a proper group to be used in oil-wet systems. Nevertheless, further investigation on parameters affecting fingering function has been performed in order to find a better correlation in both water-wet and oil-wet rocks.

$N_c\mu_r^{(x)}D^2/k$: Effect of Exponent of Viscosity Ratio

In order to study the effect of the exponent of viscosity ratio in scaling groups (the term 'X' in this case), we begin with case X =1. When X is equal to 1, the scaling group becomes:

$$\frac{N_c\mu_r D^2}{k} = \frac{v_w\,\mu_w}{\sigma_{ow}} * \frac{\mu_o}{\mu_w} * \frac{D^2}{k} \tag{4.3}$$

$$= \frac{v_w\,\mu_o}{\sigma_{ow}} * \frac{D^2}{k} \tag{4.4}$$

According to Doorwar and Mohanty (2015), the dimensionless number $N_{c,visc}$ which is called the modified capillary number is defined as:

$$N_{c,visc} = \frac{v_w\,\mu_o}{\sigma_{ow}} \tag{4.5}$$

Thus,

$$N_c\mu_r D^2/k = N_{c,visc}D^2/k \tag{4.6}$$

From this equation, the viscosity ratio is not related to this scaling group. Therefore, this group may not be reasonable. The breakthrough recovery results which are plotted in Figure 4.12 also display scattered data in both oil-wet and water-wet system, suggesting that the exponent of viscosity ratio should not be equal to 1.

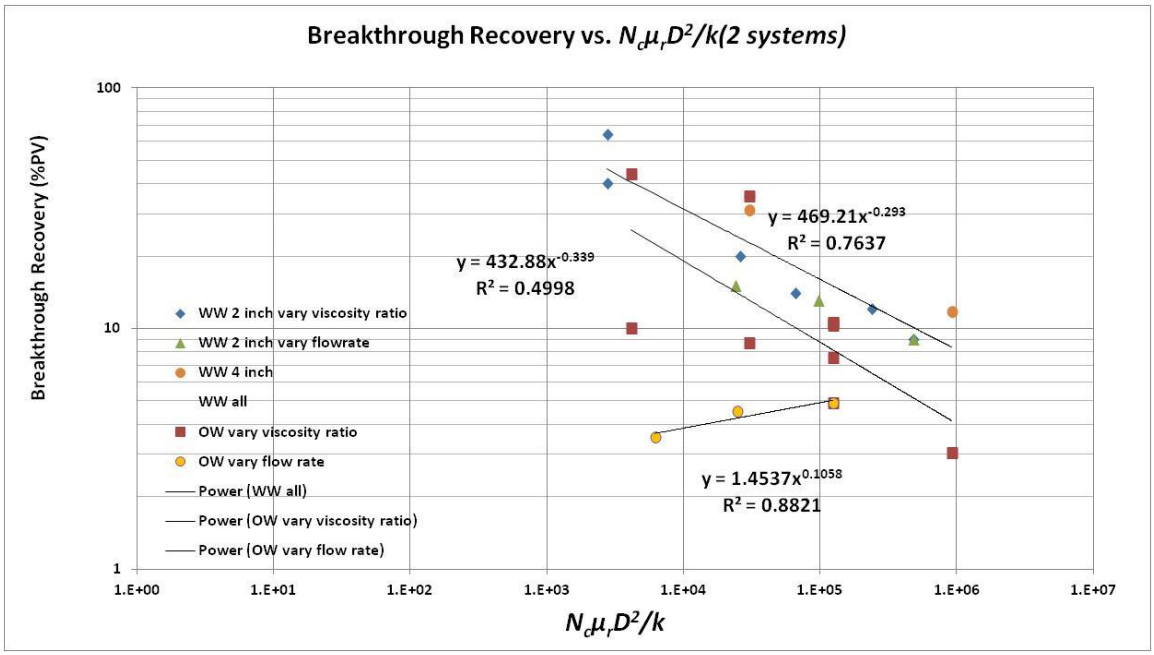

Figure 4.12: Power-law correlation between breakthrough recovery (%PV) and $N_c\mu_r D^2/k$ in water-wet and oil-wet experiments

When the exponent of the viscosity ratio is greater than 2, for example, X is equal to 3, the scaling group becomes $N_c\mu_r^3 D^2/k$. The power-law correlations between recovery and $N_c\mu_r^3 D^2/k$ are provided in Figure 4.13 and 4.14. In oil-wet experiments, the quality of correlation is slightly improved when the exponent of the viscosity ratio is higher. This character will be used to find a proper correlation between model parameters and scaling groups in the oil-wet system later.

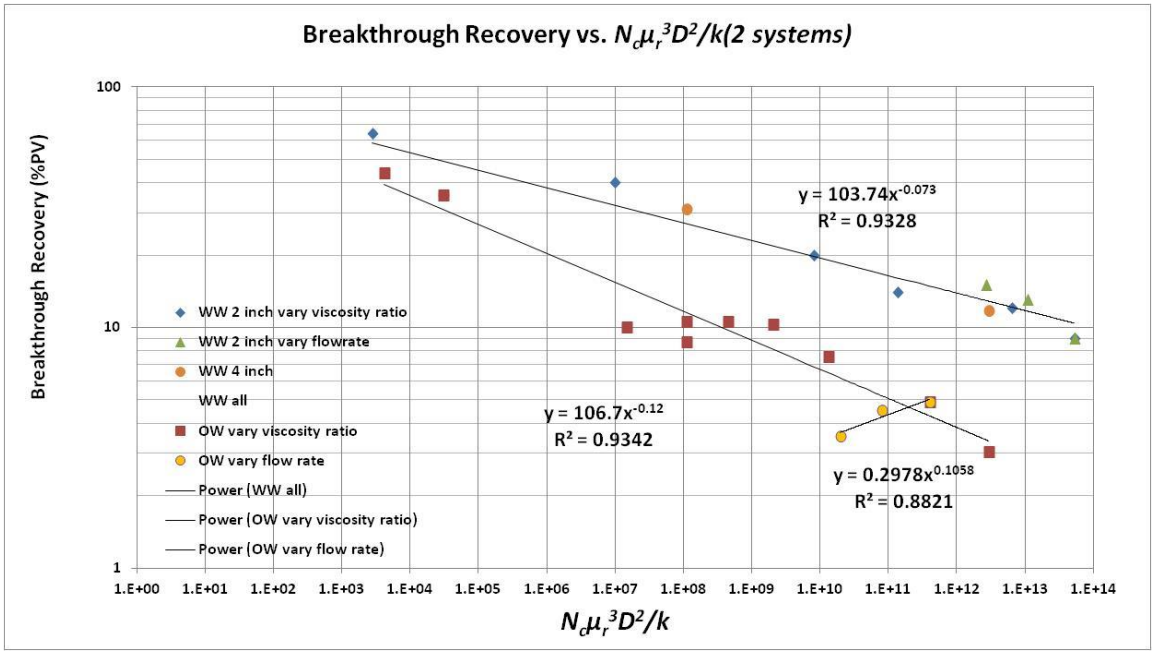

Figure 4.13: Power-law correlation between breakthrough recovery (%PV) and $N_c\mu_r^3D^2/k$ in water-wet and oil-wet experiments

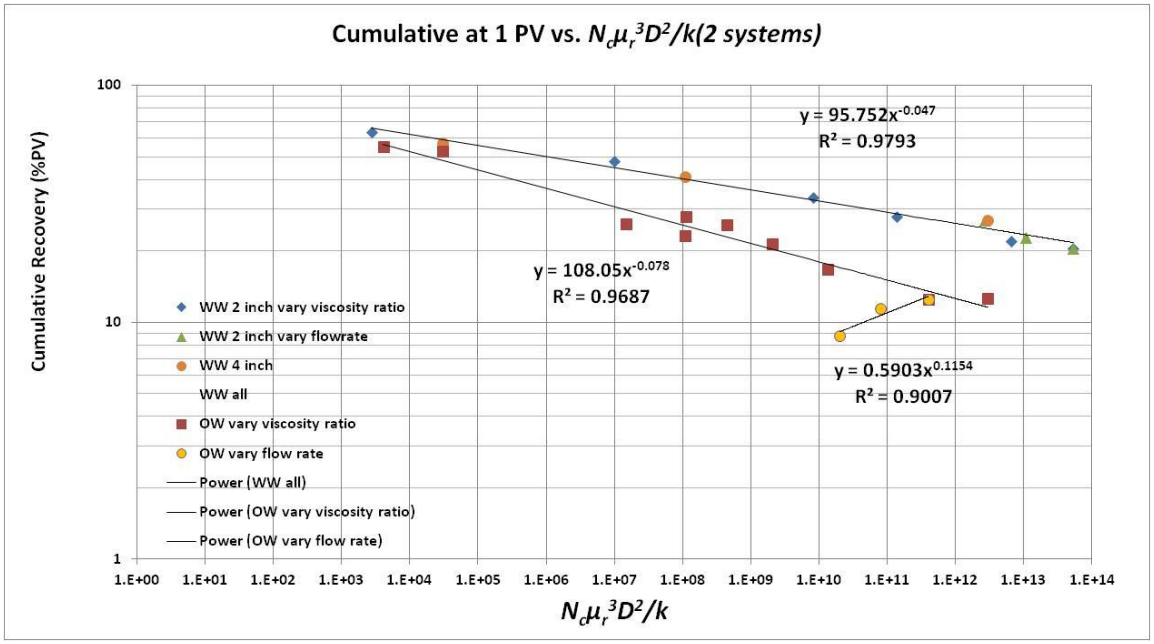

Figure 4.14: Power-law correlation between cumulative recovery at 1 injected PV (%PV) and $N_c\mu_r^3D^2/k$ in water-wet and oil-wet experiments

However, in the water-wet system, the results indicate poorer relationship when the exponent is higher than 2, thus suggesting that the term μ_r^2 is already correct for the scaling groups in this system.

$\mu_r^2 D^2/k$: Exponent of Capillary Number is Equal to Zero

When the exponent of capillary number is equal to zero, the scaling group is reduced to $\mu_r^2 D^2/k$. This means that there is no effect of flow rate and interfacial tension on viscous fingering. From Figure 4.15, although the correlation is much improved in the oil-wet system, the coreflood experimental results reveal that the higher flow rate led to a lower breakthrough recovery in water-wet rocks. Thus an inferior correlation occurs in the water-wet system. This indicates that the viscous fingering is affected by the capillary number or the flow rate. Therefore, the exponent of the capillary number should not be equal to zero.

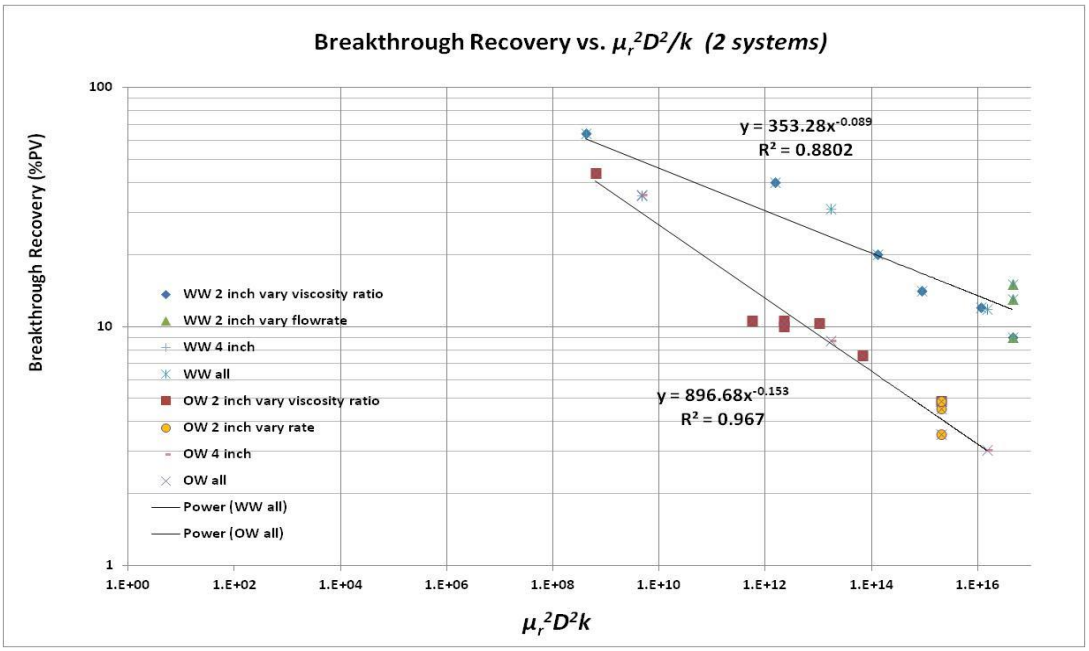

Figure 4.15: Power-law correlation between breakthrough recovery (%PV) and $\mu_r^2 D^2/k$ in water-wet and oil-wet experiments

$N_c^{(x)}\mu_r^2D^2/k$: Effect of Exponent of Capillary Number

From the previous results, in order to account for the opposite effect from the flow rate between oil-wet and water-wet systems, the exponent of capillary number has been studied. In this case, X is equal to 1 for water-wet system, displaying the original scaling group $N_c\mu_r^2D^2/k$, whereas X is equal to -1 for oil-wet system, suggesting a new scaling group $N_c^{(-1)}\mu_r^2D^2/k$.

The breakthrough and cumulative recovery at 1 PV injected are plotted against $N_c^{(x)}\mu_r^2D^2/k$ in Figure 4.16 and 4.17. For the oil-wet system, the negative exponent of capillary number demonstrates a better quality of correlation. Moreover, all data points in this system including the flow rate variation experiments can be incorporated in the whole correlation. This implies that the negative exponent is valid in oil-wet systems.

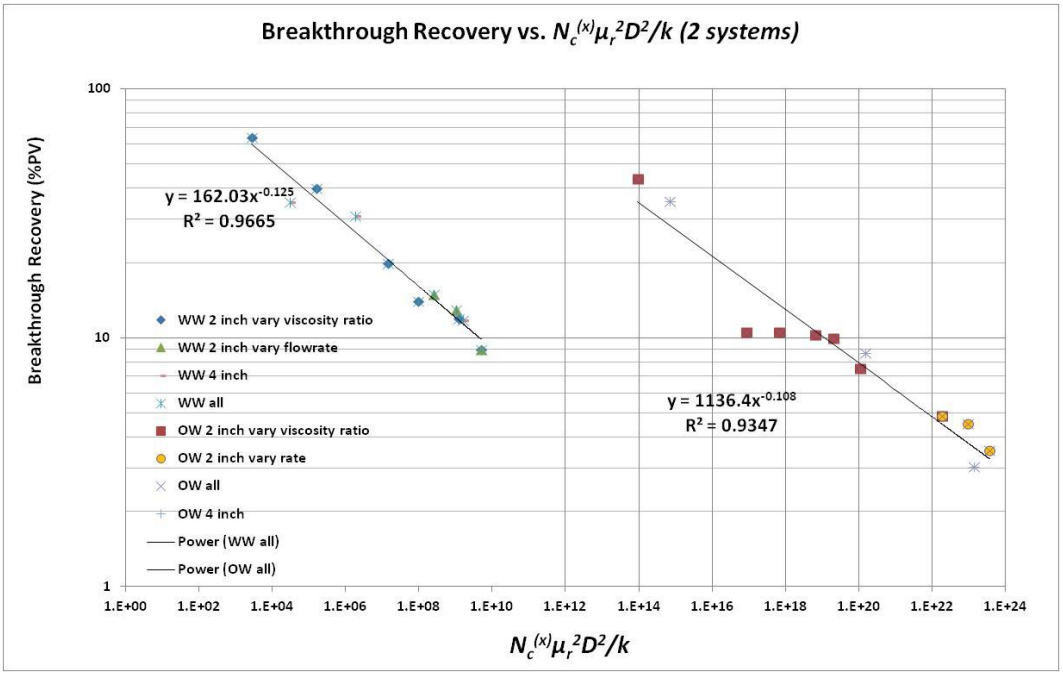

Figure 4.16: Power-law correlation between breakthrough recovery (%PV) and $N_c^{(x)}\mu_r^2D^2/k$ in water-wet and oil-wet experiments

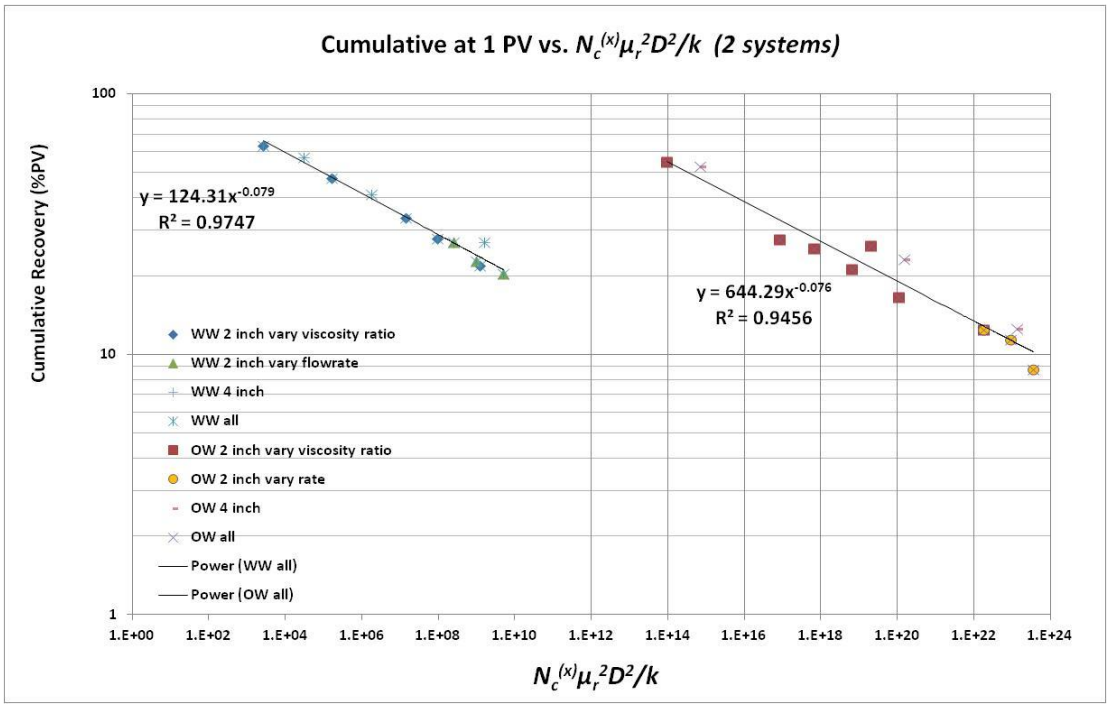

Figure 4.17: Power-law correlation between cumulative recovery at 1 injected PV (%PV) and $N_c^{(x)}\mu_r^2D^2/k$ in water-wet and oil-wet experiments

$V^{(x)}\mu_r^2D^2/k$: Effect of Exponent of Flow Velocity

Because the experiments in this study varied only the injection rate, and did not vary the interfacial tension between two fluids, the effect of the exponent of the flow rate is discussed here. Similar to the previous case, we introduce the scaling group $V^{(x)}\mu_r^2D^2/k$ where V is the water flow rate in ft/day and X is equal to 1 and -1 for the water-wet and the oil-wet system, respectively.

For the water-wet system, the scaling group becomes dimensional with a unit of ft/day. The correlation between recovery and the new scaling group is poorer than the original group $N_c\mu_r^2D^2/k$ (see Figure 4.18 and 4.19). This is because it affects the data points of 60 cp water viscosity experiments. Thus, the flow velocity should not be

separately considered in the water-wet system, instead it should be included in the capillary number.

On the other hand, in the oil-wet system, the correlation between recovery and $V^{(-1)}\mu_r^2 D^2/k$ is improved and even better than group $N_c\mu_r^3 D^2/k$. This scaling group is also developed into a dimensional group with a unit of $(ft/day)^{(-1)}$ and may cause a problem for generalization in reservoir simulation. However, due to the better correlation, this group is tested with model parameters in the simulation results section as well.

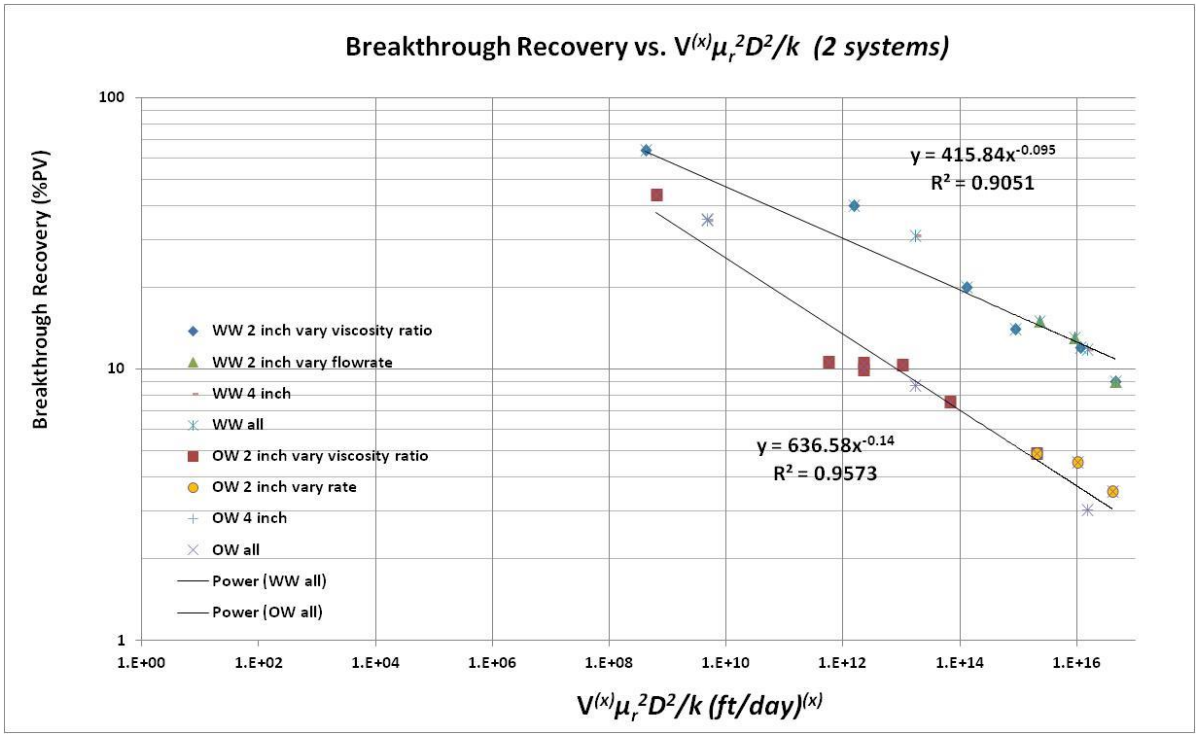

Figure 4.18: Power-law correlation between breakthrough recovery (%PV) and $V^{(x)}\mu_r^2 D^2/k$ water-wet and oil-wet experiments

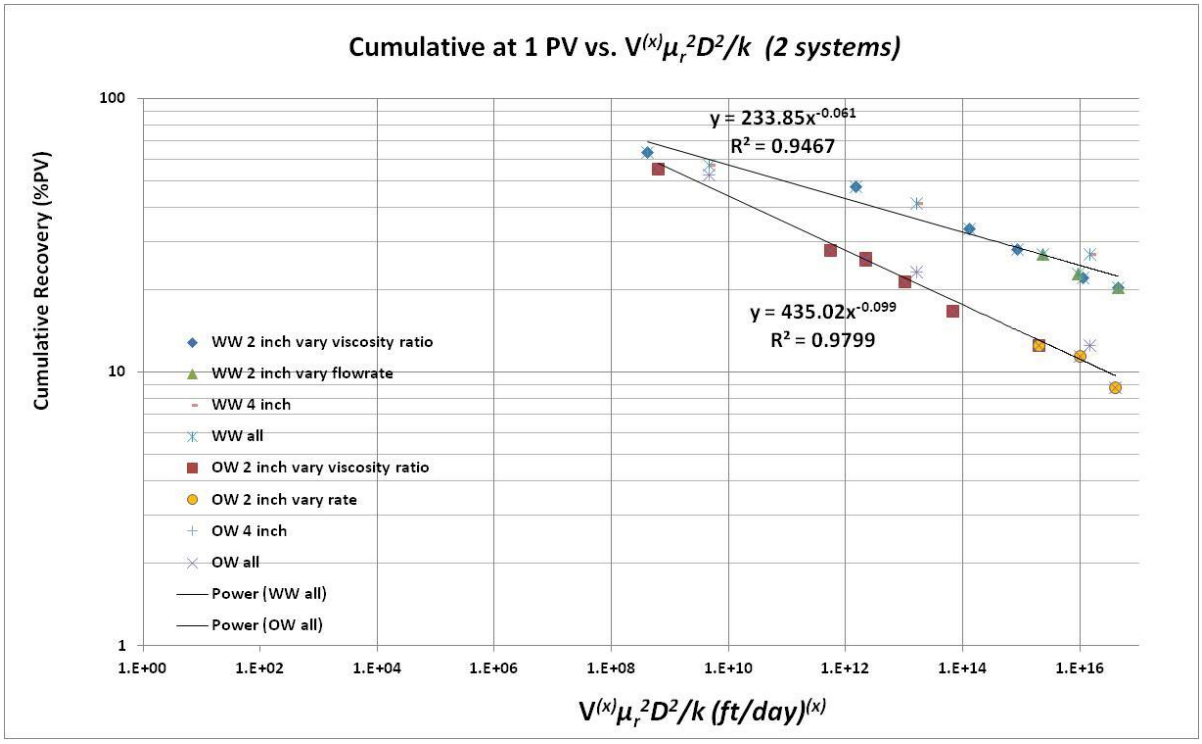

Figure 4.19: Power-law correlation between cumulative recovery at 1 injected PV (%PV) and $V^{(x)}\mu_r^2 D^2/k$ water-wet and oil-wet experiments

$N_c^{(x)}\mu_r^{(y)}D^2/k$: Combination

From the previous analysis, it is known that the exponent of capillary number should be equal to 1 for the water-wet system and -1 for the oil-wet system. Furthermore, we also know that the higher exponent of the viscosity ratio leads to the better correlation between recovery and scaling group in the oil-wet system. In an effort to find the better correlation similar to group $V^{(x)}\mu_r^2 D^2/k$ while the group is still dimensionless, the combination case was studied, specifically for the oil-wet system. In this case, the exponent of the viscosity ratio is equal to 3.

According to Figure 4.20 and 4.21, the correlations in the oil-wet system are slightly improved from the group $N_c^{(x)}\mu_r^2D^2/k$ and the R^2 values appear to be similar to the previous group ($V^{(x)}\mu_r^2D^2/k$). In contrast, the qualities of correlations for the water-wet system are worse than the original group $N_c\mu_r^2D^2/k$. This indicates that the combination group should be applied with model parameters only for the oil-wet system.

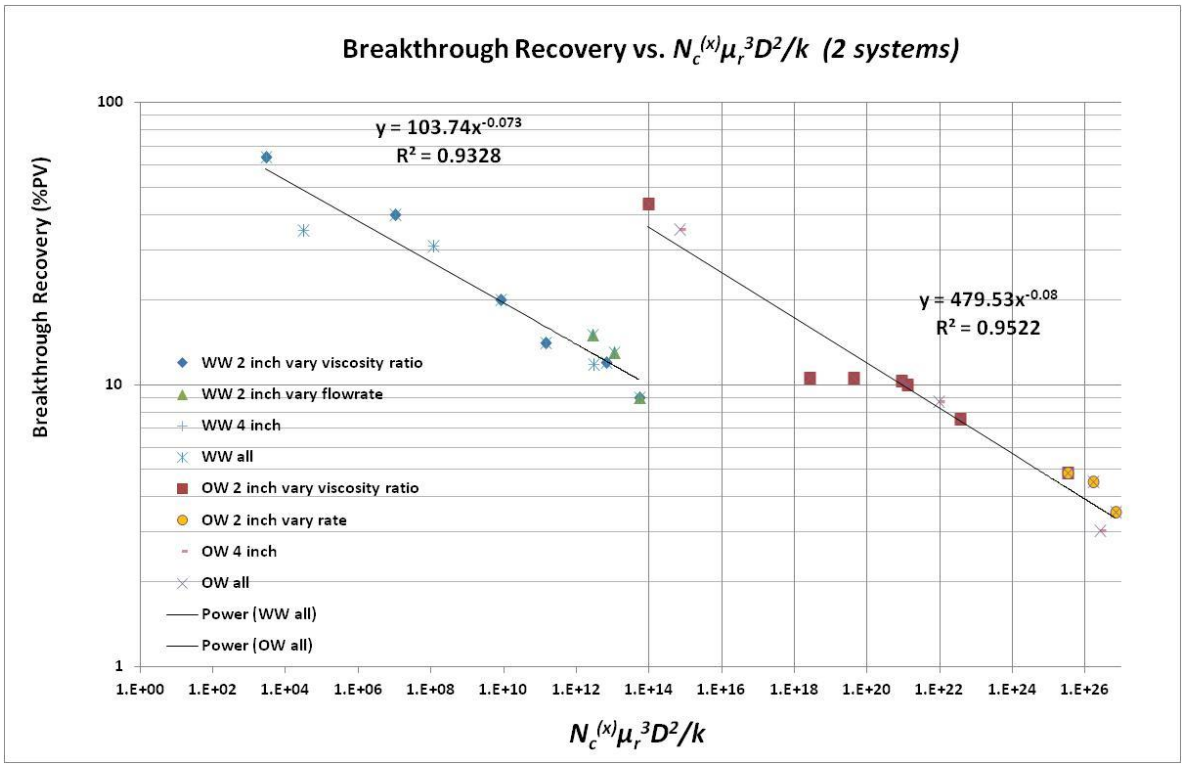

Figure 4.20: Power-law correlation between breakthrough recovery (%PV) and $N_c^{(x)}\mu_r^3D^2/k$ in water-wet and oil-wet experiments

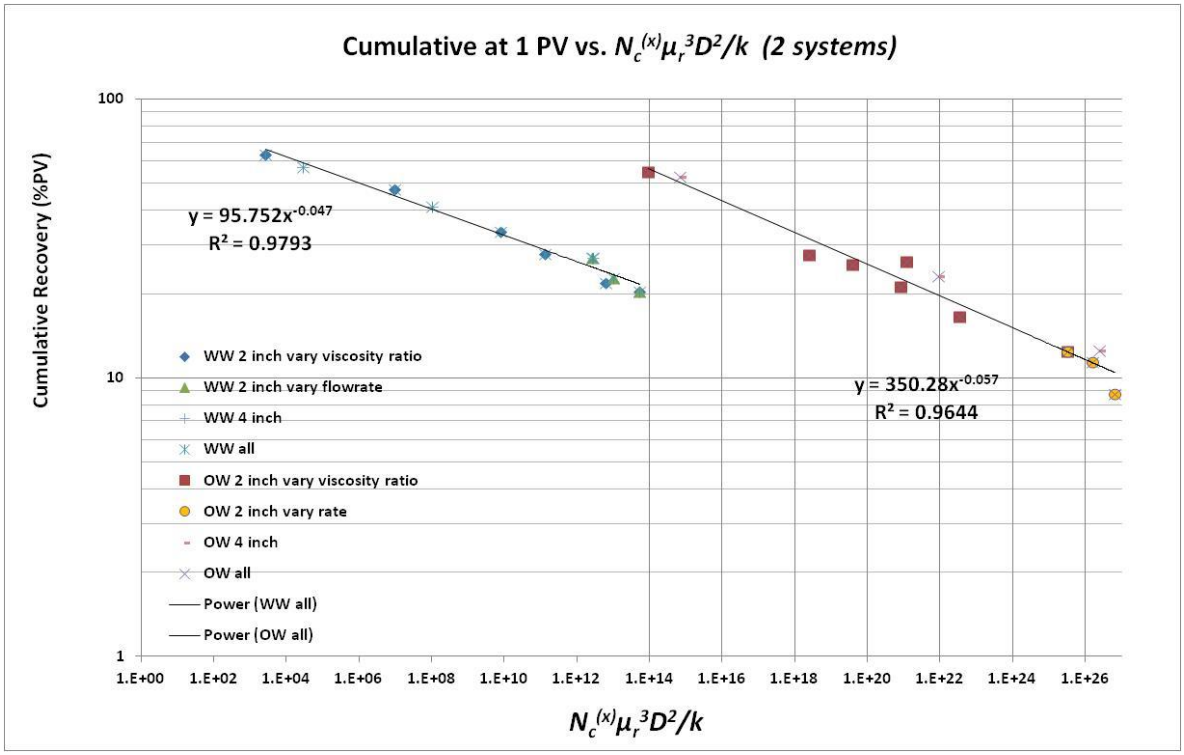

Figure 4.21: Power-law correlation between cumulative recovery at 1 injected PV (%PV) and $N_c^{(x)}\mu_r^3D^2/k$ in water-wet and oil-wet experiments

4.3.2 Estimated Residual Oil Saturation

In order to estimate the final cumulative recovery from each experiment, the graphical extrapolation technique (Jones and Roszelle, 1978) was employed. This method can be applied only with a constant flow rate waterflood. The collected volumes of effluent were used to calculate the fractional flow of oil and water versus time (PV injected). The average water saturation of the entire core ($\overline{S_w}$)at each time was calculated from:

$$\overline{S_w} = S_{wi} + \frac{N_p}{V_p} \tag{4.7}$$

where S_{wi} is the initial water saturation before the waterflood and N_p/V_p is the cumulative oil recovery in PV. The tangent to the curve between $\overline{S_w}$ and injected PV which was extended to the vertical axis at any point (it is designated as S_w^+) does not represent the water saturation at the outlet of the core (S_{w2}). This is because S_{w2} is equal to zero and does not change during waterflood until the water breakthrough. After the water breakthrough, the water saturation at this point is always less than the average water saturation until the end of the oil recovery process ($\overline{S_w} = 1 - S_{or}$ at the infinite injection). The calculation for the water saturation at the outlet of the core (S_{w2}) was derived using a material balance around a small section of the core in a linearly displacement and expressed by:

$$S_{w2} = 2\overline{S_w} - S_w^+ \tag{4.8}$$

where

$$S_w^+ = \overline{S_w} - \frac{1}{Q_i}\frac{d\overline{S_w}[1/Q_i]}{d(1/Q_i)} \tag{4.9}$$

Both $\overline{S_w}$ and S_{w2} were then plotted with the reciprocal of the injected pore volume ($1/Q_i$) for all experiments. The trends were extrapolated to the infinite injection point ($1/Q_i = 0$) which is the vertical axis. At this point, both water saturations had the same intercept value which referred to the residual oil water saturation ($\overline{S_w} = 1 - S_{or}$). The example of the extrapolation plot is presented in Figure 4.22. This example is calculated using the results from the 2-inch core experiment of the viscosity ratio of 60 (60 cp oil viscosity and 1 cp water viscosity) in the oil-wet system.

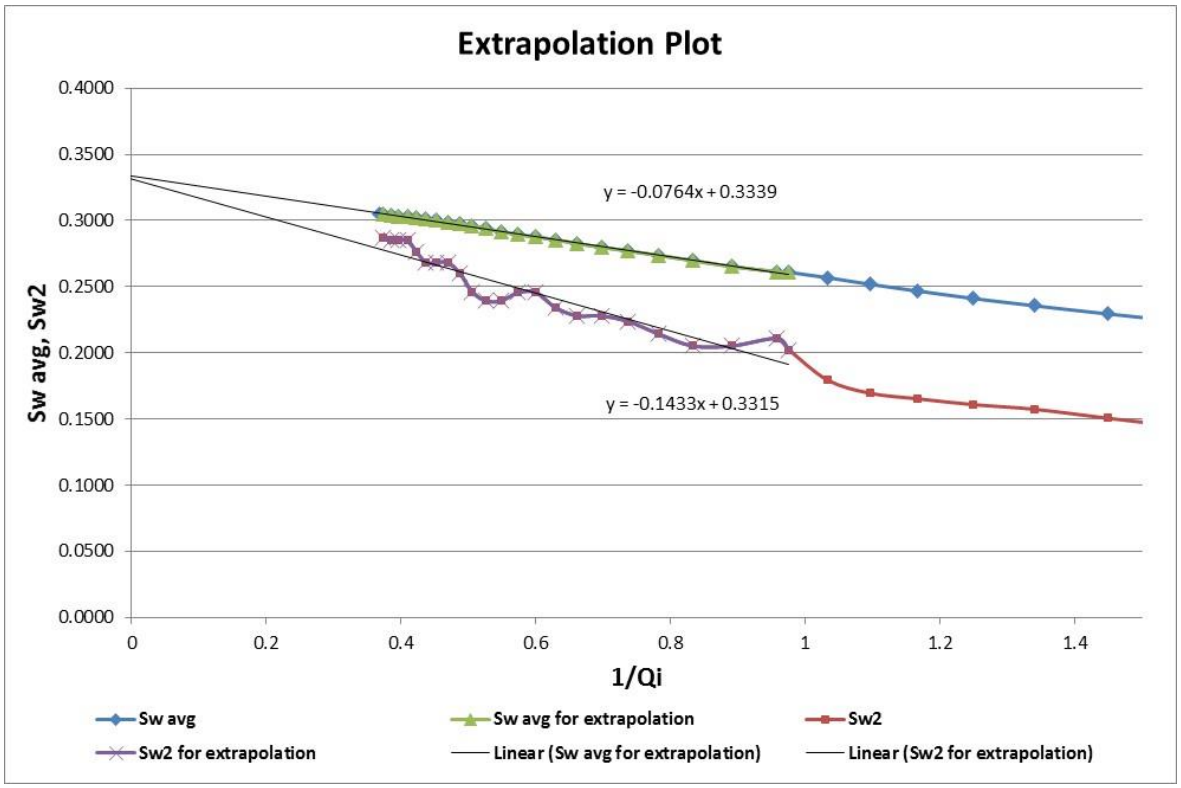

Figure 4.22: Extrapolation plot between $\overline{S_w}$ and S_{w2} versus the reciprocal injected pore volume ($1/Q_i$) for the 2-inch core experiment of the viscosity ratio of 60 in the oil-wet system

From this case, the estimated residual oil saturation (S_{or}) is approximately 0.67 (S_{or} = 1 - $\overline{S_w}$ at $1/Q_i = 0$). However, from the effective-finger model (Luo et al., 2016), there is always a bypassed-oil region which is represented by the fractional finger cross-section (1-a_e) and remains at the initial oil saturation ($S_{oi} = 1 - S_{wi}$). This means that for an unstable immiscible displacement, the extrapolated points of $\overline{S_w}$ and S_{w2} to the vertical axis does not denote the residual oil saturation which is the intrinsic property of the rocks. Instead, these extrapolated points represent the effective remaining oil saturation (S_{orem}) since it include oil remaining in both bypassed-oil region and two phase

region after the infinite volume of the waterflood. This value is related to the residual oil saturation which can be expressed by:

$$S_{orem} = (1 - a_e)(1 - S_{wr}) + a_e S_{or} \quad (4.10)$$

The first terms and the second term represent oil remaining in bypassed and two phase region, respectively. The extrapolated S_{orem} for all experiments are listed in Table 4.3. The number of experiment is in the same order as in Table 3.1 and 3.2. These results are corresponding to the viscosity ratio and flow rate. In the oil-wet system, the higher viscosity ratio results in the more unstable displacement, thus leading to the higher bypassed-oil region (higher S_{orem}). Regarding the displacement rate, the slower flow rate in the oil-wet system leads to less developed pressure and less oil recovery which also bring about the bigger bypassed-oil zone. S_{orem} from the water-wet system (experiment 13-15) also reveal the same trend as the oil-wet system for the viscosity ratio variation.

Experiment No.	S_{orem} from Graphical Extrapolation
1	0.36
2	0.67
3	0.64
4	0.69
5	0.75
6	0.82
7	0.85
8	0.86
9	0.90
10	0.40
11	0.74
12	0.83
13	0.18
14	0.34
15	0.58

Table 4.3: List of estimated S_{orem} from a graphical extrapolation technique

This relationship is important to reservoir simulation section. Regarding the residual oil saturation (S_{or}), we can estimate this value from the most stable displacement experiments. This property should not be altered during each experiment. After we obtained S_{orem} from all experiments, we can estimate the initial guess for the maximum cross-section of the effective finger (a_e), thus assisting in the history matching process. The comparison between S_{orem} from the extrapolation technique and the results from the simulation modeling will be discussed in the next chapter.

CHAPTER 5: MODELING AND SIMULATION

5.1 ASSUMPTIONS

The model used in this history matching process was proposed by Luo et al. (2016). This model is called an "effective finger model" which assumes that all the fingers within a grid block can be combined and represented by one equivalent finger in the grid block, as shown in Figure 2.10. Although it neglects the small details at the finger scale, it captures the viscous fingering effect through the pseudo-relative permeability function.

According to Figure 2.10, there are 3 main parameters involved in this model: a_e which is the maximum cross-section of finger, β_1 which is the finger growth exponent of the two-phase region, and β_2 which is the growth rate exponent of the fractional cross-section of the bypassed oil region (λ_b). Water can flow only in two-phase region or the finger zone. The fractional finger width (λ_e) depends on model parameter a_e and β_1(Equation 2.9). On the other hand, oil can be in any zone during the flow but the oil movement occurs only in two-phase region and oil single-phase region. The bypassed-oil region is the section that oil is left behind after waterflood process; thus, there is no oil flow in this region. This area is dependent on model parameter a_e and β_2(Equation 2.10). For water-wet rocks, it is shown that parameter a_e is related to the viscosity ratio and the displacement rate which are parameters in the scaling group (Luo et at., 2016). However, the relationship between these parameters and the scaling group is not yet known for oil-wet experiments. This correlation will be developed from the history matching results.

From Darcy's law and the pseudo-relative permeability concept, the effective relative permeabilities of water $\left(k_{rw,e}\right)$ and oil $\left(k_{ro,e}\right)$ are expressed as follows:

$$k_{rw,e} = \lambda_e k_{rw}^o \, (\bar{S}_w)^{n_w} \tag{5.1}$$

$$k_{ro,e} = \lambda_e k_{ro}^o \, (1 - \bar{S}_w)^{n_w} + \lambda_o k_{ro}^o \tag{5.2}$$

where k_{rw}^{o} and k_{ro}^{o} are the end point relative permeability of water and oil, and n_w and n_o are the Corey exponent of water and oil, respectively. In Equation 2.9 and 2.10, $\overline{S_w}$ is not the average water saturation as discussed in the previous chapter. Instead, it is the normalized water saturation which is defined as:

$$\overline{S_w} = \frac{S_w - S_{wr}}{1 - S_{wr} - S_{orem}} \tag{5.3}$$

From these equations, the domain of the relative permeability is changed from between S_{wr} and 1-S_{or} to S_{wr} and 1-S_{orem} due to the term $\overline{S_w}$. The end point and the curve exponent shape for both oil and water relative permeabilities are also altered because of fingering.

The experiments have been simulated using the UTCHEM simulator. Other assumptions for experimental modeling are:

1. Homogeneous core properties such as porosity and absolute permeability.
2. The waterflood process is one dimensional vertically flow upward and, at the initial state, each grid block contains the same initial water saturation throughout the core.
3. The number of grid block is 1*1*20 in X-Y-Z axis, respectively. The length of each grid block is calculated from the core length.
4. The cross-sectional geometry of the grid block is a square shape. However, the cross-sectional area of the grid block is equal to that of the core which has a circular shape.
5. Simulations predict oil recovery and pressure drop for 2 injected pore volumes.

6. The intrinsic relative permeability is assumed to be represented by a Corey function.

5.2 History Matching Results and Data Analysis

5.2.1 History Matching Process and Results

The initial values of the relative permeability curve parameters were obtained from the experimental data using JBN method from the most stable displacement for each system such as the unit viscosity ratio. Both end point relative permeability and Corey exponents were then adjusted as little as possible from the base case because we wanted to concentrate on model parameters a_e, β_1, and β_2 variation for the effective-finger model. However, some values were required to be adjusted in an effort to improve the quality of the history matching.

The initial guess of a_e was estimated from: $S_{orem}$from the extrapolation technique, S_{wr} from the experimental data, and S_{or}which is the intrinsic property of the rock. In this study, it was assumed that the initial water saturation (S_{wi}) is equal to the residual water saturation (S_{wr}). All oil-wet experiments were conducted from 100% oil saturation, thus $S_{wr}$was equal to 0 in this system. In contrast, in water-wet experiments, the cores initially contained 100% water saturation and then were injected with oil until reaching the residual water saturation point. S_{wr}values were calculated and listed in Table 5.1 for water-wet experiments. The S_{or} value was kept constant. The initial values were estimated from $S_{orem}$of the most stable displacement in each system. This is because this case tends to have the smallest bypassed-oil region; therefore, the effective remaining oil saturation is approximately equal to true residual oil saturation. The final matched values for S_{or} are around 0.39 and 0.16 for oil-wet and water-wet systems, respectively.

Experiment No.	Core diameter (inches)	Oil viscosity (cp)	Water viscosity (cp)	Viscosity ratio	Swr
13	4	60	60	1	0.23
14	4	60	1	60	0.23
15	4	1800	1	1800	0.10

Table 5.1: List of the residual oil saturation for water-wet experiments

The pressure and cumulative production data versus time were compared between the predictions obtained from simulation and the actual results from coreflood experiments. Matching parameters were changed until the results matched in the acceptable range for all experiments. The example of the comparison between experimental data and simulation forecast is illustrated in Figure 5.1. There are some pressure drop discrepancies at the early stage but the pressure drops are mostly matched with the experiment results. All history matching plots are provided in Appendix A.

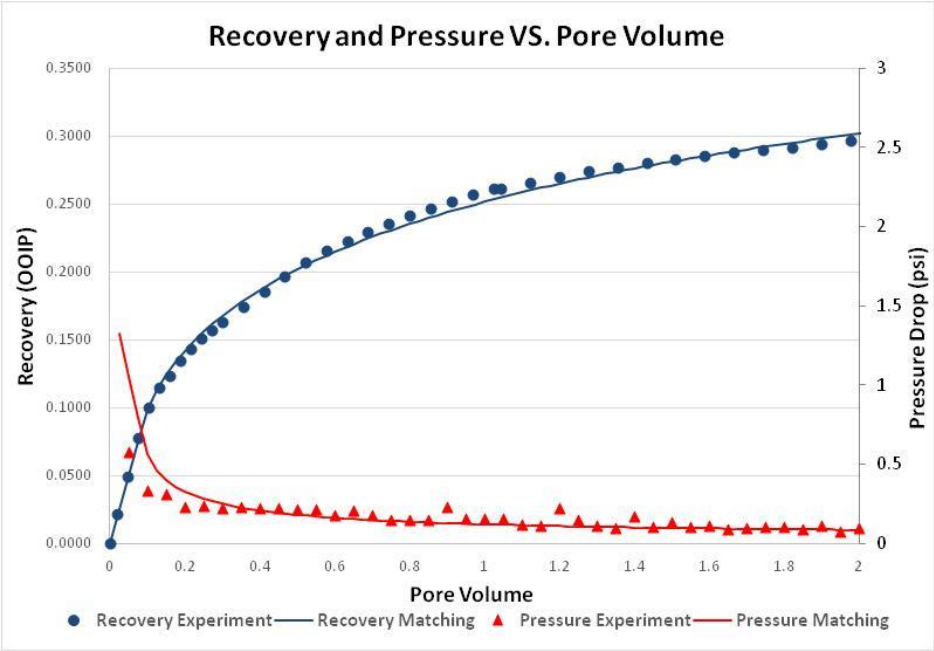

Figure 5.1: Experiment and simulation results for 2-inch coreflood of μ_r=60 (μ_o= 60 cp, μ_w= 1 cp) and displacement rate 1 ft/day in an oil-wet system

After the history matching process of the lab results, all model parameters were collected and plotted with scaling groups to find the reasonable correlation for each parameter in each system. The parameters are summarized in Table 5.2. Additional data which are obtained from previous system (experiment 16-23) are also listed in Table 5.3 (Luo et al., 2016).

Experiment No.	a_e	β_1	β_2	S_{or}
1	0.95	0.1	2.5	0.38
2	0.6	0.8	2.5	0.39
3	0.55	0.5	2.5	0.4
4	0.51	0.7	2.5	0.4
5	0.45	0.85	2.5	0.4
6	0.3	3.5	2.5	0.39
7	0.25	4.5	2.5	0.39
8	0.22	4.5	2.5	0.39
9	0.19	2	2.5	0.39
10	0.9	0.15	2.5	0.38
11	0.45	1.2	2.5	0.39
12	0.275	8	2.5	0.38
13	0.69	0.17	2.5	0.16
14	0.95	0.1	2.5	0.16
15	0.45	0.5	2.5	0.16

Table 5.2: List of model parameters results from the simulation

Experiment No.	a_e	β_1	β_2
16	N/A	N/A	N/A
17	0.79	0.1	1.5
18	0.6	0.2	2.5
19	0.47	0.33	2.4
20	0.38	0.4	2
21	0.34	0.5	1.8
22	0.4	0.4	2.6
23	0.51	0.28	2.2

Table 5.3: List of model parameters results from Luo et al. (2016)

5.2.2 Correlation with Scaling Groups

The model parameters were correlated with the scaling groups.

Oil-Wet System: Parameter a_e

Figure 5.2 shows parameter a_e plotted against the scaling group $N_c^{(-1)}\mu_r^2 D^2/k$

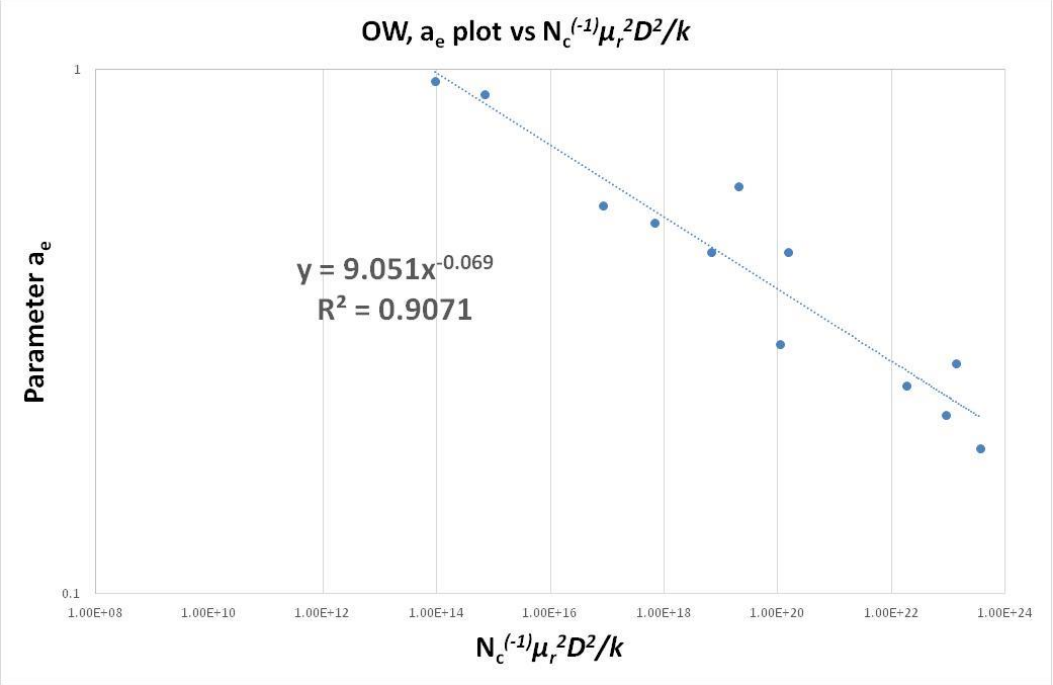

Figure 5.2: Power-law correlation between a_e and $N_c^{(-1)}\mu_r^2 D^2/k$ in an oil-wet system

This result suggests that the relationship between the scaling group and the maximum cross-section of effective finger is similar to the relationship between the same scaling group and the breakthrough recovery (or cumulative recovery) which represents viscous fingerings in porous media. A scaling group with the higher exponent of viscosity ratio ($N_c^{(-1)}\mu_r^3 D^2/k$) and a dimensional group $V^{(x)}\mu_r^2 D^2/k$ are also plotted with this parameter in Figure 5.3 and 5.4.

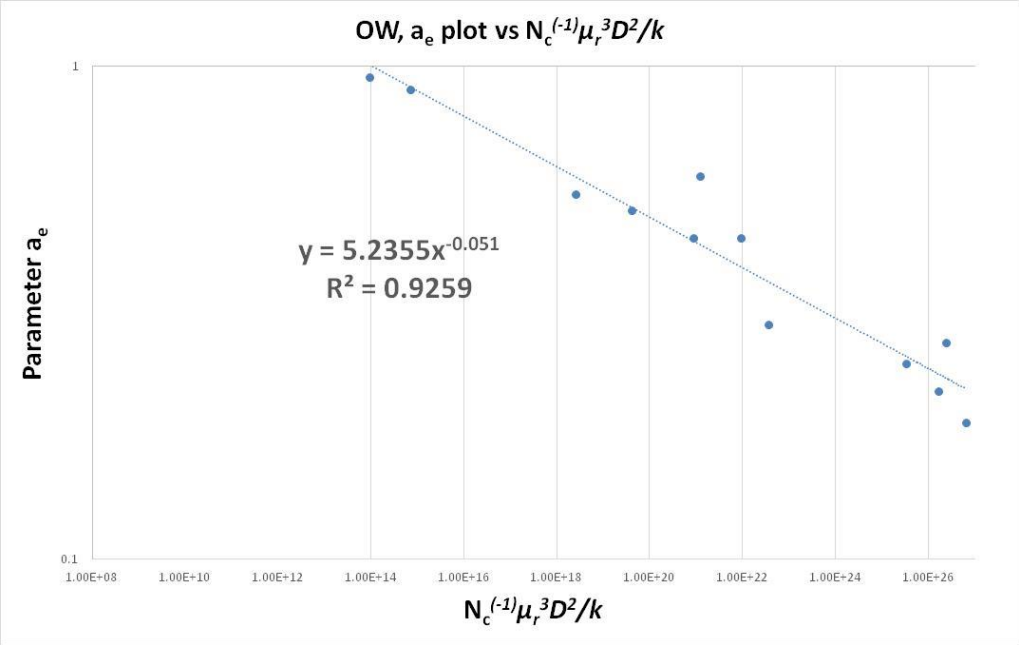

Figure 5.3: Power-law correlation between a_e and $N_c^{(-1)}\mu_r^3D^2/k$ in an oil-wet system

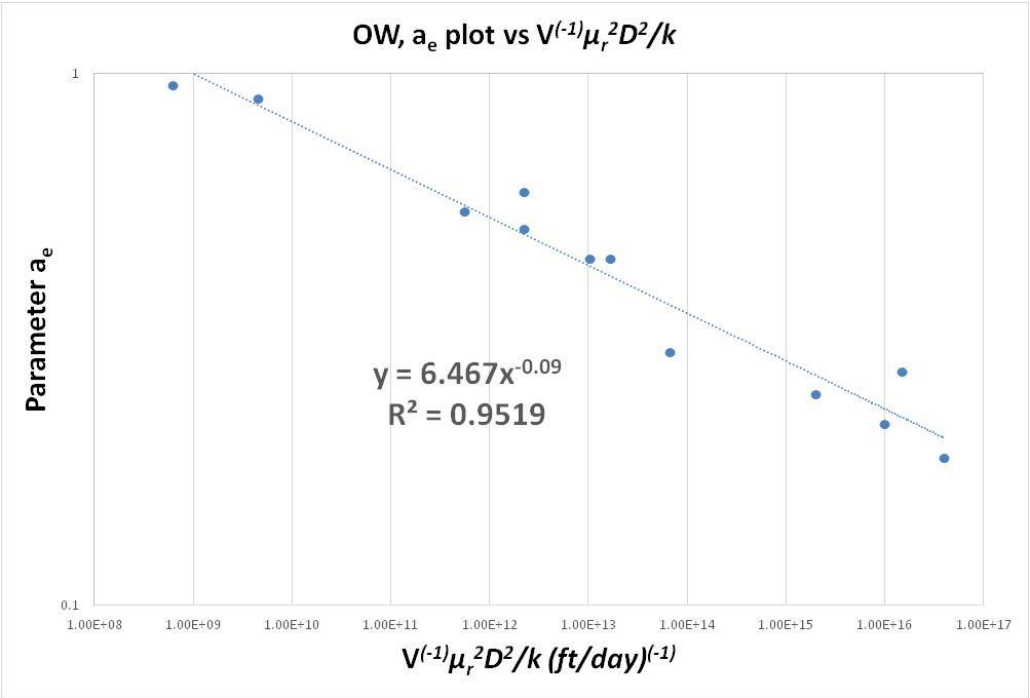

Figure 5.4: Power-law correlation between a_e and $V^{(-1)}\mu_r^2D^2/k$ in an oil-wet system

These results follow the same patterns as the breakthrough recovery (or cumulative recovery at 1 PV) plotted with these scaling groups. This indicates that the upper limit of the effective finger cross-section in an oil-wet system depends on the displacement rate, viscosity ratio, core diameter, and core permeability. The higher exponent of the viscosity ratio provides a slightly better correlation between parameter a_e and the dimensionless scaling group. A high R^2 value is also obtained in the case of $V^{(-1)}\mu_r^2 D^2/k$.

Although the scaling group $V^{(-1)}\mu_r^2 D^2/k$ offers the best correlation from this study, the dimensional scaling group may not be easy to use. In an effort to generalize the scaling group, we suggest that the scaling group $N_c^{(-1)}\mu_r^3 D^2/k$ also provides a reasonable power-law correlation with parameter a_e in an oil-wet system.

Oil-Wet System: Parameter β_1

$\beta_1$values from the simulation results range from 1 to 10. This parameter affects the shape exponent of the effective finger in the grid-blocks. Several power-law correlations between β_1 and scaling groups were plotted, similar to parameter a_e. However, the results show poor correlation. The best correlation with the previous scaling group comes from $\beta_1$and $N_c^{(-1)}\mu_r^3 D^2/k$ (as shown in Figure 5.5). Even the dimensional group $V^{(-1)}\mu_r^3 D^2/k$ provides a similar R^2 value of less than 0.9 (Figure 5.6). These results imply that the typical scaling groups in an oil-wet system from this study may not be suitable with parameter β_1.

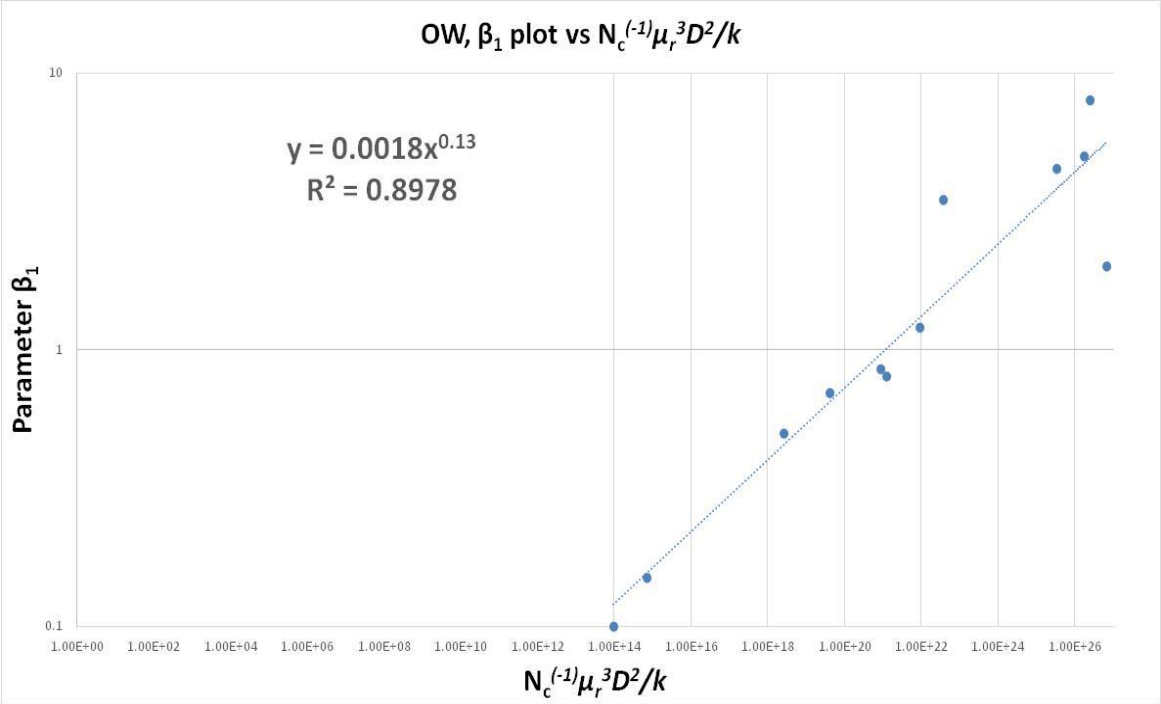

Figure 5.5: Power-law correlation between β_1 and $N_c^{(-1)}\mu_r^3 D^2/k$ in an oil-wet system

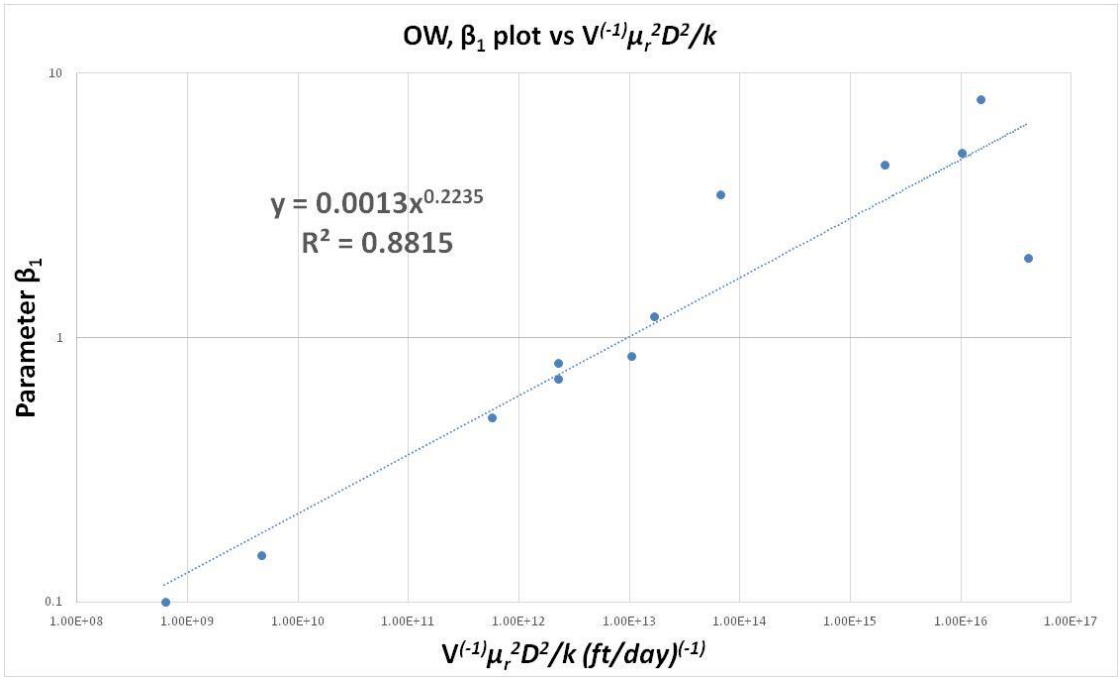

Figure 5.6: Power-law correlation between β_1 and $V^{(-1)}\mu_r^2 D^2/k$ in an oil-wet system

Water does not imbibe into the smaller pore spaces for a strongly oil-wetting surface even if it has more time to flow. We propose that the shape exponent in an oil-wet system does not depend on the displacement rate. For that reason, the dimensionless scaling group $\mu_r^2 D^2/k$ was plotted with β_1. The results illustrated in Figure 5.7 support that this hypothesis is reasonable since it provides the best power-law correlation with this new scaling group. Accordingly, this effective shape exponent $\beta_1$is dependent only on the viscosity ratio, core diameter, and core permeability.

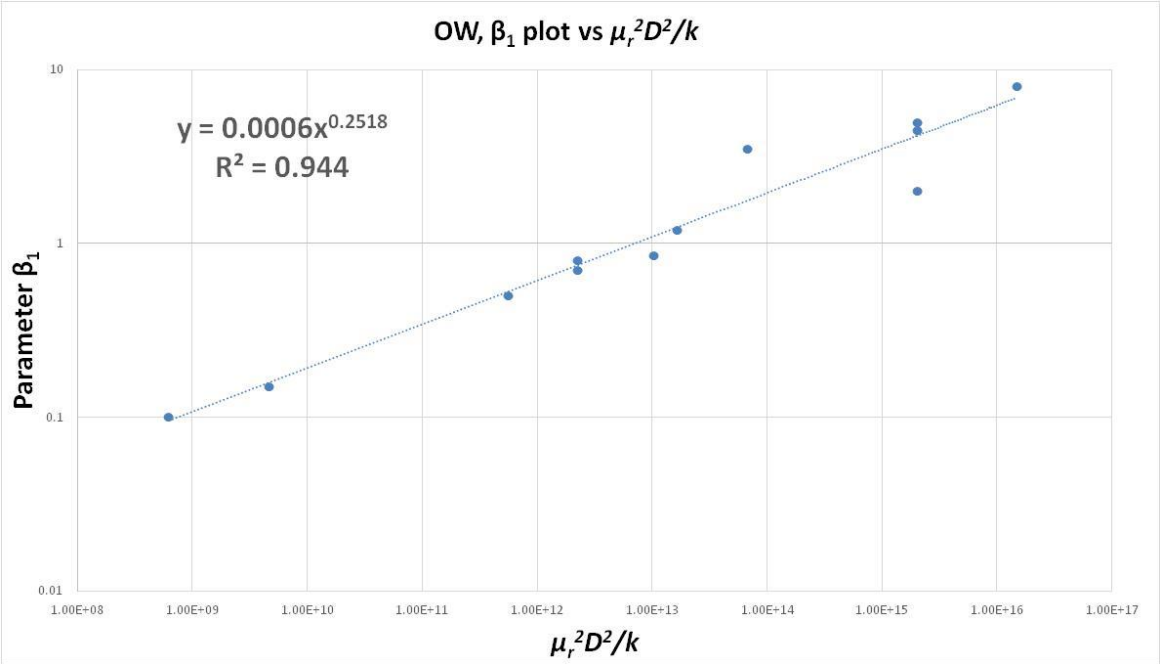

Figure 5.7: Power-law correlation between β_1 and $\mu_r^2 D^2/k$ in an oil-wet system

Water-Wet System: Parameter a_e

According to the results from the previous chapter, the scaling group $N_c\mu_r^2D^2/k$ provided the best power-law correlation to represent viscous fingerings in water-wet experiments. Including both the data from previous study (2-inch diameter core) and the new data from this study (4-inch diameter core), this scaling group was plotted with parameter a_e. As expected, the updated data points are fitted well with the power-law correlation (as can be seen in Figure 5.8). This outcome indicates that the proposed scaling group is already appropriate for determining this parameter in a water-wet system.

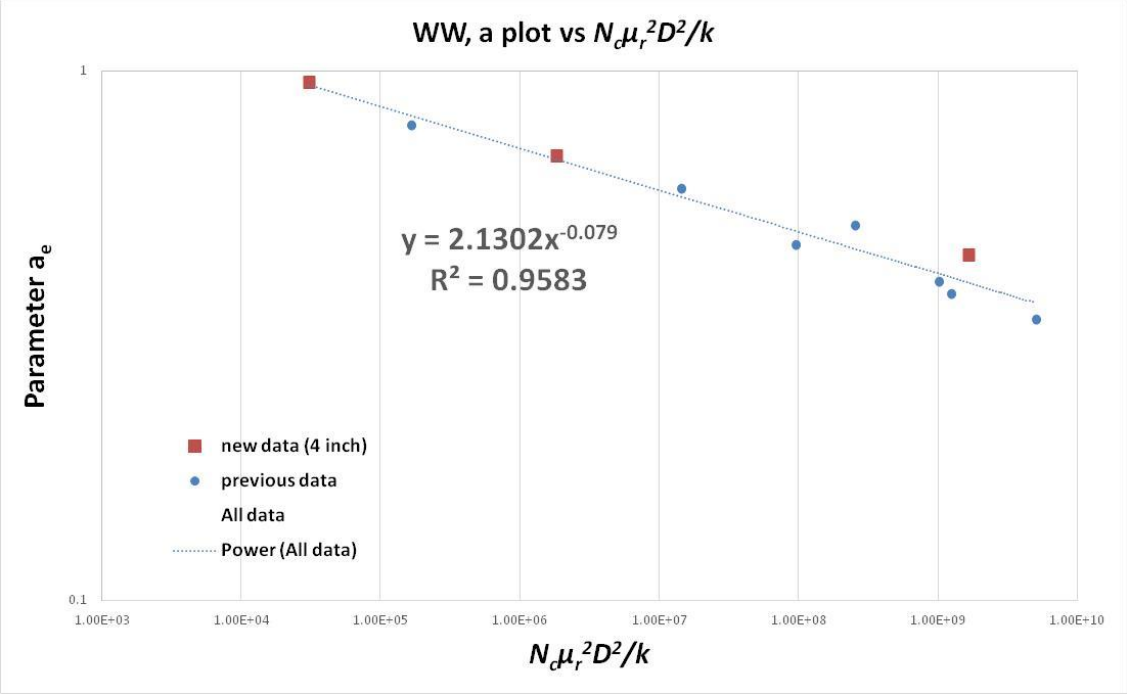

Figure 5.8: Power-law correlation between a_e and $N_c\mu_r^2D^2/k$ in a water-wet system

Water-Wet System: Parameter β_1

Similar to parameter a_e, the exponent parameter β_1 from all experiments were plotted against scaling group $N_c\mu_r^2D^2/k$ (Figure 5.9). In water-wet system, the shape exponent of the finger not only depends on the viscosity ratio, core diameter, and permeability, but also the flow velocity (in the capillary number term). This is because water can imbibe more into smaller pore throats with the slower displacement rate. The additional data also match with the proposed scaling group and provide a good power-law correlation, thus confirming that the group $N_c\mu_r^2D^2/k$ is well-related to parameter β_1 too.

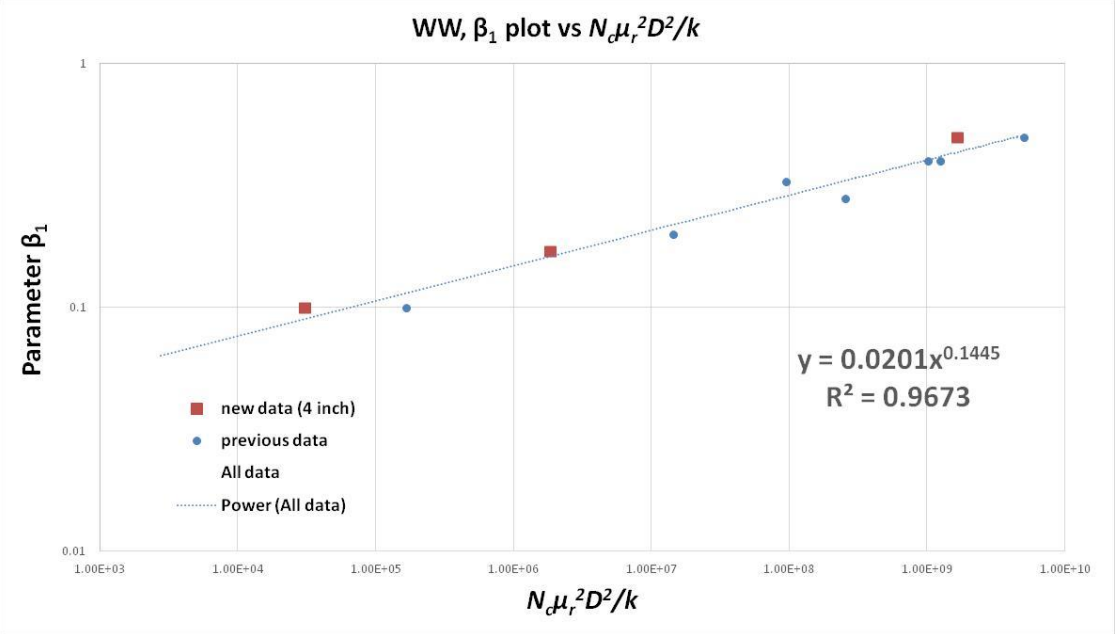

Figure 5.9: Power-law correlation between β_1 and $N_c\mu_r^2D^2/k$ in a water-wet system

Parameter β_2

According to Table 5.2, parameter β_2 is a constant at 2.5 for both oil-wet and water-wet systems. In this study, we could match production history by varying other parameters. Moreover, from previous results listed in Table 5.3, this parameter also shows no correlation with any scaling group. These results imply that the growth rate exponent of bypassed-oil zone does not depend on parameters related to viscous fingerings for both systems.

5.2.3 Effective Residual Oil Saturation Comparison

The effective residual oil saturation (S_{orem}) for all experiments was calculated from Equation 4.10. The comparison of this saturation between the simulation results and the graphical extrapolation from experimental data is listed in Table 5.4.

Experiment No.	S_{orem} from History Matching	S_{orem} from Graphical Extrapolation
1	0.41	0.36
2	0.63	0.67
3	0.67	0.64
4	0.69	0.69
5	0.73	0.75
6	0.82	0.82
7	0.85	0.85
8	0.87	0.86
9	0.88	0.90
10	0.44	0.40
11	0.73	0.74
12	0.83	0.83
13	0.19	0.18
14	0.35	0.34
15	0.56	0.58

Table 5.4: The comparison of S_{orem} from the simulation and the extrapolation technique

The information given in Table 5.4 show similar S_{orem} value, suggesting that the graphical method is reliable way to estimate the average water saturation in the core for an unstable waterflood at infinite injected pore volume. The simulation results also support the bypassed-oil region theory due to instability where the water saturation within the core never reaches 1-S_{or}.

5.2.4 Effective Relative Permeability

The viscous fingering effect is captured in the simulations through the effective relative permeability. The shape and domain of the effective relative permeability for each case was affected by model parameters a_e, β_1, and β_2.

Oil Relative Permeability

The effective oil relative permeability curves ($k_{ro,e}$) resulting from the history matching process for the 2-inch oil-wet core viscosity variation are shown in Figure 5.10. All curves begin with 100% oil saturation ($S_w = 0$). The most stable case which is the unit viscosity ratio (black line) has the largest water saturation range due to the lowest effective residual oil saturation value (S_{orem}). In general, the higher viscosity ratio leads to a smaller water saturation range, except for viscosity ratio of 30 in this plot. The end-point oil relative permeability ($k^o_{ro,e}$) is a constant of 0.4 in this model. This is because of the oil single phase-flow term in Equation 5.2. The $k^o_{ro,e}$ is assumed to be the oil relative permeability at zero water saturation since waterflood in oil-wet experiments started with 100% oil saturation in the cores. This term also leads to a high oil relative permeability at a low water saturation. However, the slope of $k_{ro,e}$ significantly drops after the water saturation starts increasing.

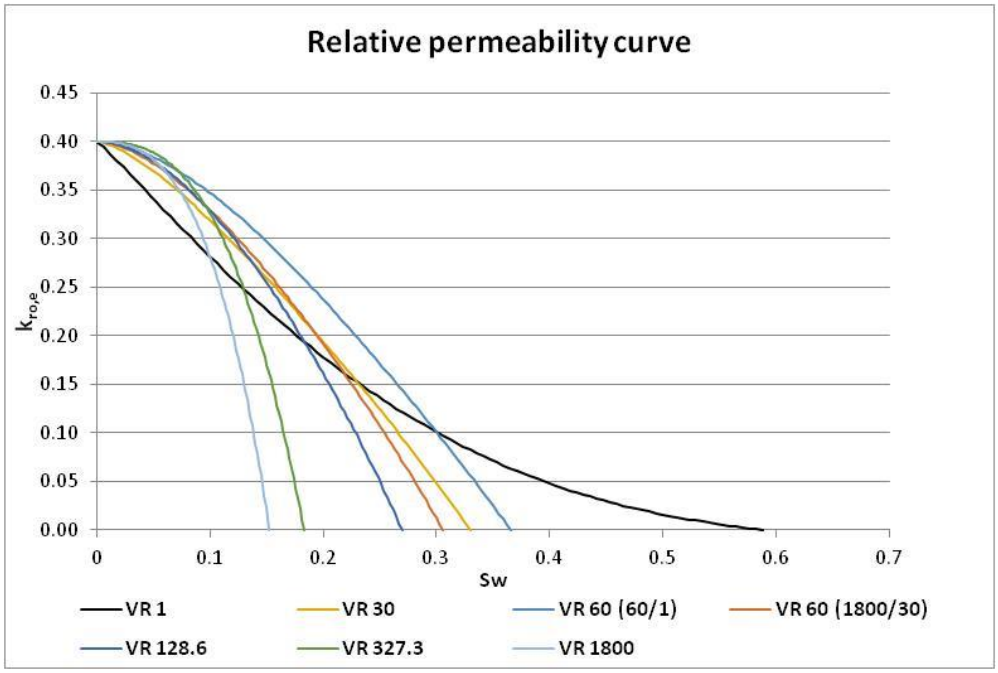

Figure 5.10: The effect of viscosity ratio on the effective relative permeability curve of oil ($k_{ro,e}$) for 2-inch oil-wet experiments

In case of flow velocity variation (Figure 5.11), the end point $k^{o}_{ro,e}$and the initial water saturation are the same as previously discussed. The highest flow rate experiment (1 ft/day) has the largest water saturation domain for relative permeability curve in oil-wet system because water displaces oil better at the higher velocity, thus leading to less bypassed-oil region. At any given water saturation, it can be seen that the effective oil relative permeability directly depends on the flow rate. Therefore, in an oil-wet system, the slower velocity results in less $k_{ro,e}$ value, causing less oil production.

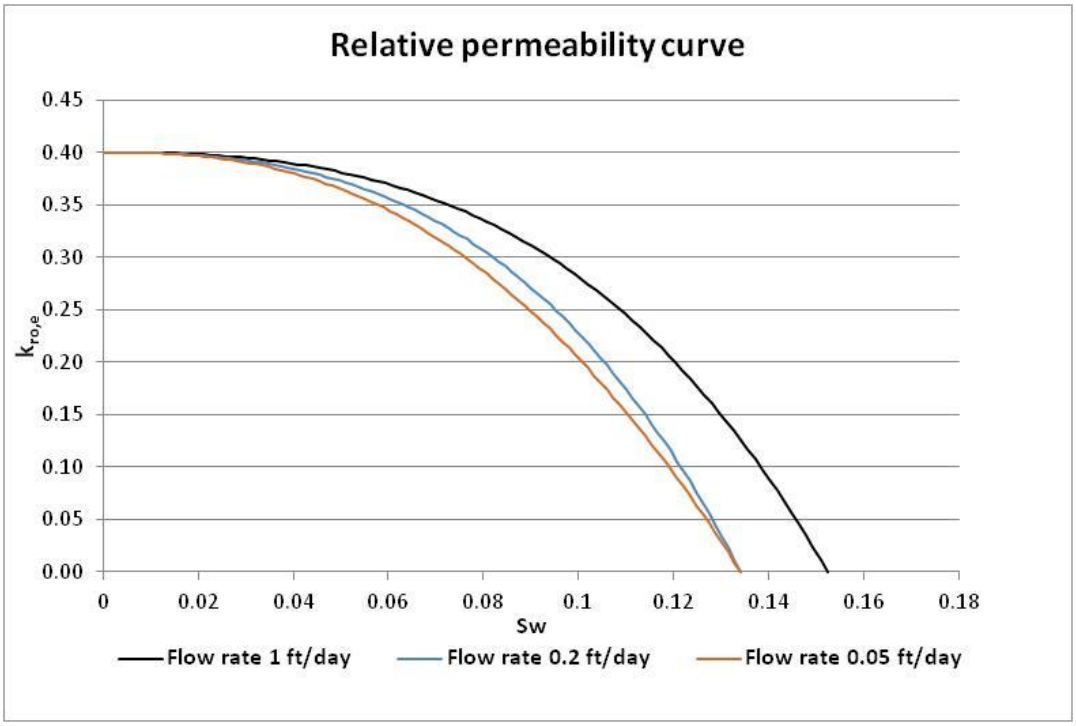

Figure 5.11: Effect of velocity on the effective relative permeability curve of oil ($k_{ro,e}$) for 2-inch oil-wet experiments

Figure 5.12 demonstrates the comparison of $k_{ro,e}$ between oil-wet and water-wet system in the same 4-inch core and at the same viscosity ratio. The dashed line and the solid line represent results from the oil-wet system and the water-wet system, respectively. In the water-wet system, the initial water saturation varied based on the oil viscosity at the initial oil saturation process. The domain of water saturation for these curves is between S_{wi} to S_{orem}. The end point $k^{o}_{ro,e}$ is affected by Equation 5.2. The shapes of $k_{ro,e}$ curves for the oil-wet and water-wet systems are similar. The end-point oil relative permeability is a constant of 1 in this model. The difference between the two wetting systems is mostly because of differences in S_{wi} and S_{orem}.

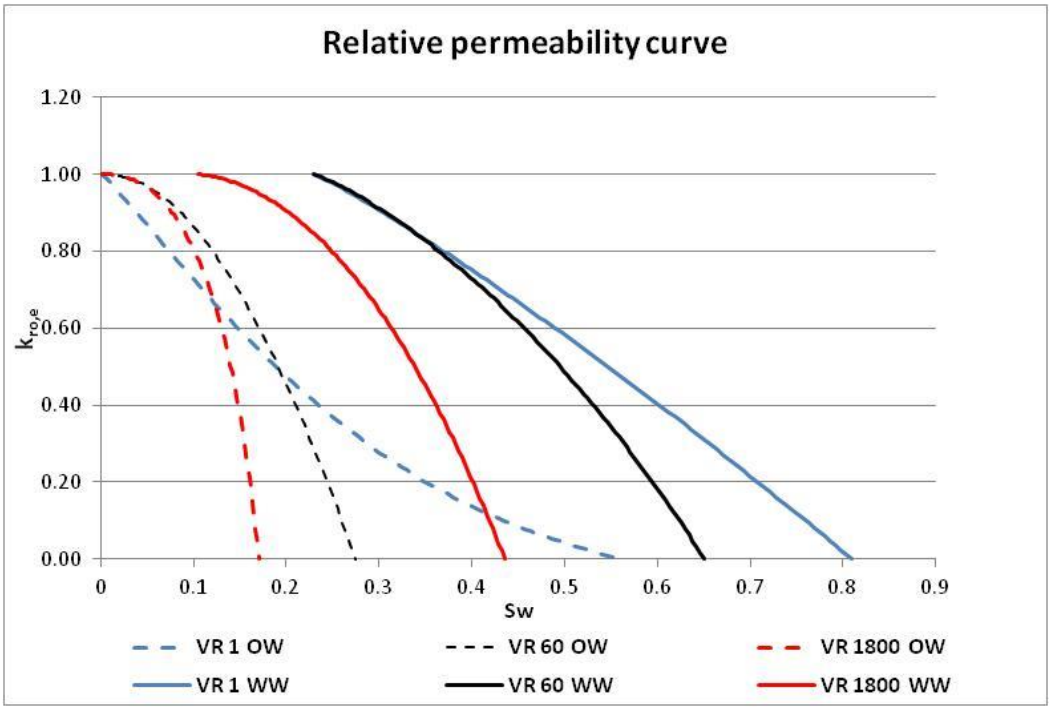

Figure 5.12: Effect of wettability and viscosity ratio on the effective relative permeability curve of oil ($k_{ro,e}$) for 4-inch experiments

Water Relative Permeability

The effective relative permeability function of water ($k_{rw,e}$) is plotted against the water saturation in Figure 5.13 for the viscosity ratio variation in the oil-wet case. The unit viscosity ratio (the most stable case) which is represented by the black line also has the largest range in water saturation. The curves shift to the left and become steeper at the higher end of water saturation as the flow is less stable. The end point water relative permeability $k^o_{rw,e}$ decreases as the viscosity ratio increases. As a result of Equation 5.1, the more unstable condition leads to a lower value of the maximum cross-section of the effective finger, which controls the water relative permeability in the two-phase region. This trend is different from the constant end point oil relative permeability $k^o_{ro,e}$.

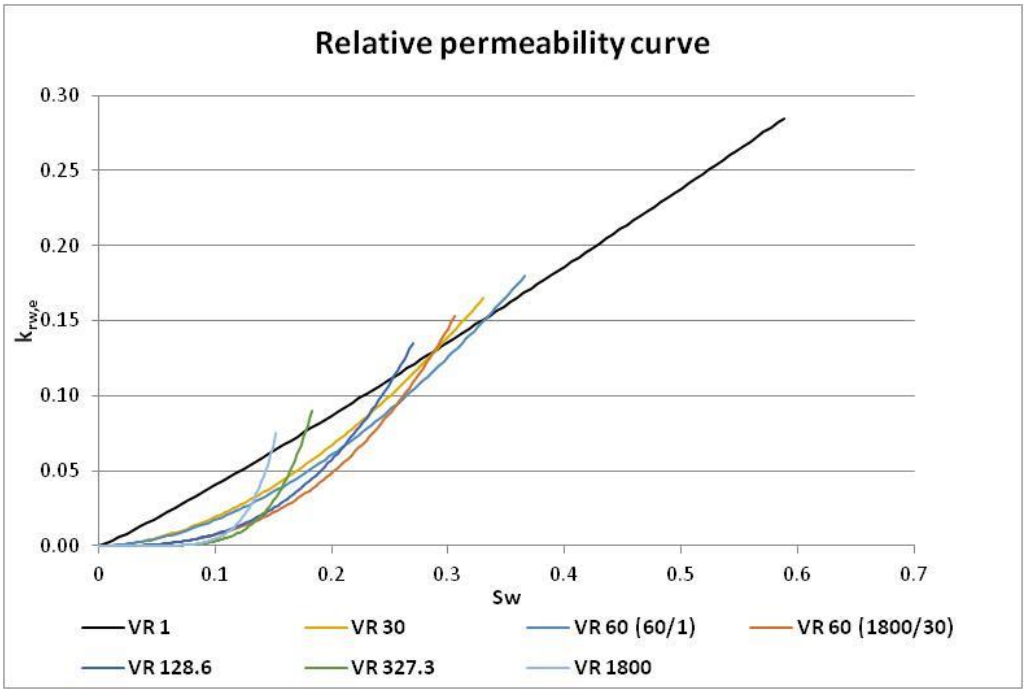

Figure 5.13: Effect of viscosity ratio on the effective relative permeability curve of water ($k_{rw,e}$) for 2-inch oil-wet experiments

The effects of flow rate variation in an oil-wet system on the effective water relative permeability curves are shown in Figure 5.14. The end points $k^o_{rw,e}$ show similar trends to the viscosity ratio variation. The slower displacement rate in an oil-wet system leads to the lower a_e value, thus decreasing the end point $k^o_{rw,e}$. Figure 5.15 compares the effective water relative permeability curves for both wetting conditions. In general, the value of $k_{rw,e}$ in the water-wet experiments is less than the oil-wet experiments, resulting in less water production and better oil recovery.

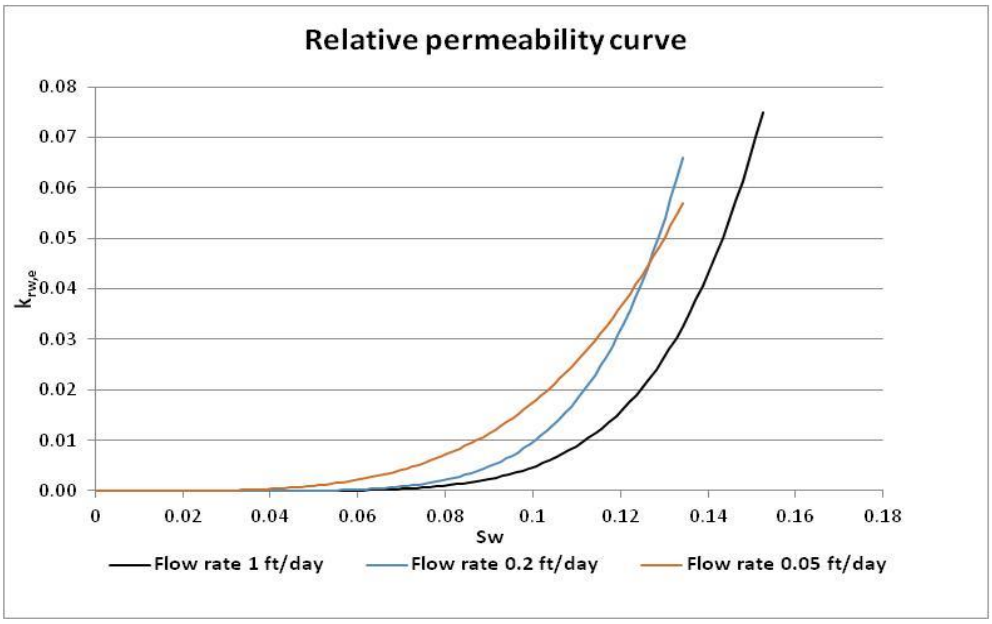

Figure 5.14: Effect of velocity on the effective relative permeability curve of water ($k_{rw,e}$) for 2-inch oil-wet experiments

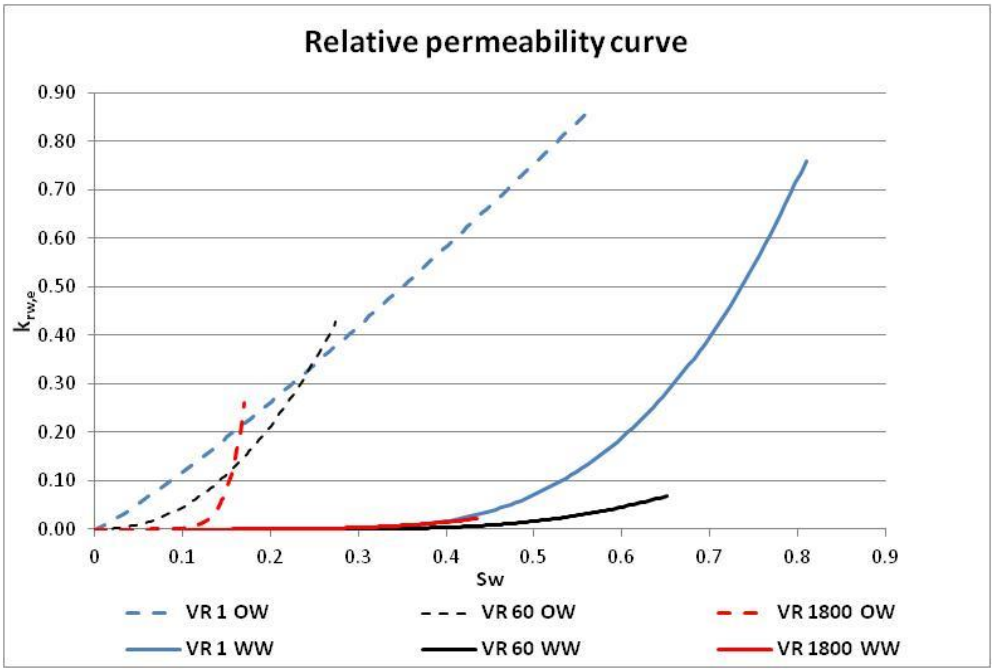

Figure 5.15: Effect of wettability and viscosity ratio on the effective relative permeability curve of water ($k_{rw,e}$) for 4-inch experiments

CHAPTER 6: CONCLUSIONS

6.1 CONCLUSIONS

1. Higher viscosity ratio leads to a more unstable flow, causing earlier breakthrough recovery in both water-wet and oil-wet rocks.

2. Based on the results in this study, the square of core diameter or the characteristic cross-sectional area also has an effect on viscous fingering. The higher the value, the earlier is the water breakthrough in both water-wet and oil-wet systems.

3. The effect of flow rate on the breakthrough recovery in oil-wet experiments is opposite to those observed in water-wet experiments. The breakthrough oil recovery and oil recovery at 1 PV injection decrease as the flow rate decreases. At slower flow rates in oil-wet experiments, the pressure drop is lower. In addition, there is no imbibition of water into the smaller pore spaces due to the non-wetting surface. These phenomena lead to less oil recovery at slower flow rates.

4. The relationship between scaling groups and the cumulative recovery (both breakthrough recovery and cumulative recovery at 1 PV) can be used to study the viscous fingering effect.

5. In the oil-wet system, the viscosity ratio raised to an exponent of slightly improves of the power-law correlation (compared to an exponent of 2).

6. The lumped fingering model parameters (a_e, β_1, and β_2) capture the viscous fingering in the flow modeling by modifying the relative permeability.

7. Model parameter a_e in the oil-wet system shows the best power-law correlation with the dimensional scaling group $V^{(-1)}\mu_r^2 D^2/k$. Nonetheless, in an effort to generalize scaling group, the dimensionless scaling group $N_c^{(-1)}\mu_r^3 D^2/k$ is proposed which also provides an acceptable power-law correlation with this parameter.

8. Model parameter $\beta_1$in the oil-wet system does not depend on flow velocity. The proposed scaling group for this parameter is $\mu_r^2 D^2/k$.

9. Model parameters a_e and β_1 in the water-wet system demonstrate the best power-law correlations with the scaling group $N_c \mu_r^2 D^2/k$. The results of the core diameter variation experiments are consistent with this scaling group.

10. The model parameter $\beta_2$was found to be a constant of 2.5 from this study.

11. The residual oil saturation estimated from graphical extrapolation method using experimental results does not represent the intrinsic residual oil saturation (during stable floods). Instead, this value corresponds to an effective residual oil saturation (S_{orem}) which depends on flow instability.

12. The effect of model parameters on the relative permeability is composed of 3 parts: the water saturation domain, the end point of relative permeability, and the shape of the curve. The first part is affected by S_{orem} which can be directly calculated from the model parameter a_e. The end point of relative permeability, $k_{ro,e}^o$ is constant for both wetting systems. However, the value of $k_{rw,e}^o$ depends on the stability of the flow since water can only flow in the two-phase zone. The shape of the relative permeability curve changes because of the extent of viscous fingering

.

6.2 RECOMMENDATIONS

1. Although the cores used in this study are different (2-inch and 4-inch diameter core), the order of magnitude of the absolute permeability is approximately the same. Boise sandstones of permeability slightly higher than 1 Darcy were used in this study. It is recommended that more experiments with the lower permeability (i.e. less than 1 Darcy) may be required in order to test the scaling groups in both systems

2. The interfacial tension (IFT) is nearly constant in all experiments. Since this value is one of the main parameter included in the capillary number, the variation of IFT is also required to investigate its effect on viscous fingering.

3. According to this research, the core's condition after oil-wet core treatment is assumed to be strongly oil-wet. Besides, the initial conditions of Boise sandstones are generally strongly water-wet. However, oil reservoirs can be "mixed-wet". Therefore, more experiments in mixed-wet system are required in order to find the appropriate scaling groups and capture the viscous fingerings in the reservoir modeling.

4. Although the scaling groups and the model parameters from the experiments are well-correlated in both systems, these correlations should be verified at the very high value of scaling groups. The maximum dimension of core is only 4 inches while the dimension of the grid blocks for the field scale is much greater.

APPENDIX

A. History Matching Results

This section provides the comparison of the cumulative oil production and the pressure drop between the experimental data and simulation predictions for all coreflood experiments.

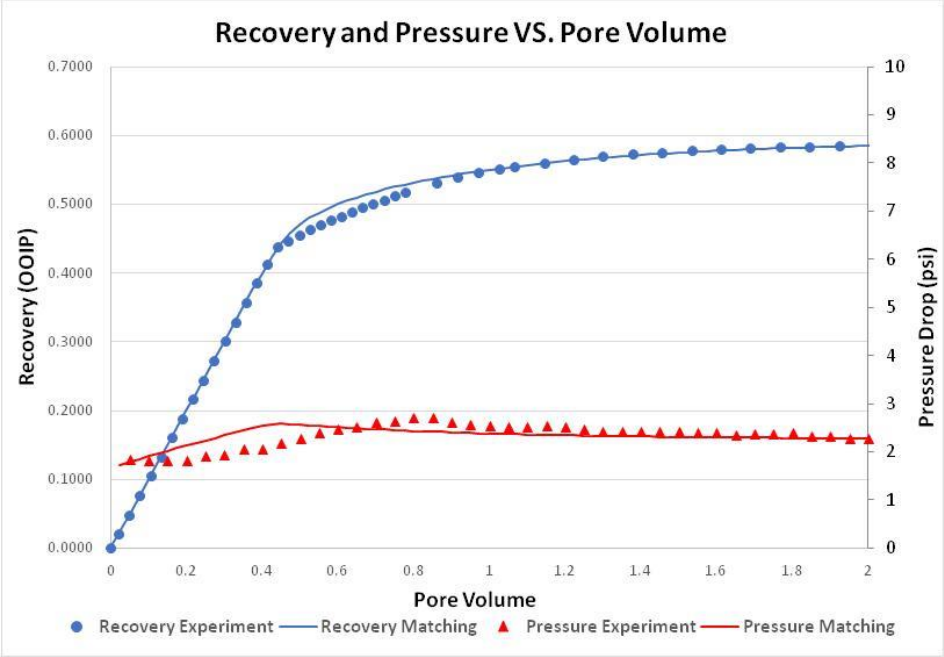

Figure A.1: Experiment and simulation results for 2-inch coreflood of μ_r=1 (μ_o= 60 cp, μ_w= 60 cp) and displacement rate 1 ft/day in the oil-wet system

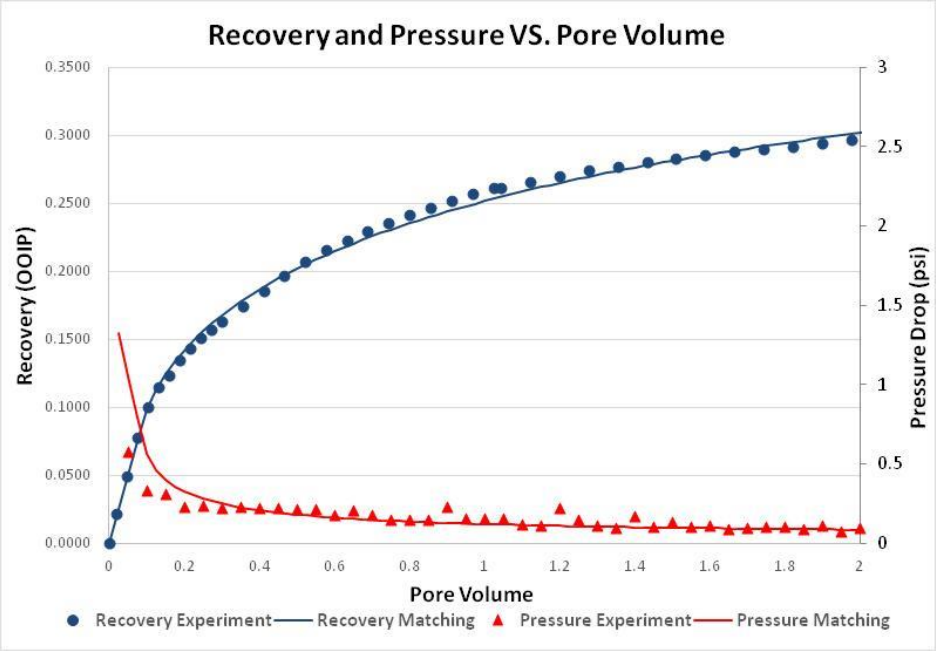

Figure A.2: Experiment and simulation results for 2-inch coreflood of μ_r=60 (μ_o= 60 cp, μ_w= 1 cp) and displacement rate 1 ft/day in the oil-wet system

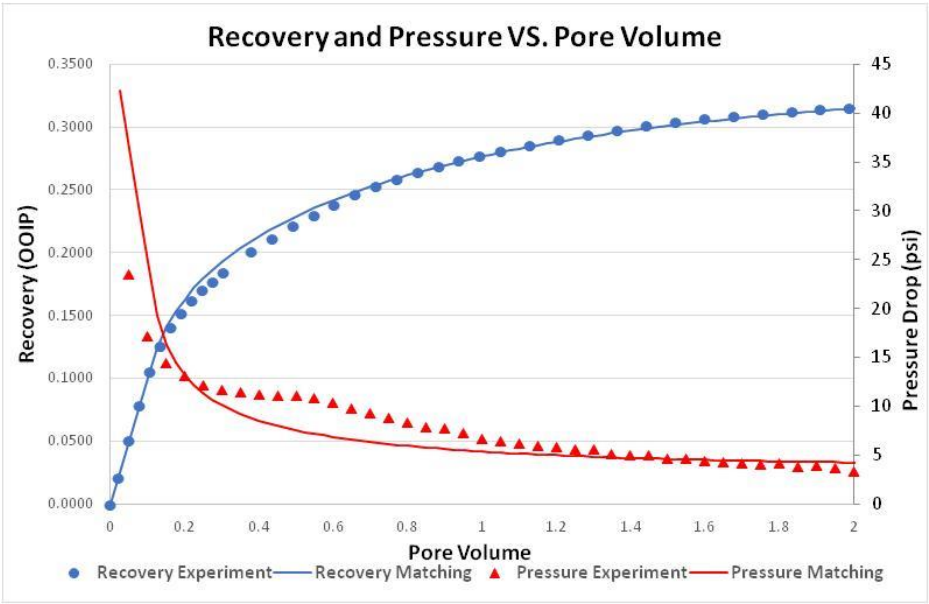

Figure A.3: Experiment and simulation results for 2-inch coreflood of μ_r=30 (μ_o= 1800 cp, μ_w= 60 cp) and displacement rate 1 ft/day in the oil-wet system

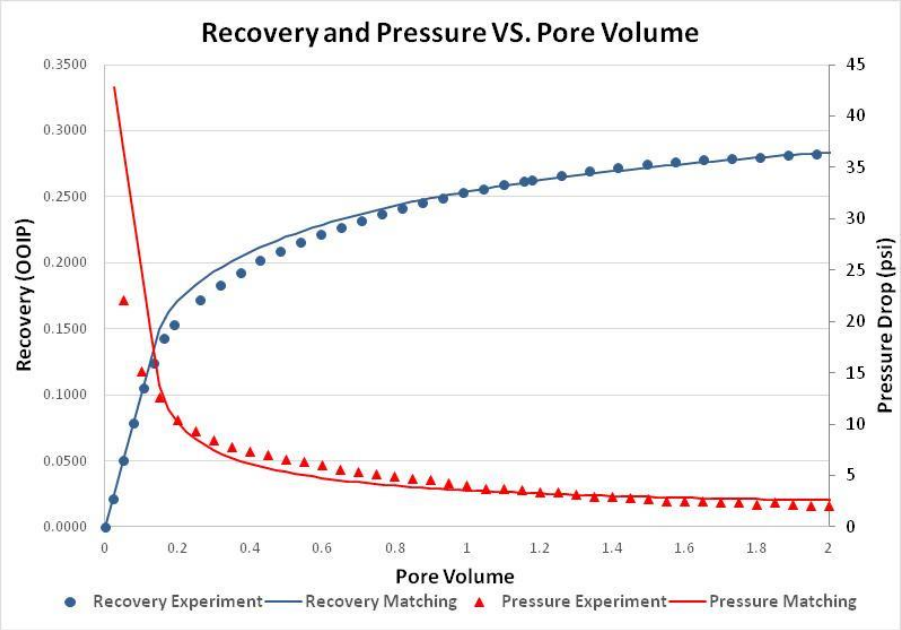

Figure A.4: Experiment and simulation results for 2-inch coreflood of μ_r=60 (μ_o= 1800 cp, μ_w= 30 cp) and displacement rate 1 ft/day in the oil-wet system

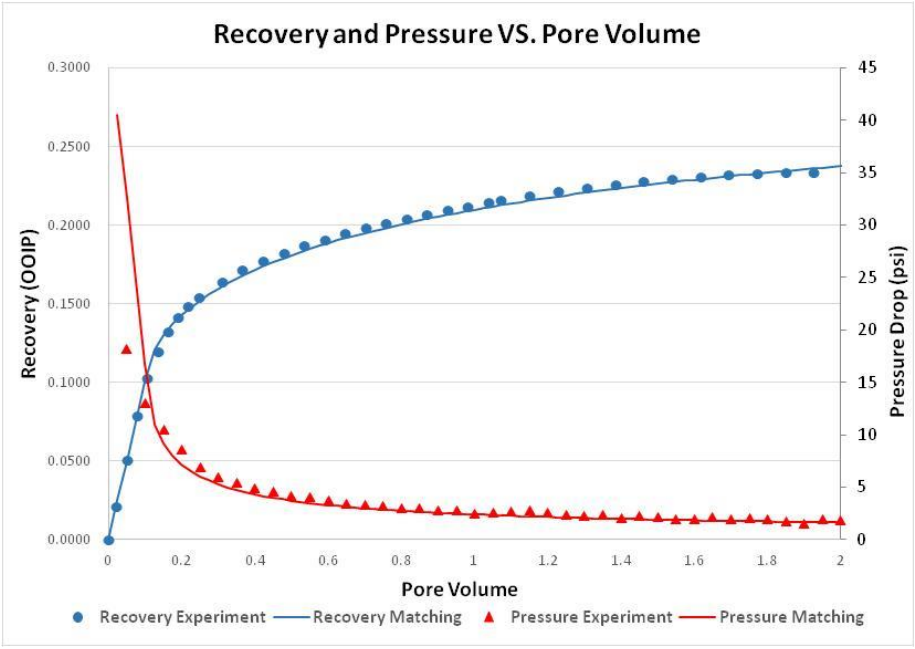

Figure A.5: Experiment and simulation results for 2-inch coreflood of μ_r=128.6 (μ_o= 1800 cp, μ_w= 14 cp) and displacement rate 1 ft/day in the oil-wet system

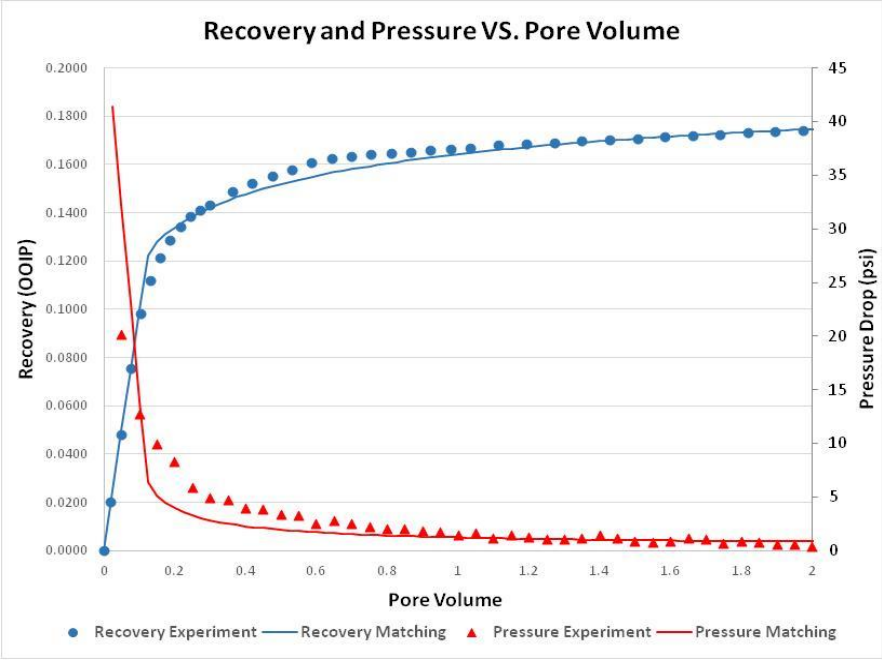

Figure A.6: Experiment and simulation results for 2-inch coreflood of μ_r=327.3 (μ_o= 1800 cp, μ_w= 5.5 cp) and displacement rate 1 ft/day in the oil-wet system

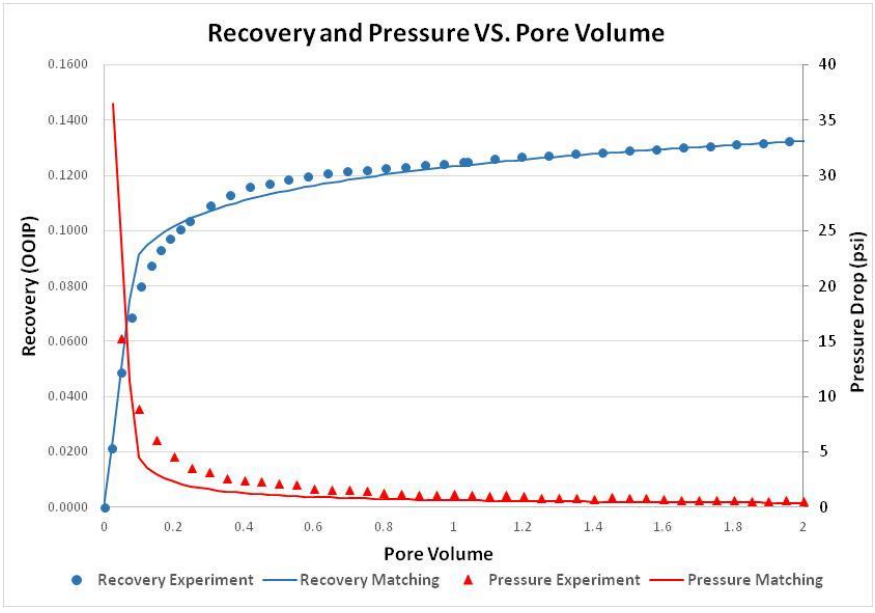

Figure A.7: Experiment and simulation results for 2-inch coreflood of μ_r=1800 (μ_o= 1800 cp, μ_w= 1 cp) and displacement rate 1 ft/day in the oil-wet system

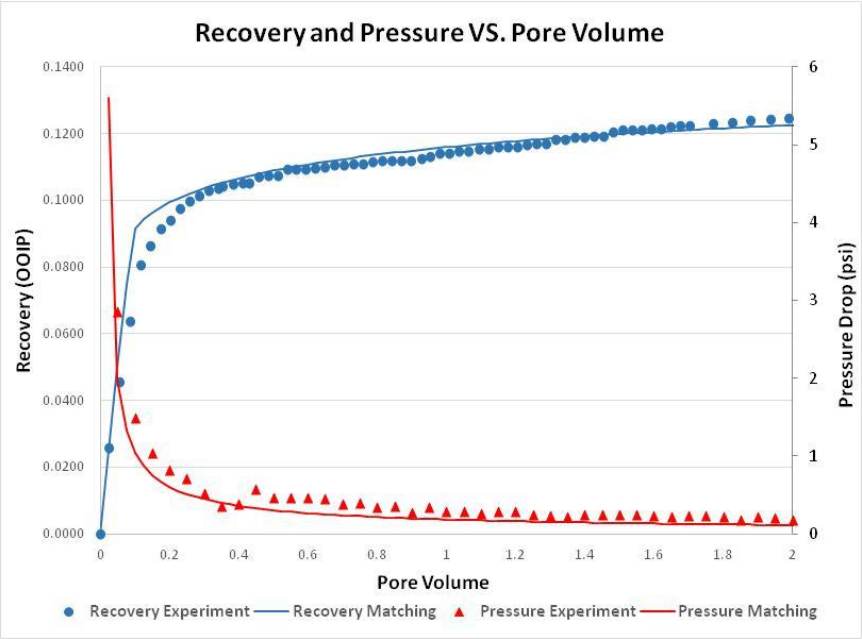

Figure A.8: Experiment and simulation results for 2-inch coreflood of μ_r=1800 (μ_o= 1800 cp, μ_w= 1 cp) and displacement rate 0.2 ft/day in the oil-wet system

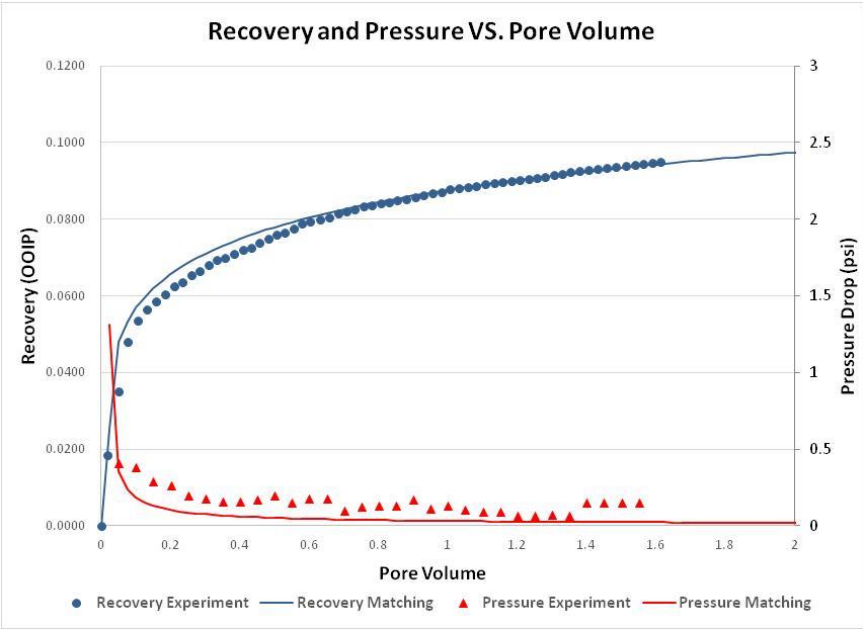

Figure A.9: Experiment and simulation results for 2-inch coreflood of μ_r=1800 (μ_o= 1800 cp, μ_w= 1 cp) and displacement rate 0.05 ft/day in the oil-wet system

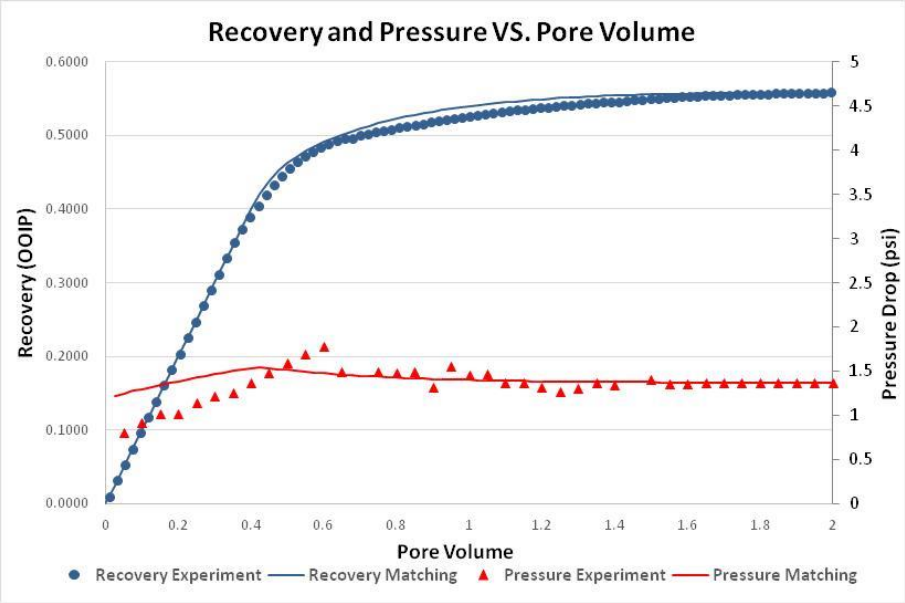

Figure A.10: Experiment and simulation results for 4-inch coreflood of μ_r=1 (μ_o= 60 cp, μ_w= 60 cp) and displacement rate 1 ft/day in the oil-wet system

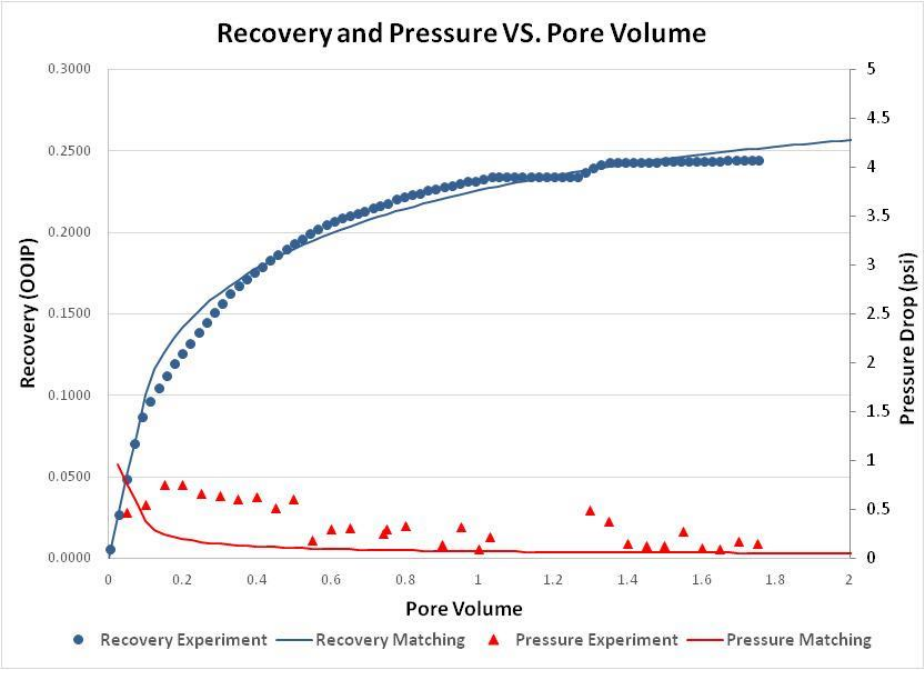

Figure A.11: Experiment and simulation results for 4-inch coreflood of μ_r=60 (μ_o= 60 cp, μ_w= 1 cp) and displacement rate 1 ft/day in the oil-wet system

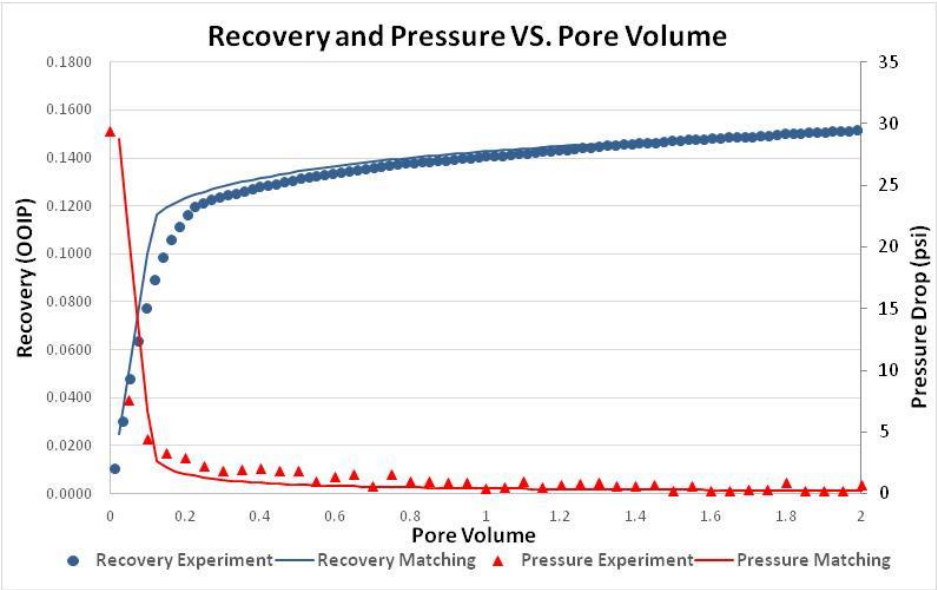

Figure A.12: Experiment and simulation results for 4-inch coreflood of μ_r=1800 (μ_o= 1800 cp, μ_w= 1 cp) and displacement rate 1 ft/day in the oil-wet system

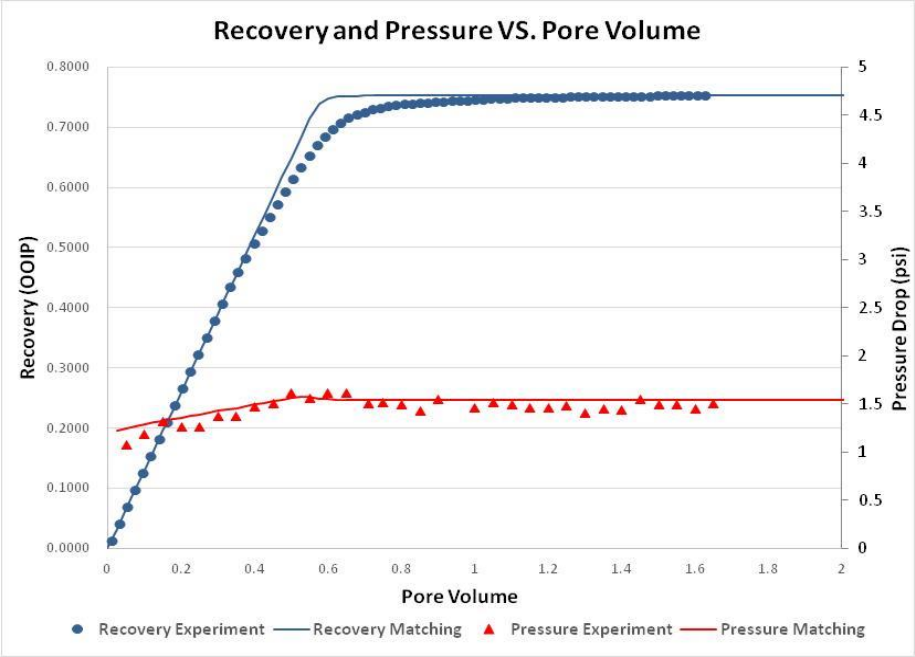

Figure A.13: Experiment and simulation results for 4-inch coreflood of μ_r=1 (μ_o= 60 cp, μ_w= 60 cp) and displacement rate 1 ft/day in the water-wet system

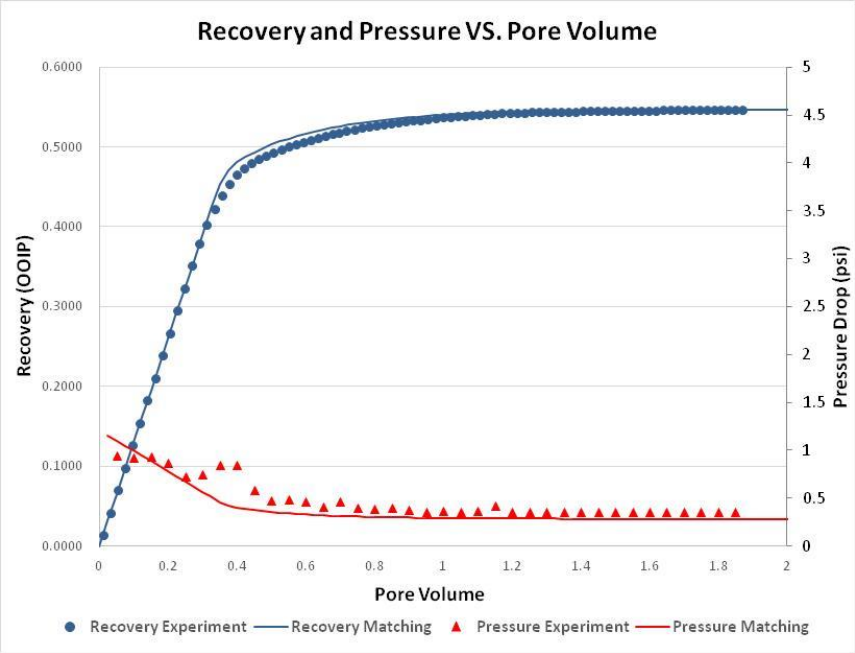

Figure A.14: Experiment and simulation results for 4-inch coreflood of μ_r=60 (μ_o= 60 cp, μ_w= 1 cp) and displacement rate 1 ft/day in the water-wet system

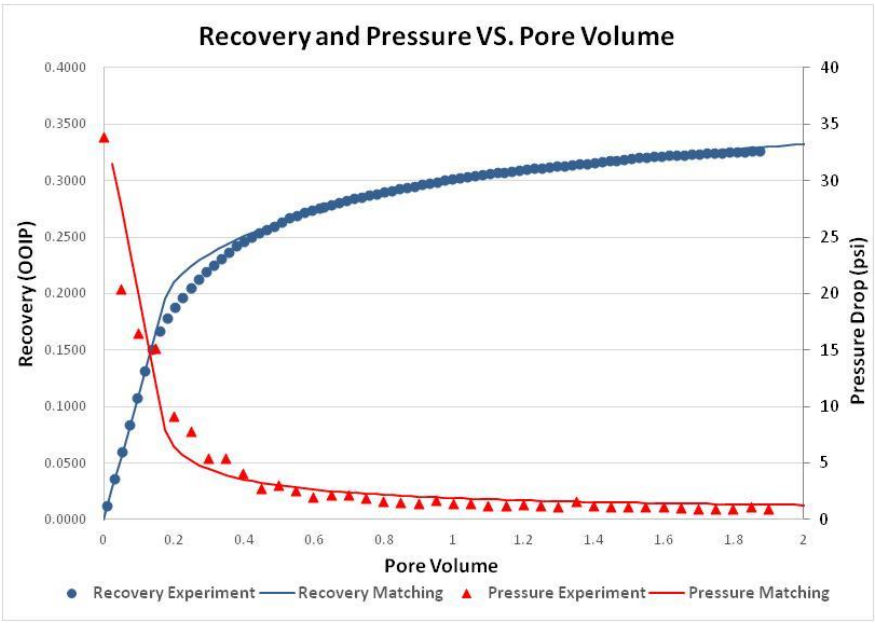

Figure A.15: Experiment and simulation results for 4-inch coreflood of μ_r=1800 (μ_o= 1800 cp, μ_w= 1 cp) and displacement rate 1 ft/day in the water-wet system

REFERENCES

Al-Shafei, M. A., & Okasha, T. M. (2009, January 1). Wettability Studies at the Pore Level of Saudi Aramco Reservoirs. Society of Petroleum Engineers. doi:10.2118/126088-MS

Anderson, W. G. (1986, October 1). Wettability Literature Survey- Part 1: Rock/Oil/Brine Interactions and the Effects of Core Handling on Wettability. Society of Petroleum Engineers. doi:10.2118/13932-PA

Anderson, W. G. (1987, November 1). Wettability Literature Survey Part 5: The Effects of Wettability on Relative Permeability. Society of Petroleum Engineers. doi:10.2118/16323-PA

Anderson, W. G. (1987, December 1). Wettability Literature Survey-Part 6: The Effects of Wettability on Waterflooding. Society of Petroleum Engineers. doi:10.2118/16471-PA

Araktingi, U. G., & Orr Jr, F. M. (1993, April 1). Viscous Fingering in Heterogeneous Porous Media. Society of Petroleum Engineers. doi:10.2118/18095-PA

Benham, A. L., & Olson, R. W. (1963, June 1). A Model Study of Viscous Fingering. Society of Petroleum Engineers. doi:10.2118/513-PA

Buckley, S. E., & Leverett, M. C. (1942, December 1). Mechanism of Fluid Displacement in Sands. Society of Petroleum Engineers. doi:10.2118/942107-G

Buckley, J. S., 1996. “Mechanisms and consequences of wettability alteration by crude oil”. PhD dissertation Heriot-Watt University

Callaway, F. H. (1959, October 1). Evaluation of Waterflood Prospects. Society of Petroleum Engineers. doi:10.2118/1258-G

Chuoke, R. L., van Meurs, P., & van der Poel, C. (1959, January 1). The Instability of Slow, Immiscible, Viscous Liquid-Liquid Displacements in Permeable Media. Society of Petroleum Engineers.

DiCarlo, D. A., Akshay, S., & Blunt, M. J. (2000, March 1). Three-Phase Relative Permeability of Water-Wet, Oil-Wet, and Mixed-Wet Sandpacks. Society of Petroleum Engineers. doi:10.2118/60767-PA

Donaldson, E. C., Thomas, R. D., & Lorenz, P. B. (1969, March 1). Wettability Determination and Its Effect on Recovery Efficiency. Society of Petroleum Engineers. doi:10.2118/2338-PA

Doorwar, S. (2015). Understanding Unstable Immiscible Displacement in Porous Media (Doctoral dissertation). Available from University of Texas at Austin, Petroleum and Geosystems Engineering Thesis and Dissertations 2015 database

Doorwar, S., & Mohanty, K. K. (2015, February 23). Fingering Function for Unstable Immiscible Flows. Society of Petroleum Engineers. doi:10.2118/173290-MS

Engelberts, W. F., & Klinkenberg, L. J. (1951, January 1). Laboratory Experiments on the Displacement of Oil by Water from Packs of Granular Material. World Petroleum Congress.

Fayers, F. J., & Newley, T. M. J. (1988, May 1). Detailed Validation of an Empirical Model for Viscous Fingering With Gravity Effects. Society of Petroleum Engineers. doi:10.2118/15993-PA

Fayers, F. J. (1988, May 1). An Approximate Model With Physically Interpretable Parameters for Representing Miscible Viscous Fingering. Society of Petroleum Engineers. doi:10.2118/13166-PA

Green, D. W., & Willhite, G. P. (1998). Enhanced oil recovery. Richardson, TX: Henry L. Doherty Memorial Fund of AIME, Society of Petroleum Engineers.

Hagoort, J. (1974, February 1). Displacement Stability of Water Drives in Water-Wet Connate-Water-Bearing Reservoirs. Society of Petroleum Engineers. doi:10.2118/4268-PA

Homsy, G. M., 1987, "Viscous fingering in porous media," Annu. Rev. Fluid Mech. 19, 271-311

Johnson, E. F., Bossler, D. P., & Bossler, V. O. N. (1959, January 1). Calculation of Relative Permeability from Displacement Experiments. Society of Petroleum Engineers.

Jones, S. C., & Roszelle, W. O. (1978, May 1). Graphical Techniques for Determining Relative Permeability From Displacement Experiments. Society of Petroleum Engineers. doi:10.2118/6045-PA

Koval, E. J. (1963, June 1). A Method for Predicting the Performance of Unstable Miscible Displacement in Heterogeneous Media. Society of Petroleum Engineers. doi:10.2118/450-PA

Krishna, I. S. (1969, January 1). The Oil-Wet Reservoir - Fact Or Fiction? Society of Petroleum Engineers.

Leimkuhler, J., & Leveille, G. (2012, February 1). Unconventional Resources. Society of Petroleum Engineers. doi:10.2118/0112-026-TWA

Lorenz, P.B., Doni1dson, E.C., and Thomas, R.D., 1974: "Use of Centrifugal Measurements of Wettability to Predict Oil Recovery, " Report 7873, U.S. Bureau of Mines, Bartlesville Energy Technology Center, Bartlesville.

Luo, H., Mohanty, K. K., Delshad, M., & Pope, G. A. (2016, April 11). Modeling and Upscaling Unstable Water and Polymer Floods: Dynamic Characterization of the Effective Finger Zone. Society of Petroleum Engineers. doi:10.2118/179648-MS

Meyer, R.F., Attanasi, E.D., and Freeman, P.A., 2007, Heavy oil and natural bitumen resources in geological basins of the world: U.S. Geological Survey Open-File Report 2007-1084, available online at http://pubs.usgs.gov/of/2007/ 1084/.

Mohanty, K. K. (1982, January 1). Multiphase Flow in Porous Media: II. Pore-level Modeling. Society of Petroleum Engineers. doi:10.2118/11018-MS

Morrow, N. R. (1990, December 1). Wettability and Its Effect on Oil Recovery. Society of Petroleum Engineers. doi:10.2118/21621-PA

Morrow, N.R., Ma, S., Zhou, X., and Zhang, X.: "Characterization of Wettability from Spontaneous Imbibition Measurements," paper CIM 94-47 presented at the 1994 Petr. Soc. of CIM Ann. Tech. Meeting and AOSTRA 1994 Ann. Tech. Conf., Calgary, June 12-15.

Owens, W. W., & Archer, D. L. (1971, July 1). The Effect of Rock Wettability on Oil-Water Relative Permeability Relationships. Society of Petroleum Engineers. doi:10.2118/3034-PA

Patel, K. K. , Mehta, M. N. , & Singh, T. R. (2014). Application of Homotopy Analysis Method in One-Dimensional Instability Phenomenon Arising in Inclined Porous Media.American Journal of Applied Mathematics and Statistics, 2(3), 106-114.

Pavone, D. (1992, May 1). Observations and Correlations for Immiscible Viscous-Fingering Experiments. Society of Petroleum Engineers. doi:10.2118/19670-PA

Peters, E. J., & Flock, D. L. (1981, April 1). The Onset of Instability During Two-Phase Immiscible Displacement in Porous Media. Society of Petroleum Engineers. doi:10.2118/8371-PA

Peters, E. J. (1983, January 1). Scaling Unstable Immiscible Displacements. Society of Petroleum Engineers.

Saffman, P. G. & Taylor, G. I., 1958, The penetration of a fluid into a porous medium or Hele-Shaw cell containing a more viscous fluid. Proc. Royal Society, 245, 312-329.

Takach, N. E., Bennett, L. B., Douglas, C. B., Andersen, M. A., & Thomas, D. C. (1989, January 1). Generation of Oil-Wet Model Sandstone Surfaces. Society of Petroleum Engineers. doi:10.2118/18465-MS

Todd, M. R., & Longstaff, W. J. (1972, July 1). The Development, Testing, and Application Of a Numerical Simulator for Predicting Miscible Flood Performance. Society of Petroleum Engineers. doi:10.2118/3484-PA